Vol. 5 No. 1 2021
pISSN 2586-1719 / eISSN 2799-3299

KJAR
Korean Journal of Abdominal Radiology

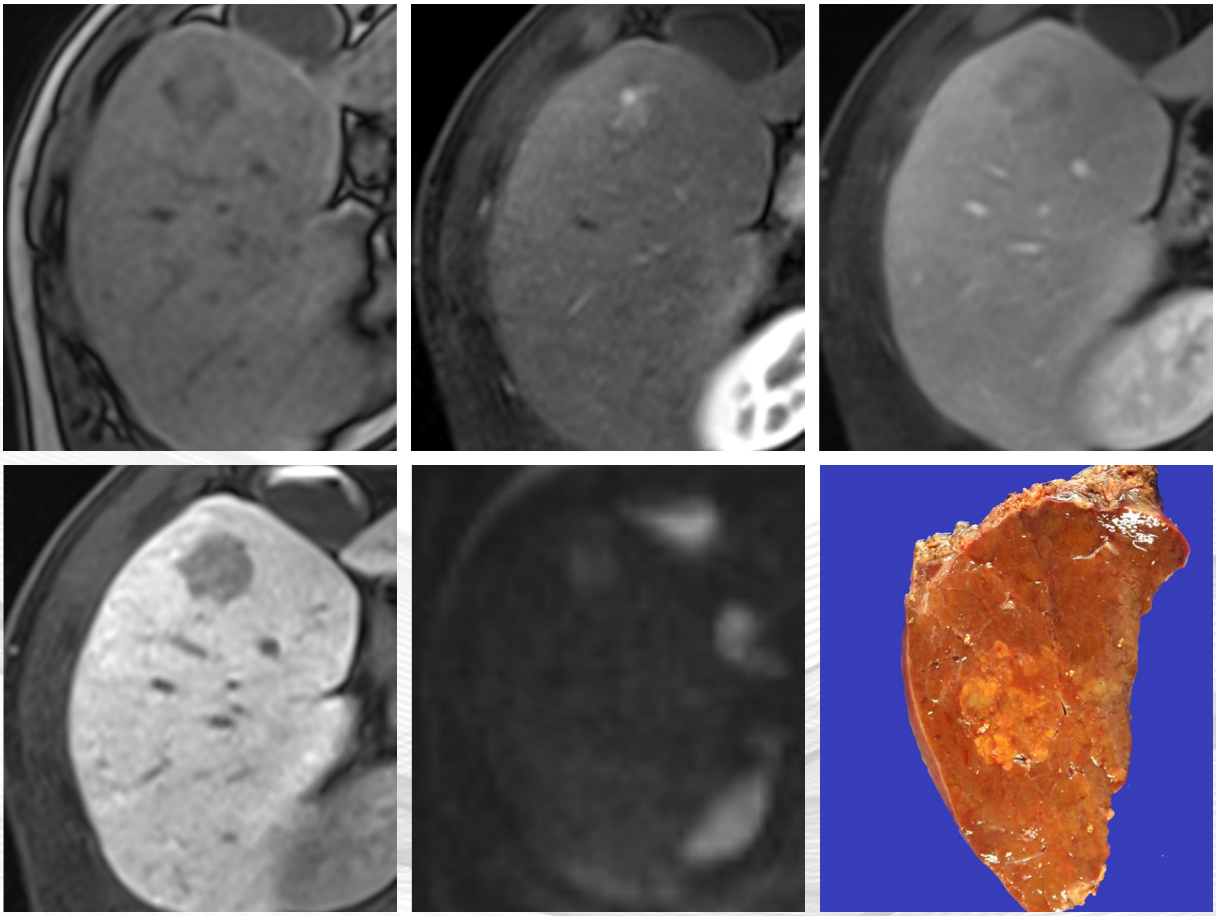

KSAR
대한복부영상의학회
Korean Society of Abdominal Radiology

KJAR
Korean Journal of Abdominal Radiology

Vol. 5 • No. 1 • July 15, 2021
pISSN 2586-1719 / eISSN 2799-3299

Publisher	Dal Mo Yang	Kyung Hee University Hospital at Gangdong
Editor-in-Chief	Jei Hee Lee	Ajou University Hospital

KJAR Editorial Office
103-1103, The Sharp Seocho, 21, Seochojungang-ro 2-gil, Seocho-gu, Seoul 06720, Korea
Tel: +82-2-3474-1983 · Fax: +82-2-3474-1982 · E-mail: office@ksar.kr

Printing Office Sungmungak
#301, 72-15 Soopyo-ro, Jung-gu, Seoul 04543, Korea
Tel: +82-2-2266-9198 · Fax: +82-2-2275-9198 · E-mail: sbgsong@chol.com

KJAR
Korean Journal of Abdominal Radiology

Vol. 5 • No. 1 • July 15, 2021
pISSN 2586-1719 / eISSN 2799-3299

종 설 | Review Article

원 저 | Original Articles

증 례 | Case Reports

www.e-kjar.org
https://doi.org/10.52668/kjar.2021.00017

pISSN 2586-1719 / eISSN 2799-3299

Korean J Abdom Radiol 2021;5:1-16

Review Article

크론병 환자의 소장조영술 판독

박성호[1,3], **박상형**[2,3], **예병덕**[2,3]
[1]울산대학교 의과대학 서울아산병원 영상의학과
[2]울산대학교 의과대학 서울아산병원 소화기내과
[3]서울아산병원 염증성장질환센터

Interpretation of Enterography in Patients with Crohn's Disease

Seong Ho Park[1,3], Sang Hyoung Park[2,3], Byong Duk Ye[2,3]
[1]Department of Radiology and Research Institute of Radiology, Asan Medical Center, University of Ulsan College of Medicine, Seoul, Korea
[2]Department of Gastroenterology, Asan Medical Center, University of Ulsan College of Medicine, Seoul, Korea
[3]Inflammatory Bowel Disease Center, Asan Medical Center, Seoul, Korea

---

Computed tomography enterography and magnetic resonance enterography are presently state-of-the-art radiological tests to examine the small bowel in patients with Crohn's disease. This review provides up-to-date practical knowledge, including high-quality exemplary figures, to make the interpretation of enterography examinations more accurate and clinically relevant for improved care of patients with Crohn's disease, emphasizing the interpretation of magnetic resonance enterography. The interpretative tasks include the diagnosis of the disease (through differential diagnosis from other mimicking conditions); specific assessment of the inflammatory activity, disease extent, and complications; assessment of the overall disease severity; diagnosis of remission; and identification of comorbidities. A good understanding of the clinical context of the patient and efforts to achieve more standardized interpretation is critical for more effective and more precise delivery of information.

Keywords: Crohn disease; Magnetic resonance imaging; Tomography, X-Ray Computed; Radiology; Diagnosis

---

서 론

크론병은 수십 년 전만 하더라도 우리나라에 매우 드문 병이었으나 발병이 지속해서 증가하여 이제는 과거보다 매우 높은 발병률을 보인다 (1). 크론병의 치료 목표도 과거에는 환자의 증상 완화에 초점이 맞추어져 있었다면 현재는 면역조절제 또는 종양괴사인자 (tumor necrosis factor) 억제제를 포함한 다양한 생물학적 제제를 이용하여 염증을 조절하고 점막 치유를 유도 및 유지함으로써 장관 손상의 진행과 장애를 예방하는 것으로 변화되었다 (2, 3). 따라서, 크론병의 초기 상태와 치료 후 질병 상태의 변화를 객관적으로 확인할 수 있는 영상 검사의 이용과 중요

Received: May 9, 2021 **Accepted:** June 19, 2021
Correspondence: Seong Ho Park, MD, PhD
Department of Radiology and Research Institute of Radiology, Asan Medical Center, University of Ulsan College of Medicine,
88 Olympic-ro 43-gil, Songpa-gu, Seoul 05505, Korea
Tel: +82-2-3010-5984 Fax: +82-2-476-4719 E-mail: seongho@amc.seoul.kr

성이 더욱 강조되고 있다. 우리나라의 인구기반 역학 연구에 따르면 크론병 진단 시점을 기준으로 대장에만 병변이 있는 경우는 9.3%에 불과하고 90.7%의 환자에서는 대장과 회장 모두에 (65.8%) 또는 회장에만 (24.9%) 병변이 있었다 (1). 이러한 이유로, 크론병을 검사할 때 당연히 회장을 포함한 소장의 검사가 중요한데, 말단 회장을 제외하고 소장의 대부분은 통상의 내시경으로 검사하기 어렵고 크론병 환자에서는 장 내강이 좁아져 캡슐내시경이 통과하지 못하는 경우가 종종 발생하기 때문에 캡슐내시경을 이용한 소장 검사도 어려운 경우가 많다. 따라서, CT나 MRI를 이용한 소장조영술이 크론병 환자의 검사에 있어 내시경과 함께 중추적인 역할을 담당하고 있다 (4, 5). 또한, CT나 MRI를 이용한 소장조영술은 내시경과는 달리 장의 전층 및 장의 외부도 확인할 수 있다는 장점이 있다.

MR 소장조영술은 CT 소장조영술에 비해 늦게 등장하였고 우리나라의 경우 아직은 CT 소장조영술에 비해 상대적으로 제한적으로 활용되고 있는 것으로 보이나 크론병 환자의 주된 검사법으로 빠르게 자리를 잡아가고 있다. CT 소장조영술의 약점 중 하나는 방사선 조사인데 방사선 조사량이 과거보다 감소하였으나 크론병 환자들은 일반적으로 젊어서 CT 소장조영술 검사를 반복적으로 시행할 경우 방사선 노출로 인한 위해의 가능성을 완전히 배제하기 어렵다. 따라서, 크론병 환자에서 MR 소장조영술의 유용성이 더 주목받으며 크론병의 발병이 높은 서양에서는 우리나라보다 MR 소장조영술이 더 활발히 이용되고 있는 것으로 보인다. 이 논문은, 이러한 현재 상황들을 고려하여 MR 소장조영술을 중심으로 크론병 환자의 소장조영술 판독을 위한 실용적인 핵심 사항들을 대표적 영상 소견들과 함께 설명한다. 모든 설명은 크론병의 진단과 치료에 대한 현재의 최신 지식들을 반영한다. 이 논문은 소장 및 연관 부위의 소견 분석을 중점적으로 다루며, 크론병의 중요한 합병증의 하나인 항문 누공은 내용이 광범위하여 이 논문의 범위를 넘어 생략하였다.

크론병의 진단

크론병의 진단을 위해서는 먼저 크론병의 소장조영술 소견을 잘 알아야 한다. 크론병에 의한 장 염증의 소장조영술 소견은 많은 연구를 통해 이미 잘 알려져 있다 (6, 7). 이 중 대표적 소견들이 Table 1에 정리되어 있으며 Fig. 1은 크론병에 의한 장 염증의 다양한 전형적 MR 소장조영술 소견들을 보여주고 있다. 이러한 소견들을 기억하는 것과 더불어 크론병에 의한 궤양 및 염증 병변들의 다양한 실제 모양과 이들이 소장조영술에서 어떻게 보이게 되는지를 하나하나 비교해 보는 것이 (Fig. 2) 소장조영술 소견을 더욱 정확히 이해하고 판독하는 데 큰 도움이 된다. 크론병의 장 병변은 초기에는 아프타성 병변이 산재하여 있는 형태로 나타나고 병변 중 일부가 점차 크기와 깊이가 증가하여 표재성 궤양을 거쳐 커다란 심부 궤양으로 진행하게 되며 나중에는 염증이 장의 전 층을 침범하게 된다. 이러한 병변들과 병변들 주변 장벽의 염증성 변화가 소장조영술에 장벽의 이상소견으로 보이게 된다. 아프타성 병변은 작아서 일반적으로 소장조영술에 이상소견이 잘 보이지 않거나 보이더라도 경미한 장벽의 비후나 조영증강 증가로 보이게 된다 (Fig. 2). 반면, 최근에는 CT와 MRI의 성능이 좋아져서, 표재성 궤양과 심부 궤양의 경우에는 궤양 자체를 소장조영술에서 명확하게 볼 수 있는 경우도 많다 (Fig. 2). 궤양이 크고 깊다고 해서 소장조영술에 반드시 잘 보이는 것은 아니며 단면 영상 평편에 대한 궤양의 방향, 장의 팽창 정도, 그리고 주변 장벽의 상태에 따라 큰 궤양이 잘 보이지 않는 경우도 있고 반면 작은 궤양이 잘 보이는 경우도 있다 (8).

이러한 염증 병변들이 장간막 쪽을 따라 위치하는 것이 크론병에 특이적인 소견으로 알려져 있다 (Fig. 3) (6, 7). 특히, 장간막 쪽에 장의 종축 방향을 따라 선형으로 배열된 종주 궤양이 크론병의 특징적 소견으로 알려져 있다 (Fig.

Table 1. Major findings of bowel inflammation in Crohn’s disease on MR enterography and CT enterography

Findings	Comment
Mural thickening (greater than 3 mm in distended bowel)	
Mural hyperenhancement	
Intramural edema*	More accurately assessed with MR (i.e., high signal on T2*)
Ulceration	
Restricted intramural diffusion	Only available with MR
Perienteric edema/inflammation	More accurately assessed with MR (i.e., high signal on T2)
Engorged vasa recta	

*T2-weighted half-Fourier sequence such as HASTE with fat suppression should be used. Caution is needed to avoid misinterpretation if steady-state free precession (SSFP) sequence is used because the bowel wall signal appears brighter on SSFP sequence than half-Fourier sequence.

2). 하지만, 병변들이 항상 이런 분포를 보이는 것은 아니며 염증이 심하면 궤양을 동반한 광범위한 염증이 장 내강 전체에 걸쳐 분포하게 된다 (Figs. 1 and 2). 장간막 쪽을 따라 장의 종축 방향으로 배열된 염증 병변에 의하여 반흔이 형성되면 장의 장간막 면의 수축으로 인해 가성주머니모양 (pseudo-sacculation)의 장 형태를 만들게 되며 이 소견도 크론병에 특이적인 소견이다 (Fig. 3B). 크론병은 특징적으로 염증 부위들이 염증이 없는 부위를 사이에 두고 비연속적으로 나타나는 건너뛰기 병변 (skipped lesion)의 소견을 보인다. 심한 염증이 있으면 크고 깊은 궤양들 사이에 남아있는 점막이 심한 부종성 변화로 인해 마치 조약돌을 깔아 놓은 듯한 양상 (cobblestone appearance)으로 보일 수 있다. 염증 병변들이 장간막 쪽을 따라 위치하는 소견이나 뒤에서 설명할 특징적인 누공을 동반하는 소견은 크론병에 특이적인 소견이지만, 크론병에서 보이는 다른 전형적 소견들은 다른 여러 염증성 장 질환들과 중복이 된다. 특히 장결핵은 크론병과 매우 유사한 영상 소견을 보일 수 있어 감별이 어렵다 (Fig. 4). 크론병과 장결핵을 구별하는데 도움을 줄 수 있는 영상소견의 차이점을 Table 2에 요약해 놓았다 (9, 10). 하지만, 이러한 구별 점이 없는 경우가 많다는 점에 항상 유의하여야 한다.

크론병의 중증도 평가

소장조영술의 판독은 크론병의 진단뿐 아니라 크론병의 중증도 (severity)를 포함하여 궁극적으로 치료 계획을 세우는데 필요한 모든 정보를 포함하여야 한다. 크론병의 중증도 평가와 관련된 소장조영술의 판독이 여러 판독자들 또는 기관 간에 일관되게 이루어지지 않는 경우가 있다. 이는 직접적으로는 크론병 중증도의 평가를 위한 영상의학적 기준이 아직 없기 때문이고 좀 더 크게 보면 Montreal 분류와 같이 (11) 크론병의 평가 및 치료를 위한 크론병 상태에 대한 분류 체계가 만들어져 이용되고 있기는 하나 이러

Table 2. Enterography findings that help the differential diagnosis of Crohn's disease and intestinal tuberculosis

Findings suggesting Crohn's disease	Findings suggesting tuberculosis
Longitudinal ulcer preferentially involving mesenteric border	Transverse ulcer
Antimesenteric pseudo-sacculation	Patulous ileocecal valve
Bowel fistula or perianal fistula	Necrotic lymphadenopathy
Cobblestone appearance	Findings of tuberculosis peritonitis (ascites or infiltration)
Fibrofatty proliferation	Pulmonary tuberculosis

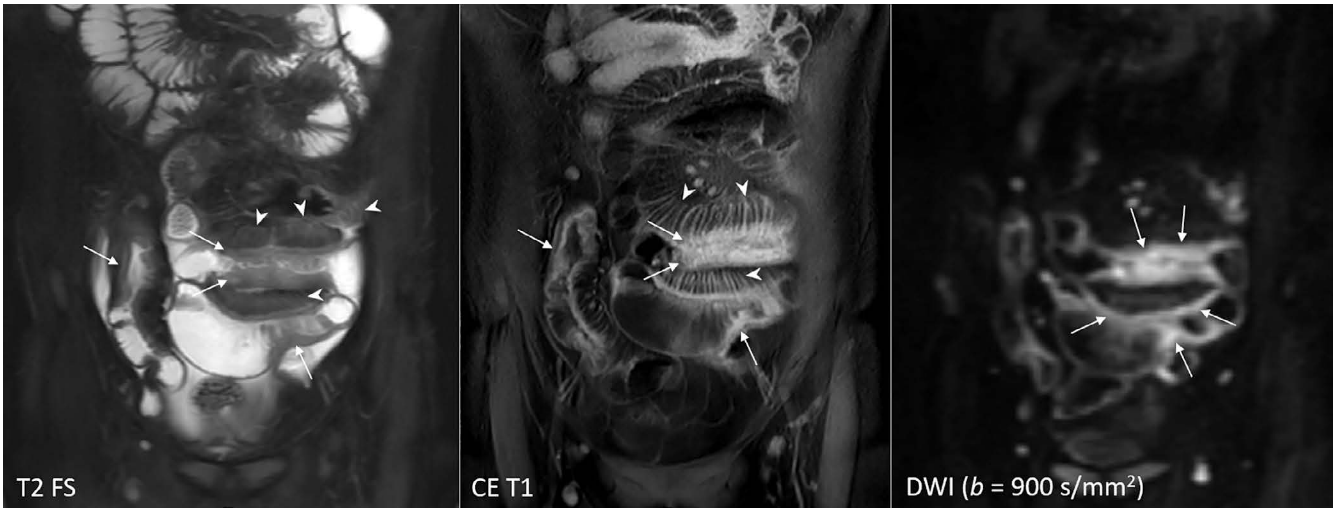

Fig. 1. Characteristic MR enterography findings of bowel inflammation in Crohn's disease.
Increased signal on T2 FS (i.e., edema), thickening, hyperenhancement, and restricted diffusion are noted in the wall of multiple ileal segments (arrows). The mural abnormalities are circumferential in some locations and involve the bowel's mesenteric side preferentially in some other locations. The mesentery adjacent to the mural abnormalities shows an increased signal on T2 FS, indicating perienteric edema (arrowheads in the left). Engorged vasa recta (arrowheads in the middle) are noted. Ulcer craters are not apparently demonstrated on these images. CE T1 = contrast-enhanced T1-weighted sequence; DWI = diffusion-weighted imaging; T2 FS = T2-weighted half-Fourier sequence with fat suppression

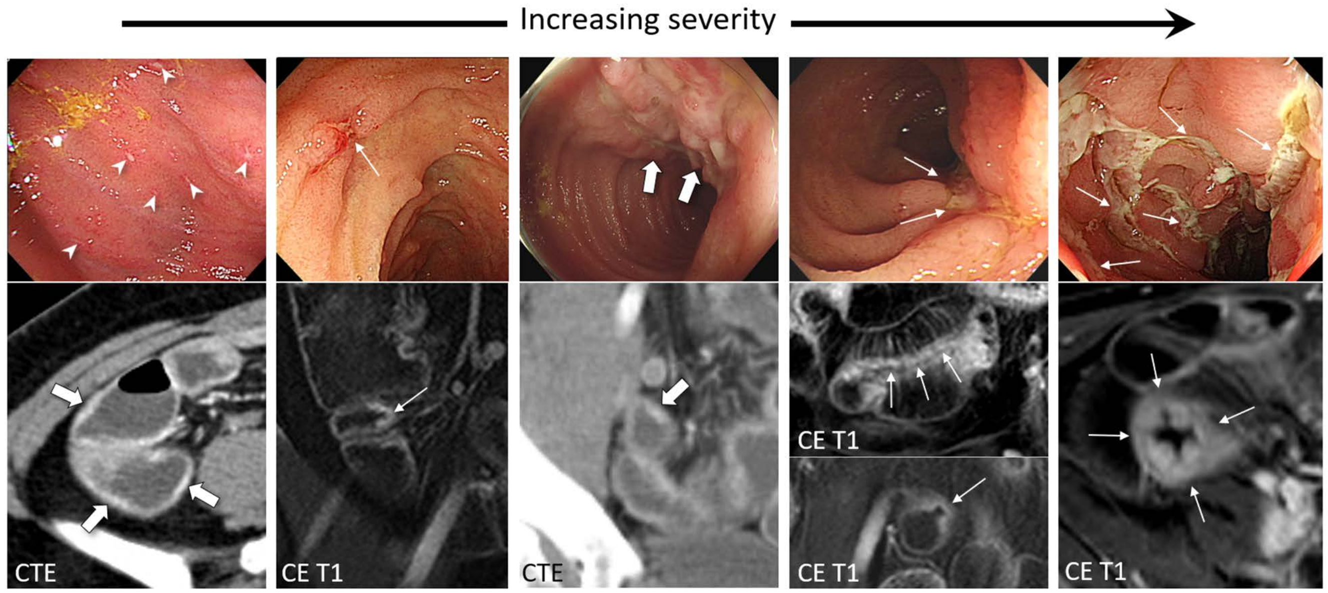

Fig. 2. Endoscopy-enterography correlation of ileal inflammation in Crohn's disease.
Various severities of inflammatory and ulcerative lesions with left-to-right increasing severities ranging from multiple tiny scattered aphthoid lesions (the leftmost) to multiple large deep longitudinal ulcers (the rightmost) are shown (arrows and arrowheads). Ulcer craters are directly seen on enterography for some of the lesions, including a small superficial ulcer (arrows in the second from the left), a deep longitudinal ulcer in the mesenteric border (arrows in the second from the right), and multiple deep longitudinal ulcers (arrows in the rightmost). The figure is in part from Park et al. (8) with permission. CE T1 = contrast-enhanced T1-weighted sequence; CTE = CT enterography

한 과거의 분류 체계는 최근의 내시경 및 영상기술의 발전을 반영하지는 못하며 질환에 대한 종합적인 중증도 평가에 적합하지 않아 질환의 중증도 평가 방법이 아직 명확하게 정립되어 있지 않기 때문이다. 크론병의 중증도는 장 염증의 중증도를 말하는 염증의 활동도 (activity)뿐 아니라 장 염증의 범위, 크론병으로 인한 장 손상 (damage)의 정도, 합병증의 유무 등 여러 측면에서 생각해 볼 수 있다. 장 염증의 활동도가 높다고 또는 낮다고 해서 크론병 질환의 전체적 중증도가 각각 반드시 심하다 또는 경하다고 말할 수 없다. 더구나, 장 염증의 활동도 하나만 생각하더라도, 소장조영술에 적용할 수 있는 여러 정량적 점수체계가 연구되어 있지만, 연구 외에 실제 진료에는 잘 활용되지 않고 있으며 (이에 대해서는 논문의 뒷부분에서 좀 더 자세히 설명한다) 장 염증의 활동도를 좀 더 간단하게 경증, 중등도 (moderate), 중증으로 대략 나누어 기술하려는 시도도 있지만, 아직 한 가지 방법으로 정의가 되어 있지는 않다 (6, 12-16). 따라서, 크론병의 소장조영술을 판독할 때 크론병의 중증도에 관한 기술에 있어 어느 정도의 혼선은 불가피한 것으로 보이며, 그래도 진단정보를 명확하게 전달하기 위해서는 "크론병이 심하다 또는 경하다"라고 막연하게 이야기하는 것보다는 크론병의 중증도를 구성하는 여러 요소를 나누어 가능한 구체적으로 기술하는 것이 좋겠다.

크론병의 중등도 분류에 대한 절대적인 표준은 없으나 현재로서는 최근에 나온 International Organization For the Study of Inflammatory Bowel Disease (IOIBD)의 전문가 합의가 좋은 참고가 될 수 있을 것 같다 (17). 이 전문가 합의는 장 염증의 활동도나 범위뿐 아니라 크론병 환자의 상태에 대한 포괄적 평가를 통해 결과적으로 향후 수술, 입원 치료, 또는 장애를 초래할 위험이 큰 고위험 환자와 저위험 환자를 구분하고 고위험 환자들에게 더욱 적극적인 치료를 적용하고 있다 (17). 고위험 환자의 기준 중 일부는 소장조영술의 소견과도 직접 관련된 것들이어서 (Table 3) 소장조영술을 판독할 때 이러한 정보들을 명확하게 포함한다면 환자 진료에 좀 더 도움을 줄 수 있을 것이다 (17).

약물치료 경과 판단

과거에는 크론병의 치료 목표가 환자의 증상 완화에 초점이 맞추어져 있었으나 현재는 면역조절제 또는 다양한 생물학적 제제를 (Table 4) 이용하여 염증을 조절하고 점막 치유를 유도 및 유지함으로써 장관 손상의 진행과 장애를 예방하는 것으로 변화되었다 (2, 3, 18). 따라서, 치료 경과 관찰에 있어 질환의 변화를 객관적으로 보여줄 수 있는 소장조영술의 중요성이 강조되고 있다. 치료 경과 관찰을

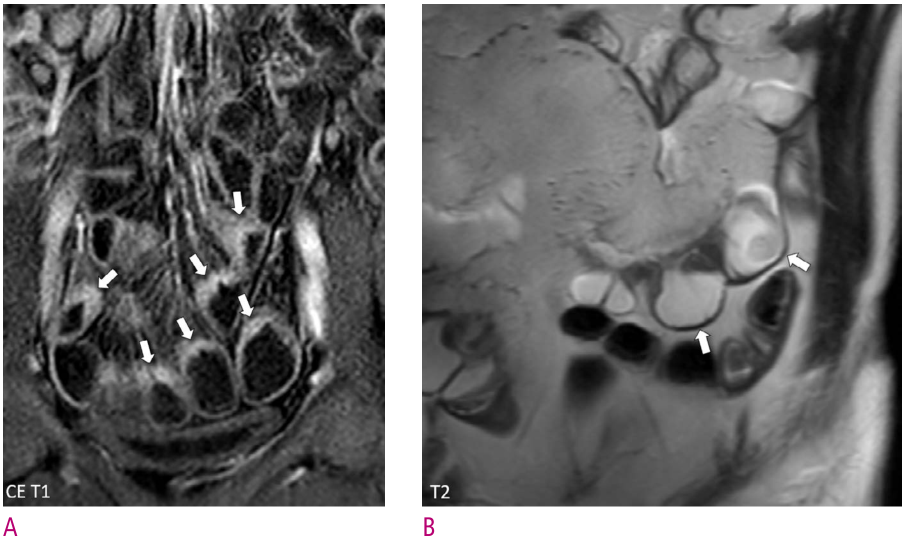

Fig. 3. Preferential involvement of the mesenteric border in Crohn's disease.
A. Mural thickening and hyper-enhancement due to inflammation are noted in the mesenteric side of multiple distal ileal segments (arrows), whereas other parts of the bowel wall appear normal. B. Shortening of the mesenteric border alone caused by scarring associated with Crohn's disease has created a pseudo-sacculation appearance in an ileal segment (arrows). CE T1 = contrast-enhanced T1-weighted sequence; T2 = T2-weighted half-Fourier sequence

Table 3. High-risk findings of Crohn's disease related to enterography interpretation according to International Organization For the Study of Inflammatory Bowel Disease

Findings
Large or deep mucosal lesions
Fistula and/or perianal abscess
Prior intestinal resections, particularly of segments >40 cm
Presence of strictures
Extensive disease (ileal involvement >40 cm or pancolitis)
Presence of stoma

Table 4. Disease-modifying medications for Crohn's disease

Category	Medication
Immune modulator	Azathioprine
	6-Mercaptopurine
	Methotrexate
Anti-TNF agent	Infliximab
	Adalimumab
	Certolizumab
Anti-integrin agent	Vedolizumab
Anti-IL-12/23 agent	Ustekinumab

TNF=tumor necrosis factor

위해서 소장조영술을 얼마나 자주 어느 시점에 시행하여야 하는지에 대해서는 아직 잘 정립되어 있지 않으며 향후 좀 더 체계적으로 정리가 되어야 할 부분이다. 내시경 검사의 시점과 빈도를 참고해 보면 (2, 3), 처음 치료를 시작하거나 치료제를 변경하고 나서 약 6-9개월 정도에 소장조영술을 이용한 평가를 고려할 수 있을 것이다. 또한, 질환의 관해가 이루어지거나 안정화가 이루어진 상황에서는 환자의 상태에 따라 1-3년에 1회 정도의 소장조영술 추적 검사를 통해 증세나 다른 검사에는 반영되지 않는 질환의 변화 여부가 있는지 확인할 수 있을 것이다. 치료 경과 관찰을 위한 목적의 소장조영술 검사의 판독에 있어 주요 평가사항은 장 염증 활동도의 변화 정도, 질환의 관해 여부, 합병증의 발생 여부 정도가 된다. 이 중 합병증에 대한 내용은 논문의 뒷부분에서 별도로 설명한다.

장 염증 활동도의 변화 평가

치료에 따른 장 염증 활동도의 감소 및 증가는 앞에서 설명한 크론병에 의한 장의 염증 소견들의 (Table 1) 변화 양상을 가지고 판단할 수 있다. 염증의 활동도와 염증의 범위가 모두 변화할 수도 있으며 염증의 범위는 큰 차이가 없이 염증 활동도만 변화할 수도 있다. 염증이 감소하면 장벽의 두께가 감소하고, T2 강조영상에서 장벽과 장 주변의 부종으로 인한 고신호강도가 감소하며, 확산강조 영상에서 확산 제한 소견도 감소한다 (Fig. 5). 영상에서 궤양을 직접 볼 수 있는 경우라면 궤양의 크기가 감소하는 것을 직접 확인할 수 있는 경우도 있다. 장벽의 조영증강 증가 소견도 염증이 감소함에 따라 일반적으로 감소하는 경향이 있으나, 장벽의 조영증강 증가는 활동성 염증 외에도 섬유화를 포함한 다양한 이유로 나타날 수 있고 조영증강의 정도는 조영제의 주입과 관련된 여러 요인, 조영제 주입 후 영상획득 시점, 환자의 혈 역학적 상태 등에 따라서도 변동될 수 있기 때문에 해석에 있어 좀 더 주의가 필요하다 (6). 앞에서 이야기한 다른 소견들도 조영증강 정도 보다 상대적으로 덜하기는 하나 해석에 함정이 있어 주의가 필요하다. 가

Fig. 4. Crohn's disease and tuberculosis in the terminal ileum showing similar enterography morphology.
Mural thickening and mild hyperenhancement in the terminal ileum (arrows) look similar between Crohn's disease (left) and tuberculosis (middle and right). In the case in the middle, a lymph node with central low attenuation indicating necrotic lymphadenopathy (arrowhead in the inset) is noted in the adjacent mesentery, which helps to suggest tuberculosis. In the case in the right, peritoneal infiltration is noted (arrowheads) in the left upper quadrant, indicating tuberculous peritonitis.

령, 치료로 인한 장벽 내 반흔과 섬유화로 인해서도 장벽의 두께 증가 소견이 보일 수 있으며 장이 경구 조영제로 채워져 잘 팽창되어 있지 않은 경우 확산강조 영상에서 위양성 확산 제한 소견이 보일 수 있다. 따라서, 어느 한 가지 소견에만 의존하지 않고 여러 가지 소견의 변화를 모두 같이 고려하여 종합적으로 판단하는 것이 중요하다 (5). MR 소장조영술은 CT 소장조영술과 비교하여 평가에 사용할 수 있는 보다 다양한 소견들을 제공하므로 장 염증 활동도의 변화를 평가하는 데 좀 더 유리하다. 이러한 소견들 외에도 장의 염증이 감소할 경우 장 주변 림프절의 크기가 감소하는 것 같은 부수적인 소견들도 평가에 부분적으로 도움을 줄 수 있다.

장 염증 활동도의 감소 및 증가를 판단하는 것은 비교적 그다지 어렵지 않으나, 만일 장 염증의 활동도 변화를 좀 더 세밀하게 정량적으로 평가를 해야 한다면 평가가 복잡해진다. 이러한 평가를 위한 목적으로 소장조영술로 장 염증의 활동도를 정량적으로 측정하기 위한 다양한 점수체계가 제시되었다. MR index of activity (MARIA), Crohn's disease MRI index (CDMI), Nancy score, Simplified MARIA 등이 상대적으로 좀 더 많이 알려진 점수체계들이다 (12-16). 이러한 점수체계는 잠재적인 장점과 유용성을 가지고 있다. 특히, 크론병의 장 염증 활동도를 서로 다른 환자들 사이에서 일관되게 평가, 구분, 비교하는 데 도움을 줄 수 있을 것이다. 가령 혈액검사 결과처럼 장 염증 활동도의 정도를 숫자로 제시하고 점수의 범위에 따라 경증, 중등도, 중증을 나누는 방법을 적용해 볼 수 있을 것이다. 하지만 실제로는 여러 제약으로 인해 이러한 점수체계들은 거의 연구에서만 사용되며 임상 진료에는 잘 이용되지 않고 있다 (4, 5). 먼저, 이들 점수는 측정을 시행하는 해당 부위에 부여되는 값으로 장의 어느 부위에서 점수를 매기는지에 따라 값이 변할 수 있다. 커다란 고형장기나 종괴와는 달리 크기가 작은 장벽에서 측정을 하는 것은 쉽지 않으며 오류가 발생할 수 있다. 일부 정량적인 측정치는 영상획득의 세부 조건들에 따라 값이 달라질 수 있다. 또한, 이러한 정량적 평가는 영상의학의 일반적 판독 업무 환경 및 상황과는 약간 차이가 있어 판독 업무 흐름에 방해를 주지 않는 방식으로 도입을 하려면 별도의 고려가 필요하다. 이러한 이유로 정량적 평가에 영향을 줄 수 있는 여러 요인이 잘 관리될 수 있는 연구 환경이 아닌 일반 진료 환경에서는 이 점수체계들을 연구 환경처럼 정확하고 일관되게 널리 사용하기는 어렵다. 또한, 여러 서로 다른 점수체계가 있다는 것은 어떤 점수체계도 만족스럽지 않다는 것을 보여주는 것으로 생각할 수도 있다. 이러한 제한점들을 극복하고자 과거 점수체계인 MARIA를 좀 더 쉽게 개선한 Simplified MARIA를 만드는 노력도 있었는데, 향후 정량적 점수체계가 임상 진료에 도입될 수 있을지는 좀 더 두고 보아야 한

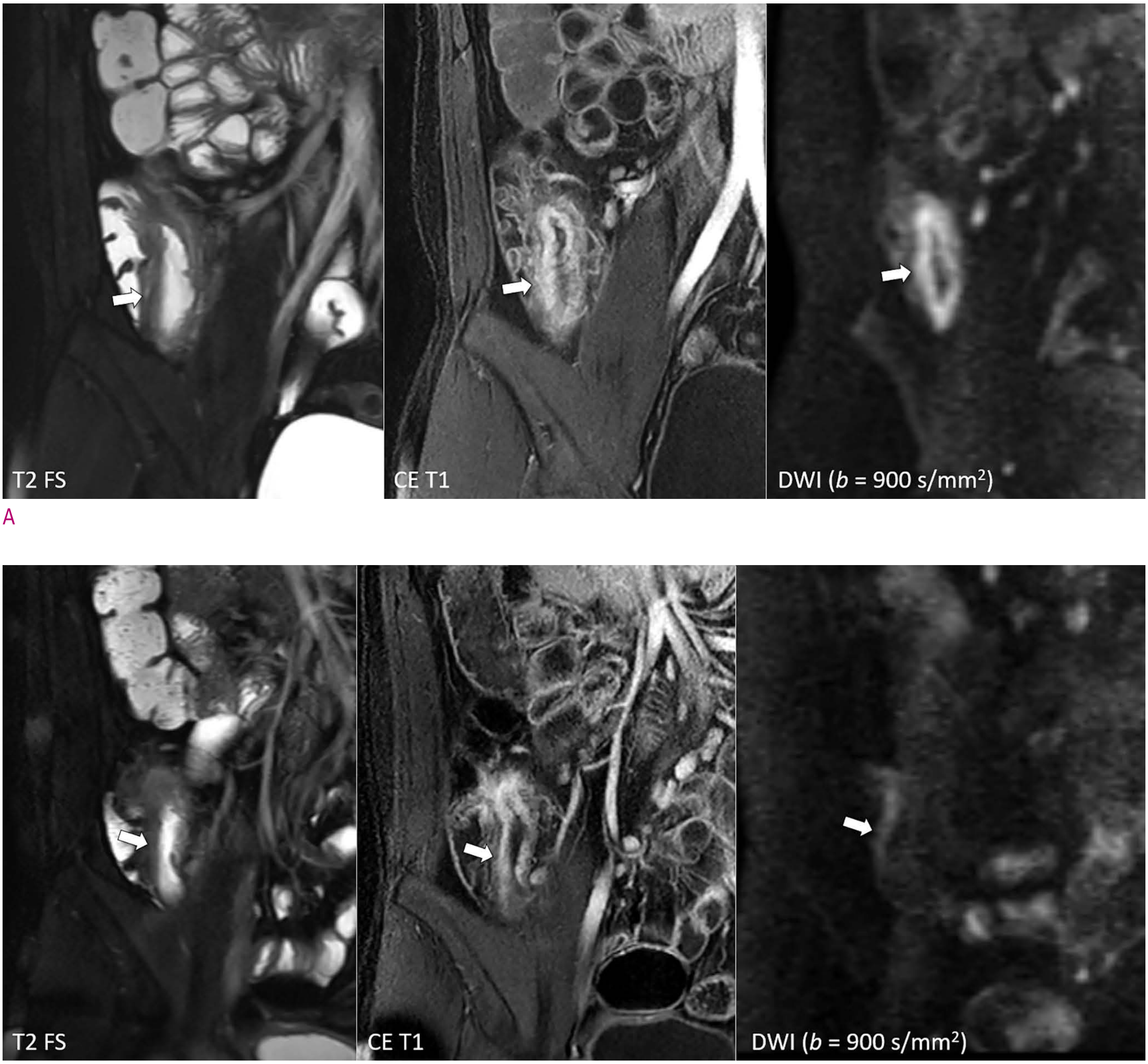

Fig. 5. Decreased inflammation of Crohn's disease in the terminal ileum after treatment with azathioprine.
A. MR enterography before therapy shows remarkable thickening, high signal on T2-weighted sequence, hyperenhancement, and diffusion restriction in the wall of the terminal ileum (arrows) and high signal in the perienteric fat on T2-weighted sequence. B. MR enterography obtained after 15 months of treatment with azathioprine shows decreased thickness, signal on T2-weighted sequence, and diffusion restriction in the terminal ileal wall (arrows). Hyperenhancement of the terminal ileal wall is still similarly noted. CE T1 = contrast-enhanced T1-weighted sequence; DWI = diffusion-weighted imaging; T2 FS = T2-weighted half-Fourier sequence with fat suppression

다 (12, 16).

관해의 평가

소장조영술에서 어떠한 소견을 크론병의 관해로 보아야 할지는 아직 분명히 정립되지 않았다. 이는 부분적으로는 크론병의 관해에 대한 정의가 현재 하나로 정해져 있지 않기 때문이다. 현재 관해를 판단하는 일반적인 기준은 내시경적 관해에 해당하는 점막 치유이다. 내시경적 관해가 된

예들의 소장조영술 소견에 대해서는 보고된 연구들이 있다. 내시경적 관해를 보이는 환자들의 대다수는 염증으로 인한 장벽의 비후, 비정상 신호강도, 그리고 조영증강 증가 소견이 모두 소실되어 장벽이 사실상 거의 정상으로 보이게 된다 (Figs. 6 and 7). 다만 장벽의 이상 소견들이 모두 소실되더라도 염증 후 남아있는 약간의 반흔으로 인해 장의 윤곽은 약간 변형될 수 있다 (Fig. 7). 반면, 내시경적 관해가 된 환자 중 많게는 약 30-40% 정도의 환자에서 점막 치유에도 불구하고 장벽의 이상 소견이 MR 소장조영술이나 CT 소장조영술에 어느 정도 계속 남아 있는 것으로 알려져 있다 (19-21). 이처럼 장벽의 이상소견이 남아 있다 하더라도 치료 전보다는 감소한 상태로 대부분의 경우에는 경미한 장벽의 비후, 비정상 신호강도, 또는 조영증강 증가로 보이는데 (Fig. 8) 드물게 심한 이상 소견이 남아 있는 경우도 있다.

내시경적으로 관해가 된 장을 수술로 절제해서 분석해 보거나 할 수는 없기 때문에, 내시경적 관해에도 불구하고 소장조영술에 남아 있는 장벽의 이상소견이 병리학적으로는 어떤 상태인지 정확히 알기는 어렵다. 한 연구는 간접적인 자료 분석을 통해 이처럼 남아 있는 장벽의 이상 소견이

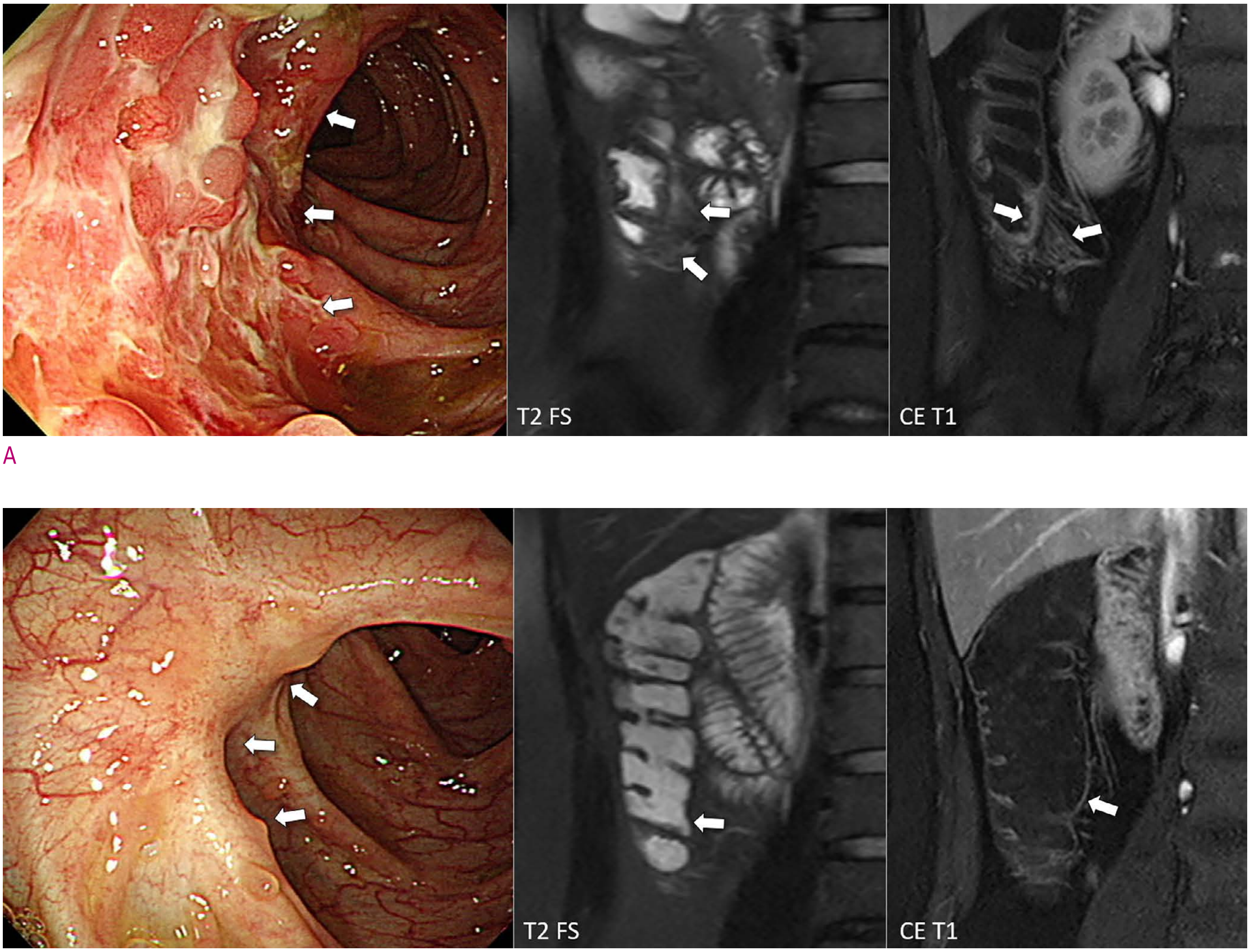

Fig. 6. MR enterography findings of endoscopic mucosal healing of Crohn's disease in the ascending colon after treatment with 6-mercaptopurine.

A. MR enterography before therapy shows inflammatory changes in the medial wall of the ascending colon and adjacent pericolic area due to inflammation (arrows), as shown on the colonoscopic image (left). B. All the inflammatory findings have resolved at MR enterography (arrows) with the achievement of endoscopic remission after a 1-year treatment with 6-mercaptopurine. The figure is from Park et al. (5) with permission. CE T1 = contrast-enhanced T1-weighted sequence; T2 FS = T2-weighted half-Fourier sequence with fat suppression

치유된 점막 아래에 숨어 있는 염증이라기보다는 크론병으로 인한 장 손상의 소견일 것이라 제시하였다 (19). 내시경적 관해와 더불어 소장조영술에서도 장벽의 이상소견이 모두 소실된 경우를 내시경적 관해인 점막 치유와 구분하여 전 층 (transmural) 치유 또는 관해라 하는데, 한 연구에 따르면, 내시경적 점막 치유는 되었으나 MR 소장조영술에서 장벽에 이상이 남아 있는 환자들이 전 층 치유가 된 환자들에 비해서 향후 추적 관찰에서 크론병으로 인한 수술, 입원, 그리고 약물치료를 강화하게 되는 위험이 더 높아 나쁜 경과를 보였다 (22).

수술 후 재발 평가

크론병 환자의 수술 후 경과 관찰에 있어 별도의 고려가 필요한 부분은 수술 후 병변의 재발을 발견하기 위한 조기 검사와 관련된 것이다. 크론병으로 장 절제 수술을 받은 환자에서 수술 후 크론병의 재발이 흔하게 일어나는 것으로 알려져 있으며, 많은 환자에서 수술 후 조기에 재발이 나타난다. 한 메타분석에 따르면, 무작위 임상시험의 결과를 종합하여 보았을 때 54%의 환자에서 수술 후 1년 이내에 내시경에서 재발이 확인되었으며 이 중 약 절반의 환자가 임상적으로 재발을 의심할 만한 증상이나 다른 소견이 없었다 (23). 따라서, 크론병으로 장 절제 수술을 받은 환자들에 대해서 재발이 의심되는 증상이 보일 때까지 기다리지 말고 수술 후 6개월 정도에 대장내시경으로 먼저 적극적으로 검사를 할 것이 권고된다 (24, 25). 이른 시기에 무증상 환자에서 적극적으로 검사를 시행하여 재발을 일찍 발견하고 적절히 치료를 시행하면 환자의 예후를 향상시킬 수 있다 (26). 크론병으로 장 절제 수술을 받은 경우 재발은 문합 부위 주변에 잘 발생한다. 크론병으로 인한 장 절제 수술의 대표적인 형태는 회맹판을 포함하여 소장과 대장의 일부를 절제하고 소장과 대장간 문합을 만드는 수술인데 이때 문합부의 소장 쪽으로 크론병이 재발하는 특징이 있다.

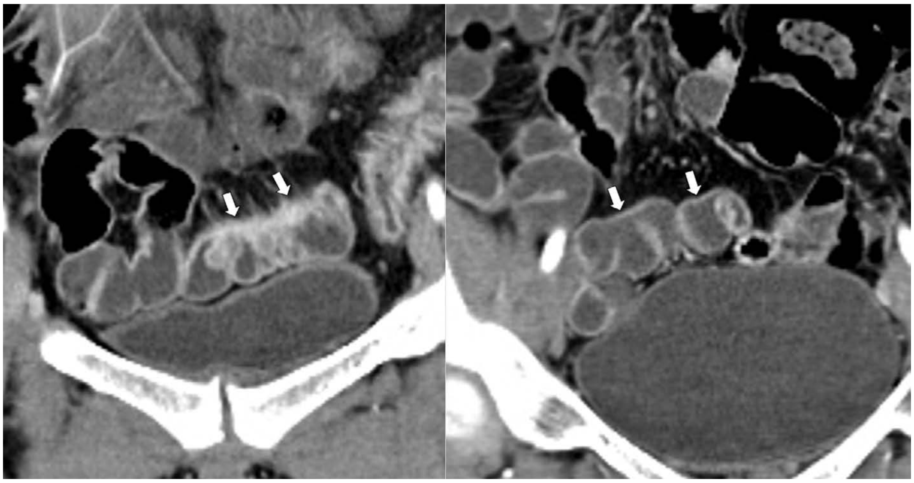

Fig. 7. CT enterography findings of endoscopic mucosal healing of Crohn's disease in the distal ileum after treatment with infliximab and azathioprine. Inflammatory changes are noted in the mesenteric side of the pelvic ileum before treatment (arrows in the left). The inflammatory findings have completely resolved after a 2-year treatment with infliximab and azathioprine, leaving shortening and flattening of the bowel contour (arrows in the right) due to scarring.

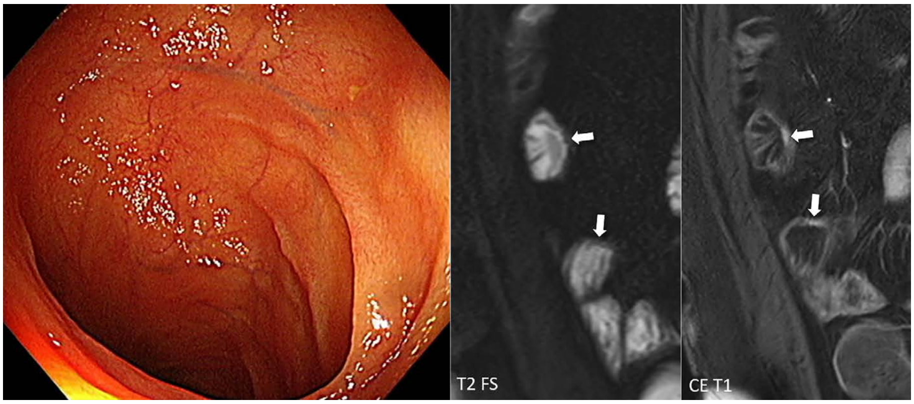

Fig. 8. Subtle residual mural abnormalities at MR enterography despite endoscopic mucosal healing of Crohn's disease. Endoscopy of the neo-terminal ileum (left; status post ileocecal resection) shows no demonstrable inflammation, whereas MR enterography shows slight mural thickening and hyperenhancement (arrows in the right). The mural signal on the T2-weighted sequence is only slightly increased (arrows in the middle). CE T1 = contrast-enhanced T1-weighted sequence; T2 FS = T2-weighted half-Fourier sequence with fat suppression

수술 후 이른 시기에 증상과 무관하게 소장조영술 검사를 시행하는 것에 대한 연구 결과는 많지 않다. 크론병으로 장 절제술을 받은 환자의 검사를 위해 소장조영술을 이용한 대부분의 연구는 재발이 의심되는 증세를 보이는 환자를 대상으로 하거나 수술 후 좀 더 늦은 시기에 소장조영술을 이용한 연구들이다. CT 소장조영술을 수술 후 1년 이내에 증상과 무관한 검사로서 이용하는 것을 분석한 한 연구에 따르면 소장-대장 문합부 근처의 크론병 재발 진단에 있어 CT 소장조영술의 예민도와 특이도는 각각 92%와 83%이었다 (27). 소장조영술을 수술 후 이른 시기에 시행하는 경우 판독에 있어 눈여겨보아야 할 점은, 앞서 이야기한 것처럼 재발이 소장-대장 문합부의 소장 쪽에 발생한다는 점과 (Fig. 9) 재발 초기의 병변은 경미한 이상소견 만을 보일 수 있다는 점 정도로 생각된다 (Fig. 9A).

질환의 악화가 의심되는 경우

장 염증의 증가, 합병증의 발생, 다른 질환의 발생 등 다양한 가능성에 대해서 영상소견을 잘 확인하여야 한다. 크론병 자체의 변화에 대한 평가는 앞의 설명을 보기 바라며 합병증의 평가에 대해서는 뒤에서 설명한다. 크론병에 대한 평가와 더불어 복부 및 골반의 다른 여러 질환 유무에 대한 평가가 같이 이루어져야 한다. 단지 영상만 보고 판독하는 것보다는 환자의 증세를 확인하고 증세를 설명할 만한 영상 소견이 있는지 확인을 해 보는 것이 좋다.

합병증의 평가

크론병의 대표적인 합병증은 장 협착과 누공이다. 크론병 장 염증의 활동도와 합병증은 분리하여 생각하고 기술하여야 한다. 합병증은 장 염증의 활동도 보다는 장손상의 소견이다. 심한 장 염증이 지속되면 장손상과 이로 인한 합병증의 발생 위험이 증가한다. 하지만 합병증이 있다고 해서 현재 장 염증이 반드시 심하게 있는 것은 아니며 합병증이 새롭게 발생하였다고 해서 반드시 장 염증의 활동도가 증가한 것은 아니다. 가령, 장 염증이 치료되는 과정에서 반흔이 증가하면서 장 협착이 발생할 수도 있다. 또한, 장-장 누공이 형성된 경우에도 염증의 활동도는 그다지 높지 않고 누공만 유지될 수도 있다.

장 협착

크론병에서 장 협착은 염증에 의한 점막 부종 또는 만성적 염증으로 인한 장벽 내 섬유화에 의해 발생할 수 있다. 소장조영술을 판독할 때 장 협착에 대한 해석을 보다 일관되게 할 수 있도록 최근 전문가 협의를 거쳐 장 협착의 영상의학적 기준이 제시되었는데, 소장조영술에서 소장의 협착은 내강이 좁아진 소장 분절의 상방으로 소장의 너비가 3 cm 이상으로 늘어나 있을 때로 정의된다 (6). 이는 특이도가 높은 기준으로 위양성의 가능성은 매우 낮으나 상대적으로 예민도는 높지 않아 실제 증상을 유발하는 소장 협착이 이 기준을 만족하지 않을 수도 있다. 따라서, 상방 소장의 너비가 3 cm를 넘지는 않지만, 소장 내강이 좁아진 부위가 하나의 정지 영상이 아닌 영화 영상 (cine), 여러 영상 시퀀스, 또는 추적 검사 결과에서 변함없이 보일 경우 장 협착 의심 (probable stricture) 이라고 별도로 이야기한다 (6). 대장의 경우 상부 대장의 확장 및 수분, 공기 및 대변의 저류 소견으로 판단할 수 있으나 소장의 협착과는 달리 대장의 협착에 대한 영상의학적 기준이 하나로 마련되어 있지는 않다.

크론병 환자에서 다양한 급성 감염성 장염과 같은 비특이적 염증이 동반되거나 유착과 같은 다른 원인으로도 크론병으로 인한 장 협착과 비슷한 증세를 유발할 수 있다. 따라서, 장 협착이 의심되는 크론병 환자의 영상 검사를 판독할 때 먼저 이러한 다른 원인이 있는지 확인을 하여야 한다 (Fig. 10) (28). 장 협착이 의심되는 크론병 환자들의 경우 급성 복통으로 인해 응급실을 방문하여 CT로 검사를 하는 경우가 많은데, 일반적으로 장벽의 조영증강이 두드러지게 보이는 크론병의 염증과는 달리, 비특이적 급성 장염의 경우에는 장벽의 부종으로 인해 CT에서 두꺼워진 장벽이 전체적으로 균일하게 저음영을 보이는 차이가 있다 (Fig. 11). 크론병으로 인한 장 협착이 확인되면 약물에 의한 치료가 가능한 주로 염증으로 인한 협착인지 수술이나 내시경 풍선확장술과 같은 비약물적 치료가 필요한 섬유화로 인한 협착인지 구별을 하여야 한다 (Fig. 10). 협착 부위에 T2 강조영상에서 높은 신호강도가 보이면 염증을 시사하는 소견이고 혈관 내로 조영제 주입 후 지연기 영상에서 두드러진 조영증강이 있으면 섬유화를 시사하는 것으로 일반적으로 알려져 있으나 이러한 구분이 항상 잘 맞는 것은 아니며 실제로는 대부분의 환자에서 염증과 섬유화가 다양하게 섞이어 있기 때문에 구별이 어려운 경우가 많다 (29-33). 탄성 영상 및 자화전이 영상을 이용하여 크론병으로 인한 장 벽 내 섬유화를 평가해 보려는 연구들도 보고되어 있기는 하지만 아직은 실험단계이다 (34-39). 따라서, 현재로서는 크론병으로 인한 협착 부위의 섬유화 정도를 잘 평가할 수 있는 적절한 영상 방법이 없는 상태이다. 이러한 영상진단의 제한점 들과 크론병의 치료에 있어 장 수술을 가급적 최소화 하려는 원칙을 고려할 때, 크론병으로 인한 장 협착을 염증형 협착과 섬유형 협착으로 배타적으로 구분하려 하는 것보다는, 염증이 동반된 협착과 염증이 동반되지 않은 협착으로 구분하는 것이 더 효과적이다 (Figs. 10 and 12) (28). 염증이 동반된 협착에 대해서는 먼저 약물치료를 시도해 보고 효과가 없으면 비약물적 치료로 진

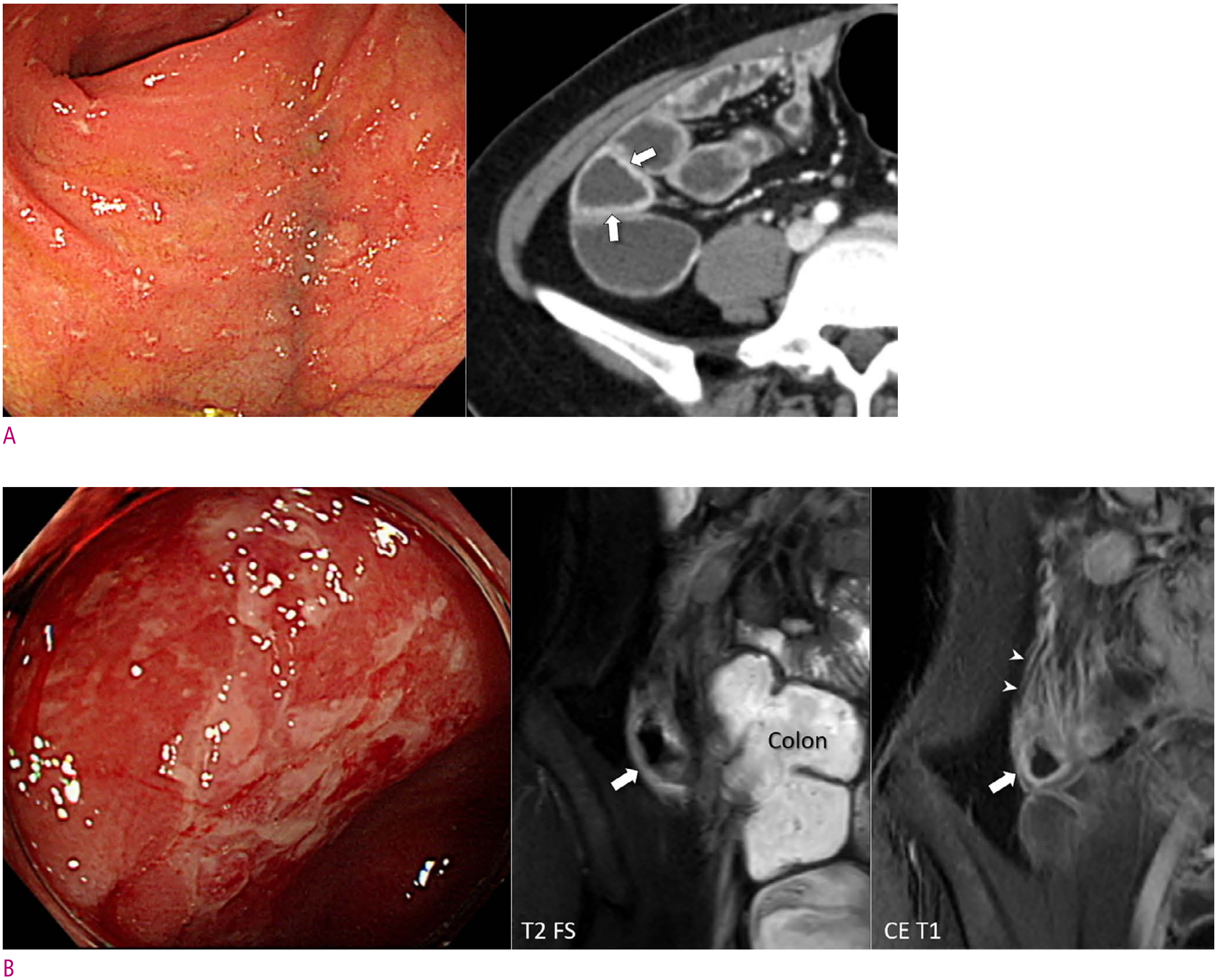

Fig. 9. Examples of recurred Crohn's disease near the ileocolic anastomosis.
A. CT enterography shows slight wall thickening and mural hyperenhancement in the neo-terminal ileum (arrows). Endoscopy image shows numerous scattered aphthoid lesions, which corresponds to Rutgeert i2. B. MR enterography in another patient shows more severe inflammatory changes than the patient in A in the wall of the neo-terminal ileum (arrows) and engorged vasa recta (arrowheads). Endoscopy image shows more severe inflammation and ulcerations than the patient in A, which corresponds to Rutgeerts i3. CE T1 = contrast-enhanced T1-weighted sequence; T2 FS = T2-weighted half-Fourier sequence with fat suppression

행하는 접근이 권고된다 (Fig. 10) (28).

장 누공

크론병으로 인한 장 누공은 크론병에서 높은 빈도로 동반되는 합병증으로 장 협착과 동반되는 경우가 많다 (40). 크론병으로 인한 장 누공은 장 천공과 구분되어야 한다. 후자는 복강 내로 유리된 공기 및 복막염을 동반하는 경우를 말하며 크론병에서는 드물게 발생한다. 이와는 달리, 장 누공은 복강 내로 유리된 공기나 복막염의 소견은 드물며 장 주변 지방조직에 누공에 의한 염증성 종괴 또는 농양을 형성하거나 인접 장기나 구조물까지 누공이 진행되어 연결될 수 있다 (Fig. 13). 염증성 종괴는 고형상태의 염증성 병변을 말하며 농양은 내부에 액상의 저류나 공기가 있고 이를 둘러싸는 가장자리로 조영증강을 보이는 형태의 병변을 말한다 (Fig. 14). 염증성 종괴는 농양과는 달리 배액술의 대상이 아니며 두 경우에 대한 치료가 다를 수 있기 때문에 구분해서 판독하는 것이 중요하다. 영어에 phlegmon이란 단어가 있는데 둘 중 어떤 경우를 이야기하는지 모호하기 때문에 사용하지 않는 것이 좋다 (6, 7). 이러한 병변들을 모두 통상 누공이라고 이야기하지만, 영어로는 상피세포

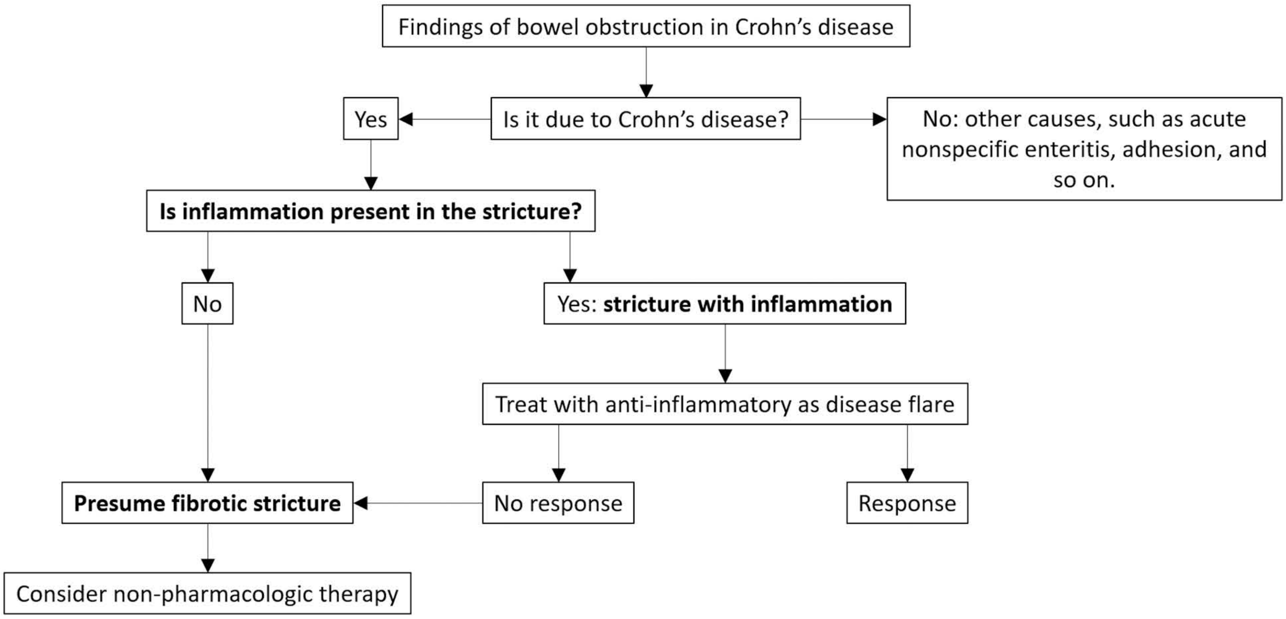

Fig. 10. Suggested approach for assessment of suspected bowel stricture in Crohn's disease.

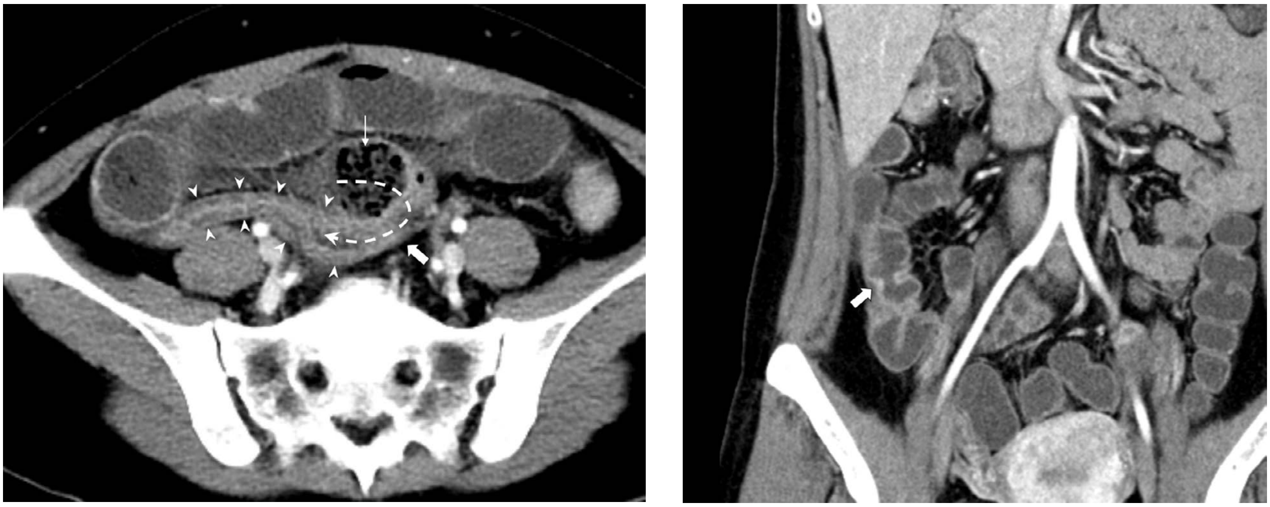
A
B

Fig. 11. Small bowel obstruction due to nonspecific acute enteritis in a patient with Crohn's disease.
A. CT at presentation shows dilated small bowel segments and small bowel feces sign (thin arrow). The thick arrow points to the level of obstruction (the exact obstruction site is not completely included in this image due to the curved configuration of the bowel). The dashed arrow shows the course of the bowel. The wall of the long bowel segment just distal to the obstruction site shows mild diffuse thickening with low attenuation (arrowheads) due to edema. B. CT obtained after 4 days of general management with intravenous fluid and cessation of oral intake shows resolution of small bowel obstruction. The previous obstruction site (arrow) shows a slight wall thickening and mild luminal narrowing, presumably as an underlying change from the previous involvement of Crohn's disease. The patient was free of any findings of bowel stricture or obstruction for the next 2 years.

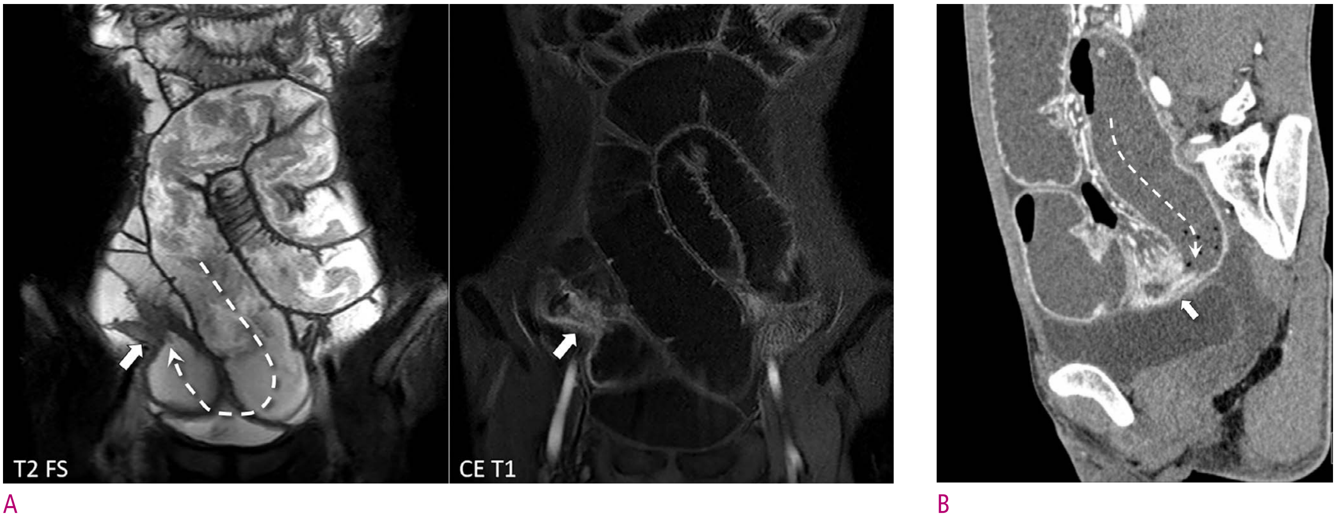

Fig. 12. Stricture with inflammation (not inflammatory stricture) in the ileum due to Crohn's disease.
A. MR enterography shows a short-segmental ileal stricture (arrows) causing an obstruction. The dashed arrow shows the course of the bowel. The stricture shows several findings of inflammation, including wall thickening with high signal intensity on T2-weighed sequence and hyperenhancement. The figure is in part from Park et al. (5) with permission. B. Follow-up CT obtained a month later after anti-inflammatory medical therapy shows no improvement of the bowel obstruction (arrow), indicating irreversible nature of the stricture. The dashed arrow shows the course of the bowel. It is a stricture with inflammation instead of an inflammatory stricture. CE T1 = contrast-enhanced T1-weighted sequence; T2 FS = T2-weighted half-Fourier sequence with fat suppression

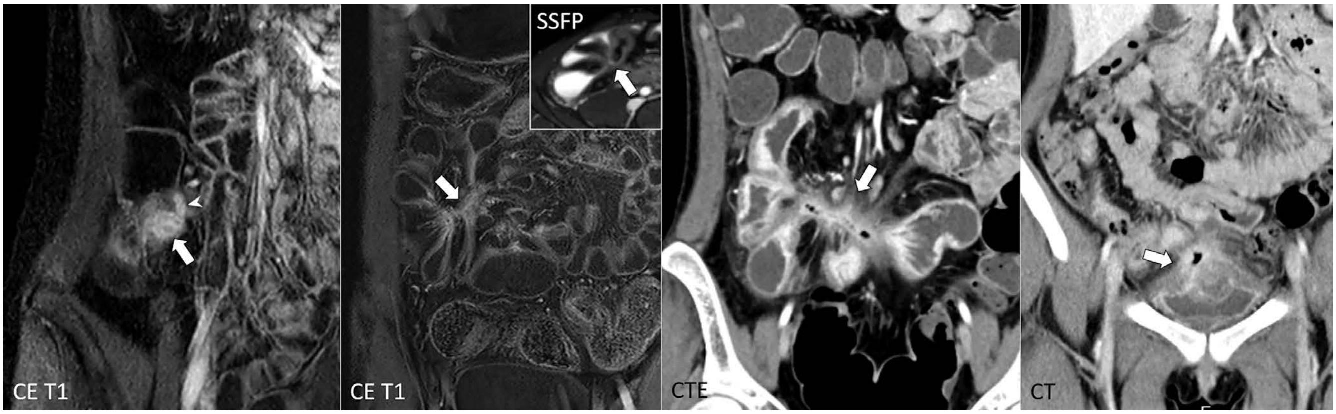

Fig. 13. Examples of enteric penetration in Crohn's disease.
From left to right, a small sinus tract (arrowhead) from the inflamed terminal ileum (arrow), enteroenteric fistula (arrow) associated with only mild inflammatory change (i.e., no peri-tract edema on the inset SSFP), enteroenteric fistula with remarkable inflammation around the tract (arrow), and enterovesical fistula (arrow) are shown. CE T1 = contrast-enhanced T1-weighted sequence; CTE = CT enterography; SSFP = steady-state free precession sequence

로 둘러싸인 장기나 구조물 간에 연결이 생긴 경우 (예, 장-장 누공, 장-방광 누공, 장-피 누공 등)를 fistula라고 하고 단지 장 주변 지방조직으로만 누공이 연장된 경우를 sinus tract이라 하여 구분한다 (Fig. 13) (6, 7). 그리고 fistula와 sinus tract를 모두 포함하는 용어로 penetration을 사용한다. 인접한 소장 분절 사이에 누공이 생긴 경우보다 소장으로부터 에스결장, 십이지장, 방광, 피부와 같이 기능적으로 크게 분리된 부위나 위장관 외 장기로 누공을 만든 경우 특히 더 문제가 될 수 있다. 따라서, 이러한 소견들이 있는지 주의 깊게 보아야 한다.

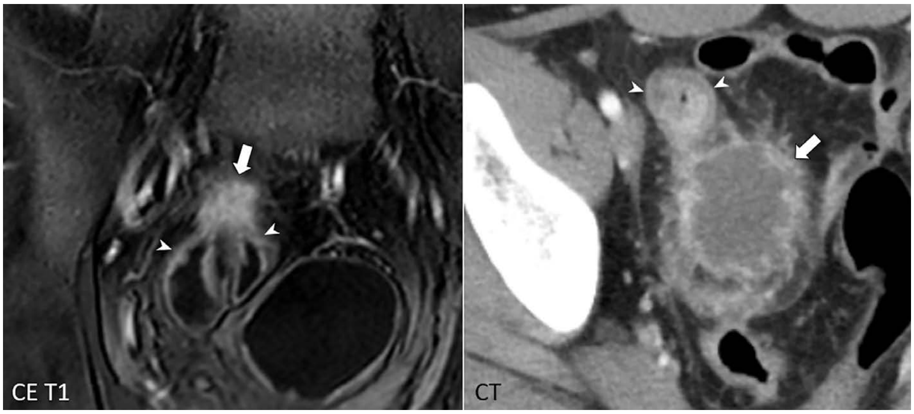

Fig. 14. Inflammatory mass and abscess associated with bowel penetration in Crohn’s disease.
From left to right, an inflammatory mass appearing as a solid enhancing nodule (arrow) and an abscess with a low-attenuating center surrounded by an irregular enhancing rim (arrow) are shown adjacent to inflamed bowel segments due to Crohn’s disease (arrowheads).

기타

이상 설명한 소견들 외에도 크론병은 소장조영술에 여러 다양한 소견들로 보일 수 있다. 이에 대해서는 최근 발표된 크론병의 소장조영술 판독에 대한 다학제 합의 권고안을 추가로 찾아볼 것을 권장한다 (6, 7).

결 론

이 논문은, 크론병의 진단과 치료에 대한 현재의 최신 지식에 맞추어 MR 소장조영술을 중심으로 크론병 환자의 소장조영술 판독을 위한 실용적인 핵심 사항들을 대표적 영상 예들과 함께 설명하였다. 크론병과 관련된 소장조영술 판독은 유사 질환과의 감별을 포함한 크론병의 진단, 크론병의 중증도 평가, 합병증의 평가 등 다양한 구성요소를 포함한다. 환자 진료에 더욱 도움이 되는 효과적인 판독과 영상정보의 제공을 위해서는 소장조영술을 하게 된 임상적 맥락을 고려해야 하고 보다 일관되고 표준화된 판독이 되도록 노력하여야 한다. 이 논문의 설명이 도움이 되었을 것으로 생각한다.

ORCID: Seong Ho Park: https://orcid.org/0000-0002-1257-8315; Sang Hyoung Park: https://orcid.org/0000-0002-5366-5749; Byong Duk Ye: https://orcid.org/0000-0001-6647-6325

References

1. Park SH, Kim YJ, Rhee KH, Kim YH, Hong SN, Kim KH, et al. A 30-year Trend Analysis in the Epidemiology of Inflammatory Bowel Disease in the Songpa-Kangdong District of Seoul, Korea in 1986-2015. J Crohns Colitis 2019;13:1410-1417.
2. Peyrin-Biroulet L, Sandborn W, Sands BE, Reinisch W, Bemelman W, Bryant RV, et al. Selecting Therapeutic Targets in Inflammatory Bowel Disease (STRIDE): Determining Therapeutic Goals for Treat-to-Target. Am J Gastroenterol 2015;110:1324-1338.
3. Turner D, Ricciuto A, Lewis A, D'Amico F, Dhaliwal J, Griffiths AM, et al. STRIDE-II: An Update on the Selecting Therapeutic Targets in Inflammatory Bowel Disease (STRIDE) Initiative of the International Organization for the Study of IBD (IOIBD): Determining Therapeutic Goals for Treat-to-Target strategies in IBD. Gastroenterology 2021;160:1570-1583.
4. Bruining DH, Bhatnagar G, Rimola J, Taylor S, Zimmermann EM, Fletcher JG. CT and MR enterography in Crohn's disease: current and future applications. Abdom Imaging 2015;40:965-974.
5. Park SH, Ye BD, Lee TY, Fletcher JG. Computed Tomography and Magnetic Resonance Small Bowel Enterography: Current Status and Future Trends Focusing on Crohn's Disease. Gastroenterol Clin North Am 2018;47:475-499.
6. Bruining DH, Zimmermann EM, Loftus EV, Sandborn W, Sauer CG, Strong SA, et al. Consensus Recommendations for Evaluation, Interpretation and Utilization of CT and MR Enterography in Patients with Small Bowel Crohn's Disease. Radiology 2018;286:776-799.
7. Guglielmo FF, Anupindi SA, Fletcher JG, Al-Hawary MM, Dillman JR, Grand DJ, et al. Small Bowel Crohn Disease at CT and MR Enterography: Imaging Atlas and Glossary of Terms. Radiographics 2020;40:354-375.
8. Park SH, Park SH. Simplified Magnetic Resonance Index of Activity for Crohn's Disease-Let's Try to Kick It Up a Notch. Gastroenterology 2020;158:281-282.e281.
9. Park SH, Park BJ, Huh J, Choi SH, Kang BK, Jang YJ. Small intestine. In Korean Society of Abdominal Radiology, ed. Abdominal radiology. 4th ed. Seoul: Ilchokak, 2020;167-241.
10. Limsrivilai J, Pausawasdi N. Intestinal tuberculosis or Crohn's

disease: a review of the diagnostic models designed to differentiate between these two gastrointestinal diseases. Intest Res 2021;19:21-32.

11. Silverberg MS, Satsangi J, Ahmad T, Arnott ID, Bernstein CN, Brant SR, et al. Toward an integrated clinical, molecular and serological classification of inflammatory bowel disease: report of a Working Party of the 2005 Montreal World Congress of Gastroenterology. Can J Gastroenterol 2005;19 Suppl A:5a-36a.
12. Rimola J, Rodriguez S, Garcia-Bosch O, Ordas I, Ayala E, Aceituno M, et al. Magnetic resonance for assessment of disease activity and severity in ileocolonic Crohn's disease. Gut 2009;58:1113-1120.
13. Oussalah A, Laurent V, Bruot O, Bressenot A, Bigard MA, Regent D, et al. Diffusion-weighted magnetic resonance without bowel preparation for detecting colonic inflammation in inflammatory bowel disease. Gut 2010;59:1056-1065.
14. Steward MJ, Punwani S, Proctor I, Adjei-Gyamfi Y, Chatterjee F, Bloom S, et al. Non-perforating small bowel Crohn's disease assessed by MRI enterography: derivation and histopathological validation of an MR-based activity index. Eur J Radiol 2012;81:2080-2088.
15. Tielbeek JA, Makanyanga JC, Bipat S, Pendse DA, Nio CY, Vos FM, et al. Grading Crohn disease activity with MRI: interobserver variability of MRI features, MRI scoring of severity, and correlation with Crohn disease endoscopic index of severity. AJR Am J Roentgenol 2013;201:1220-1228.
16. Ordás I, Rimola J, Alfaro I, Rodríguez S, Castro-Poceiro J, Ramírez-Morros A, et al. Development and Validation of a Simplified Magnetic Resonance Index of Activity for Crohn's Disease. Gastroenterology 2019;157:432-439.e431.
17. Siegel CA, Whitman CB, Spiegel BMR, Feagan B, Sands B, Loftus EV, Jr., et al. Development of an index to define overall disease severity in IBD. Gut 2018;67:244-254.
18. Cushing K, Higgins PDR. Management of Crohn Disease: A Review. JAMA 2021;325:69-80.
19. Rimola J, Alfaro I, Fernández-Clotet A, Castro-Poceiro J, Vas D, Rodríguez S, et al. Persistent damage on magnetic resonance enterography in patients with Crohn's disease in endoscopic remission. Aliment Pharmacol Ther 2018;48:1232-1241.
20. Kim C, Park SH, Yang SK, Ye BD, Park SH, Lee JS, et al. Endoscopic Complete Remission of Crohn Disease After Anti-Tumor Necrosis Factor-alpha Therapy: CT Enterographic Findings and Their Clinical Implications. AJR Am J Roentgenol 2016;206:1208-1216.
21. Ordas I, Rimola J, Rodriguez S, Paredes JM, Martinez-Perez MJ, Blanc E, et al. Accuracy of magnetic resonance enterography in assessing response to therapy and mucosal healing in patients with Crohn's disease. Gastroenterology 2014;146:374-382.e371.
22. Fernandes SR, Rodrigues RV, Bernardo S, Cortez-Pinto J, Rosa I, da Silva JP, et al. Transmural Healing Is Associated with Improved Long-term Outcomes of Patients with Crohn's Disease. Inflamm Bowel Dis 2017;23:1403-1409.
23. Buisson A, Chevaux JB, Allen PB, Bommelaer G, Peyrin-Biroulet L. Review article: the natural history of postoperative Crohn's disease recurrence. Aliment Pharmacol Ther 2012;35:625-633.
24. Lichtenstein GR, Loftus EV, Isaacs KL, Regueiro MD, Gerson LB, Sands BE. ACG Clinical Guideline: Management of Crohn's Disease in Adults. Am J Gastroenterol 2018;113:481-517.
25. Lamb CA, Kennedy NA, Raine T, Hendy PA, Smith PJ, Limdi JK, et al. British Society of Gastroenterology consensus guidelines on the management of inflammatory bowel disease in adults. Gut 2019;68:s1-s106.
26. De Cruz P, Kamm MA, Hamilton AL, Ritchie KJ, Krejany EO, Gorelik A, et al. Crohn's disease management after intestinal resection: a randomised trial. Lancet 2015;385:1406-1417.
27. Choi IY, Park SH, Park SH, Yu CS, Yoon YS, Lee JL, et al. CT Enterography for Surveillance of Anastomotic Recurrence within 12 Months of Bowel Resection in Patients with Crohn's Disease: An Observational Study Using an 8-Year Registry. Korean J Radiol 2017;18:906-914.
28. Rieder F, Zimmermann EM, Remzi FH, Sandborn WJ. Crohn's disease complicated by strictures: a systematic review. Gut 2013;62:1072-1084.
29. Adler J, Punglia DR, Dillman JR, Polydorides AD, Dave M, Al-Hawary MM, et al. Computed tomography enterography findings correlate with tissue inflammation, not fibrosis in resected small bowel Crohn's disease. Inflamm Bowel Dis 2012;18:849-856.
30. Chiorean MV, Sandrasegaran K, Saxena R, Maglinte DD, Nakeeb A, Johnson CS. Correlation of CT enteroclysis with surgical pathology in Crohn's disease. Am J Gastroenterol 2007;102:2541-2550.
31. Zappa M, Stefanescu C, Cazals-Hatem D, Bretagnol F, Deschamps L, Attar A, et al. Which magnetic resonance

imaging findings accurately evaluate inflammation in small bowel Crohn's disease? A retrospective comparison with surgical pathologic analysis. Inflamm Bowel Dis 2011;17:984-993.

32. Bouhnik Y, Carbonnel F, Laharie D, Stefanescu C, Hebuterne X, Abitbol V, et al. Efficacy of adalimumab in patients with Crohn's disease and symptomatic small bowel stricture: a multicentre, prospective, observational cohort (CREOLE) study. Gut 2017;67:53-60.
33. Rimola J, Planell N, Rodriguez S, Delgado S, Ordas I, Ramirez-Morros A, et al. Characterization of inflammation and fibrosis in Crohn's disease lesions by magnetic resonance imaging. Am J Gastroenterol 2015;110:432-440.
34. Branchi F, Caprioli F, Orlando S, Conte D, Fraquelli M. Non-invasive evaluation of intestinal disorders: The role of elastographic techniques. World J Gastroenterol 2017;23:2832-2840.
35. Lu C, Gui X, Chen W, Fung T, Novak K, Wilson SR. Ultrasound Shear Wave Elastography and Contrast Enhancement: Effective Biomarkers in Crohn's Disease Strictures. Inflamm Bowel Dis 2017;23:421-430.
36. Orlando S, Fraquelli M, Coletta M, Branchi F, Magarotto A, Conti CB, et al. Ultrasound Elasticity Imaging predicts therapeutic outcomes of patients with Crohn's disease treated with anti-tumor necrosis factor antibodies. J Crohns Colitis 2018;12:63-70.
37. Stidham RW, Higgins PD. Imaging of intestinal fibrosis: current challenges and future methods. United European Gastroenterol J 2016;4:515-522.
38. Adler J, Swanson SD, Schmiedlin-Ren P, Higgins PD, Golembeski CP, Polydorides AD, et al. Magnetization transfer helps detect intestinal fibrosis in an animal model of Crohn disease. Radiology 2011;259:127-135.
39. Dillman JR, Swanson SD, Johnson LA, Moons DS, Adler J, Stidham RW, et al. Comparison of noncontrast MRI magnetization transfer and T2 -Weighted signal intensity ratios for detection of bowel wall fibrosis in a Crohn's disease animal model. J Magn Reson Imaging 2015;42:801-810.
40. Schwartz DA, Tagarro I, Carmen Díez M, Sandborn WJ. Prevalence of Fistulizing Crohn's Disease in the United States: Estimate From a Systematic Literature Review Attempt and Population-Based Database Analysis. Inflamm Bowel Dis 2019;25:1773-1779.

크론병 환자의 소장조영술 판독

박성호[1,3], 박상형[2,3], 예병덕[2,3]

[1]울산대학교 의과대학 서울아산병원 영상의학과
[2]울산대학교 의과대학 서울아산병원 소화기내과
[3]서울아산병원 염증성장질환센터

초 록

CT 소장조영술과 MR 소장조영술은 현재 크론병 환자의 소장을 평가하기 위한 영상의학적 검사 중 가장 발전된 검사이다. 이 종설은 소장조영술을 보다 정확하고 임상적 맥락에 부합하도록 판독하는데 필요한 최신의 실용적 지식을 양질의 대표적 영상과 함께 설명하며, 이를 통하여 환자의 진료 향상에 기여할 수 있도록 한다. 특히 MR 소장조영술의 해석을 중점적으로 설명한다. 소장조영술의 판독은 크론병의 진단 및 다른 유사 질환과의 감별, 장 염증의 활동도 및 범위의 평가, 합병증의 평가, 질환의 전체적 중증도 평가, 관해의 진단, 동반 질환의 발견을 포함한다. 영상소견을 좀 더 효과적으로 정확하게 임상의들에게 전달하기 위해서는 판독자가 환자들의 임상적 상황에 대해서 잘 이해를 하고 좀 더 표준화된 판독을 하려는 노력이 필요하다.

www.e-kjar.org
https://doi.org/10.52668/kjar.2021.00024

pISSN 2586-1719 / eISSN 2799-3299

Korean J Abdom Radiol 2021;5:17-31

Original Article

Gadoxetic Acid-Enhanced and Diffusion-Weighted Magnetic Resonance Imaging of Histologically Defined Early Hepatocellular Carcinoma

Nieun Seo[1], Myeong-Jin Kim[1], Young Nyun Park[2], Mi-Suk Park[1], Jin-Young Choi[1], Yong Eun Chung[1]
[1]*Department of Radiology, Severance Hospital, Yonsei University College of Medicine, Seoul, Korea*
[2]*Department of Pathology, Severance Hospital, Yonsei University College of Medicine, Seoul, Korea*

Purpose: To describe the imaging features of histologically defined early hepatocellular carcinoma (eHCC) on gadoxetate disodium-enhanced MRI (EOB-MRI) and diffusion-weighted imaging (DWI).
Materials and Methods: We enrolled 173 surgically confirmed eHCCs in 119 patients examined by preoperative EOB-MRI and DWI between January 2006 and September 2017. The imaging features of preoperatively detected eHCCs were retrospectively analyzed by two radiologists. The clinical and imaging characteristics associated with false-negative detection were evaluated.
Results: Of the 173 eHCCs, 118 (68%) in 78 patients were prospectively reported on preoperative EOB-MRI. After retrospective review, 17 eHCCs in 13 patients were additionally detected, with a per-lesion detection sensitivity of 78% (135/173). Thus, the imaging features of 135 eHCCs in 91 patients were analyzed. Most eHCCs exhibited hepatobiliary hypointensity (90%, 122/135). Arterial phase hyperenhancement, washout, and capsule appearance were seen in 68 (50%), 79 (59%), and 11 (8%) detected lesions, respectively. Diffusion restriction and fatty change were noted in 30 (22%) and 39 (29%) lesions, respectively; most eHCCs exhibited T1 and T2 isointensity (80 [59%] and 89 [66%], respectively). False-negative detection was associated with small lesion size (< 1 cm), history of HCC treatment (odds ratio, 0.34 [95% confidence interval, 0.13-0.92]), number of HCC lesions (≥ 2; odds ratio, 0.08 [0.01-0.66]), and poor functional liver imaging score (< 4; odds ratio, 0.13 [0.04-0.51]).
Conclusions: Histologically defined eHCCs typically appear as hepatobiliary phase hypointensity. Detection sensitivity of eHCC may be affected by lesion size, history of HCC treatment, number of HCCs, and hepatobiliary enhancement.

Keywords: Hepatocellular carcinoma; Early diagnosis; Detection; Magnetic resonance imaging; Diffusion-weighted imaging

---

Received: May 12, 2021 **Revised:** June 17, 2021 **Accepted:** June 19, 2021
Correspondence: Myeong-Jin Kim, MD, PhD
Department of Radiology, Severance Hospital, Yonsei University College of Medicine, 50-1 Yonsei-ro, Seodaemun-gu, Seoul 03722, Korea
Tel: +82-2-2228-7400 Fax: +82-2-2227-8337 E-mail: kimnex@yuhs.ac

Introduction

Hepatocellular carcinoma (HCC) is a major cause of cancer-related mortality worldwide (1, 2). HCC develops via multistep carcinogenesis in a background of chronic liver disease, where an early HCC (eHCC) develops from a premalignant dysplastic lesion, then eventually to a progressed (moderately or poorly differentiated) HCC (3, 4). Early HCCs are histologically defined as vaguely nodular, well-differentiated HCCs with stromal invasion (5, 6), and are characterized by a lower risk of recurrence and higher 5-year survival rate than progressed HCCs after treatment (7, 8). Therefore, the detection of eHCCs may help decrease mortality associated with HCC, and increase opportunities for curative treatment (9, 10).

The detection and characterization of eHCCs is more difficult than progressed HCCs, given that the former are usually small (< 2 cm) and demonstrate fewer discernible findings via computed tomography (CT) and extracellular contrast-enhanced magnetic resonance imaging (MRI) (11-14). Diagnostic imaging via gadoxetate disodium-enhanced MRI (EOB-MRI) is superior to multiphase dynamic CT, as eHCCs are depicted as hypointense nodules in hepatobiliary phase (HBP) images (15-19). However, the reported features of eHCCs on EOB-MRI are highly variable. Importantly, the incidence of arterial phase hyperenhancement (APHE), a hallmark for HCC diagnosis, ranges widely, from 13% (15) to 37% (16). Moreover, although diffusion-weighted imaging (DWI) has been recognized as an important tool in HCC diagnosis, especially in non-hypervascular HCCs (20-22), the appearance of eHCC by DWI is limited to only a few reports with relatively small subject numbers (11, 17).

Therefore, the aim of this study was to describe the imaging features of histologically defined eHCCs based on EOB-MRI and DWI in a relatively large number of subjects.

Materials and Methods

Patients

This retrospective study was approved by our Institutional Review Board, and the requirement for informed consent was waived. From January 2006 to September 2017, 218 adult patients who presented with at least one pathologically confirmed eHCC were identified from institutional electronic medical records. The study inclusion criteria were as follows: (a) patients who underwent surgery for eHCC; (b) those with preoperative EOB-MRI. Ninety-nine patients were excluded from the study for the following reasons: (a) biopsy-confirmed eHCC without surgery (n = 3; to exclude the possibility of biopsy tissue sampling an eHCC portion of a progressed HCC); (b) no contrast-enhanced liver MRI (n = 19); (c) MRI using contrast agents other than gadoxetate disodium (n = 32); (d) interval between liver MRI and surgery > 3 months (n = 40); (e) > 5 nodules in the pathological specimen (n = 5; due to difficulty in correlating the radiological and pathological findings). Thus, 119 patients were included in our study (Fig. 1). The median interval between MRI and surgery was 26 days (range, 0-86 days).

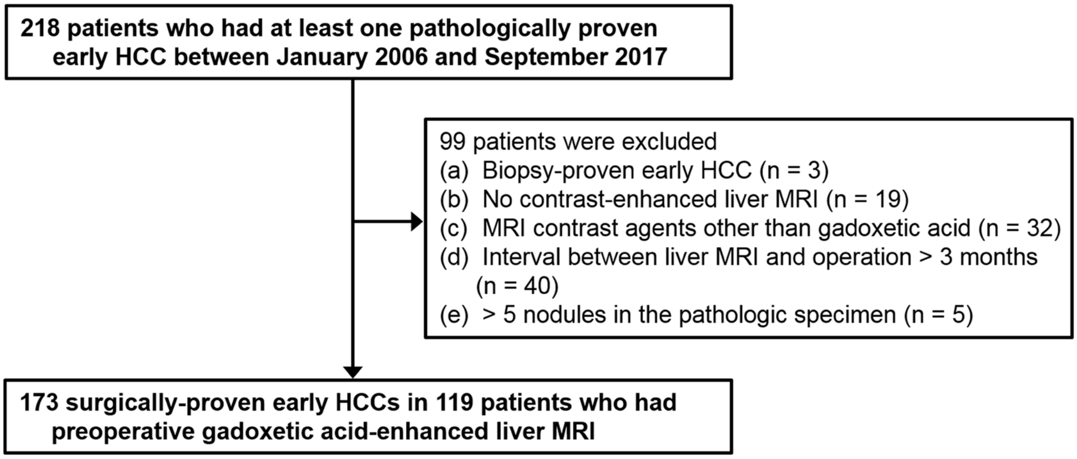

218 patients who had at least one pathologically proven early HCC between January 2006 and September 2017

99 patients were excluded
(a) Biopsy-proven early HCC (n = 3)
(b) No contrast-enhanced liver MRI (n = 19)
(c) MRI contrast agents other than gadoxetic acid (n = 32)
(d) Interval between liver MRI and operation > 3 months (n = 40)
(e) > 5 nodules in the pathologic specimen (n = 5)

173 surgically-proven early HCCs in 119 patients who had preoperative gadoxetic acid-enhanced liver MRI

Fig. 1. Flow diagram of the patient enrollment process.

Electronic medical records were retrospectively reviewed for clinical findings and laboratory data. Clinical findings included patient characteristics, chronic liver disease etiology, history of HCC treatment, and type of liver surgery. Laboratory data included serum albumin, total bilirubin, aspartate transaminase, alanine transaminase, and alpha fetoprotein. The Child-Pugh score and albumin-bilirubin (ALBI) grade were both calculated to evaluate the hepatic function of the study population (23-25).

Pathological diagnosis

Pathological examination was performed by a senior liver pathologist (with more than 20 years of experience in hepatic pathology), together with one or two residents or a fellow. The pathological reports included the fibrosis grade of the non-tumor-bearing liver parenchyma and the location, size, and number of eHCCs and progressed HCCs. Diagnosis of eHCC was based on the established histological criteria of a small, well-differentiated HCC of a vaguely nodular type, with combinations of the following histological features: (a) increased cell density more than two times that of the surrounding parenchyma, with an increased nuclear/cytoplasm ratio and irregular thin-trabecular pattern; (b) varying numbers of intratumoral portal tracts; (c) pseudoglandular pattern; (d) fatty change; (e) varying numbers of unpaired arteries (6). Importantly, the presence of stromal invasion was useful for differentiating high-grade dysplastic nodules from eHCCs (6, 26). When morphologic criteria, such as stromal invasion, were difficult to assess, a panel of immunohistochemical markers were used to establish the diagnosis, including glypican-3, heat shock protein 70, and glutamine synthetase; eHCC was diagnosed when two or more immune-markers were positive (26).

Magnetic resonance imaging

Liver MRI was performed using a 3.0-T (MAGNETOM Tim Trio, Siemens Healthineers; Intera Achieva or Ingenia, Philips Healthcare) or a 1.5-T system (Intera Achieva or Ingenia, Philips Healthcare). Routine liver MRI sequences included dual-echo spoiled gradient-echo T1-weighted in-phase and opposed-phase images, multi-shot and single-shot turbo spin-echo T2-weighted images (T2WI), single-shot echo planar DWI with b values of 50, 400, and 800 sec/mm^2, and dynamic T1-weighted images (T1WI). Dynamic fat-suppressed spoiled gradient-echo T1WI was acquired before and after gadoxetate disodium injection (Primovist, Bayer Pharma AG) at a dose of 0.1 mL/kg (0.025 mmol/kg), followed by a 20-mL saline flush at an injection rate of 1 mL/sec. To determine the timing of the arterial phase, a bolus-tracking method was used. Subsequent dynamic phases were acquired at approximately 30 sec intervals; each dynamic phase required 16-22 sec. The HBP images were obtained 20 min after contrast injection.

Image analysis

The detection sensitivity of eHCC was calculated from both prospective and retrospective reading sessions. A study coordinator (an abdominal radiologist with 5 years of experience in liver imaging) performed radiologic-pathologic correlations (through review of the MRI and pathological reports) by matching the size and location of the hepatic lesions. Prospective detection sensitivity was determined from the preoperative reports of MRI examinations conducted by one of five faculty radiologists (all with more than 5 years of experience in abdominal MRI), together with one or two residents and/or fellows. A lesion was defined as “detected” when an eHCC, documented on the pathologic report, was identified and mentioned in the preoperative MRI. The original radiologic impressions of histologically confirmed eHCCs were divided into one of the following six categories: definite benign, probably benign, indeterminate, probably HCC, definitely HCC, or other malignancy such as metastasis. Thereafter, retrospective analyses were performed by the study coordinator to identify missed or unreported eHCCs; any lesions identified were included in the calculation of overall detection sensitivity and review of MRI findings.

To investigate whether the detection sensitivity was affected by image quality or hepatic function, two abdominal radiologists, with 25 and 5 years of experience in liver MRI, reviewed the MRI using a picture archiving and communication system (Centricity version 4, GE healthcare). The image quality of the HBP of EOB-MRI was evaluated using the functional liver imaging score (FLIS), previously validated in liver transplant recipients (27). The FLIS was calculated as the sum of the following three parameters: liver parenchymal enhancement relative to the kidney (EnQS: 0, hypointense; 1, isointense; 2, hyperintense); biliary contrast excretion (ExQS: 0, no excretion; 1, excretion into peripheral intrahepatic bile ducts; 2, excretion into the common hepatic duct, common bile duct, or duodenum); and signal intensity (SI) of the portal vein relative to the liver (PVsQS: 0, hyperintense; 1, isointense; 2, hypointense). A higher FLIS indicates better image quality of the HBP. The image qualities of other sequences, including dynamic T1WI, T2WI, and DWI, were graded using a four-point scale: 1, poor; 2, fair; 3, good; and 4, excellent.

Subsequently, the same two radiologists independently evaluated the MRI features of the detected eHCCs. The reviewers were informed of the size and location of the detected eHCCs via series/image numbers and arrows on the picture archiving and communication system. Each MRI finding was evaluated for: the presence of fatty change, APHE, washout, capsule appearance, and SI on pre-contrast T1WI, T2WI, DWI, and HBP. The definition of each finding was based on the 2017 Liver Imaging Reporting and Data System (28). For example, washout was determined from the portal venous phase only. The presence of fatty change was determined by comparison of in- and opposed- phase T1-weighted gradient-echo images. The presence of a smooth hypointense rim on HBP (HBP capsule appearance) was noted in addition to the conventional capsular appearance (29). Capsular appearance was considered positive when it appeared around at least two-thirds of the tumor border (29, 30). Discrepancies between reviewers were resolved by consensus review, and the consensus data were used for analysis. Original data from the independent review were used to calculate interobserver agreement.

Statistical analysis

Both per-patient and per-lesion detection sensitivities were calculated. If all eHCCs were detected in a patient, we considered this "detected" on a per-patient basis. If any eHCC was missed in a patient, we classified this as "undetected" in terms of per-patient sensitivity. Both preoperatively reported lesions and retrospectively identified lesions were regarded as detected lesions for image review, as well as for the calculation of detection sensitivity. The per-lesion detection sensitivity was also calculated according to the size of the eHCC. For per-lesion analysis, generalized estimating equations were used to adjust for possible clustering effects caused by multiple lesions in a patient. Detection sensitivities were compared among different sized groups of eHCC using logistic regression with generalized estimating equations. Baseline patient demographics and MRI quality were compared between patients with and without false-negative lesions using independent t-tests for continuous variables and Pearson's chi-squared test or Fisher's exact test for categorical variables. Per-patient analyses of factors affecting the detection of eHCCs were performed using logistic regression. Multivariate analysis was performed for significant factors identified by univariate analysis. The interobserver agreement regarding MRI quality and imaging findings of detected eHCCs were assessed using weighted κ statistics as follows: κ values < 0.20, poor; 0.21-0.40, fair; 0.41-0.60, moderate; 0.61-0.80, good; 0.81-1.00, excellent (31). Statistical analyses were performed using SPSS v23.0 software (IBM Corp.). P values < 0.05 were considered statistically significant.

Results

Detection rate of early hepatocellular carcinoma

The prospective per-patient and per-lesion detection sensitivities of eHCCs from preoperative MRI reports were 66% (78/119) and 68% (118/173), respectively. The radiologic impressions of 118 originally detected lesions were as follows: HCC, 52% (n = 61); probably HCC, 21% (n = 25); indeterminate, 25% (n = 29); probably benign, 1% (n = 1); metastasis in patients with history of other malignancy, 2% (n = 2). After retrospective review, 17 eHCCs were additionally identified in 13 patients. Thus, retrospective per-patient and per-lesion detection sensitivities were 77% (91/119) and 78% (135/173), respectively. Per-lesion sensitivity increased with eHCC size: < 1-cm lesions, 63% (35/56); 1- to 2-cm lesions, 82% (72/88); ≥ 2-cm lesions, 97% (28/29). Per-lesion detection sensitivity differed significantly between < 1-cm and ≥ 1-cm lesions (56% and 85%, respectively; P = 0.001). Detected eHCCs (mean ± standard deviation, 1.5 ± 0.6 cm) were significantly larger than undetected eHCCs (1.0 ± 0.5 cm; P < 0.001).

Patients and magnetic resonance imaging quality

The comparisons of the patient demographics and MRI quality between patients with and without false-negative findings are summarized in Table 1. Patients with

Table 1. Patient characteristics and magnetic resonance image quality

	With FN (n = 28)	Without FN (n = 91)	P value
Clinicopathologic findings			
Age (years)	65.0 ± 6.9	61.7 ± 8.2	0.058
Sex			0.771
Male	23 (82)	77 (85)	
Female	5 (18)	14 (15)	
Cause of CLD			0.515
HBV	22 (79)	73 (80)	
HCV	4 (14)	7 (8)	
Alcoholic	1 (4)	9 (10)	
Others	1 (4)	2 (2)	
History of HCC			0.014
No	16 (57)	73 (80)	
Yes	12 (43)	18 (20)	
Type of surgery			0.008
Resection	12 (43)	64 (70)	
LT	16 (57)	27 (30)	
Pathologic cirrhosis			0.054
No	3 (11)	26 (29)	
Yes	25 (89)	65 (71)	
Number of HCC			0.003
One	1 (4)	27 (30)	
Two	10 (36)	37 (41)	
Three or more	17 (61)	27 (30)	
Number of eHCC			0.014
One	15 (54)	72 (79)	
Two	5 (18)	12 (13)	
Three or more	8 (29)	7 (8)	
Presence of progressed HCC			0.742
No	8 (29)	29 (32)	
Yes	20 (71)	62 (68)	
Largest size of eHCC (cm)	1.3 ± 0.8	1.4 ± 0.7	0.451
Albumin (g/dL)	3.7 ± 0.8	3.8 ± 0.7	0.746
Total bilirubin (mg/dL)	1.4 ± 1.1	1.0 ± 0.7	0.150
AST (IU/L)	42.7 ± 20.1	51.0 ± 38.2	0.273
ALT (IU/L)	34.8 ± 22.4	47.1 ± 41.6	0.138
AFP (ng/mL)	126.1 ± 369.5	238.6 ± 1081.6	0.591
Child-Pugh score			0.188
A	20 (71)	76 (84)	
B	6 (21)	14 (15)	
C	2 (7)	1 (1)	
ALBI grade			0.650
1	14 (50)	50 (55)	
2	9 (32)	31 (34)	
3	5 (18)	10 (11)	
MR image quality			
Hepatobiliary phase			
EnQS			0.038
0	5 (18)	3 (3)	
1	4 (14)	10 (11)	
2	19 (68)	78 (86)	
ExQS			0.336
0	2 (7)	2 (2)	
1	4 (14)	8 (9)	
2	22 (79)	81 (89)	
PVsQS			0.217
0	2 (7)	2 (2)	
1	6 (21)	11 (12)	
2	20 (71)	78 (86)	
FLIS			0.004
0-3	8 (29)	6 (7)	
4-6	20 (71)	85 (93)	
Dynamic phase			0.464
Poor-fair	6 (21)	14 (15)	
Good-excellent	22 (79)	77 (85)	
T2WI			0.032
Poor-fair	5 (18)	4 (4)	
Good-excellent	23 (82)	87 (96)	
DWI			0.130
Poor-fair	7 (25)	11 (12)	
Good-excellent	21 (75)	80 (88)	

The data are expressed as means ± standard deviations.

The data in parentheses are percentages. Percentages may not sum to 100% because of rounding.

FN, false-negative; CLD, chronic liver disease; HBV, hepatitis B virus; HCV, hepatitis C virus; HCC, hepatocellular carcinoma; LT, liver transplantation; eHCC, early hepatocellular carcinoma; AST, aspartate transaminase; ALT, alanine transaminase; AFP, alpha fetoprotein; ALBI, albumin-bilirubin; EnQS, enhancement quality score; ExQS, excretion quality score; PVsQS, portal vein sign quality score; FLIS, functional liver imaging score; T2WI, T2-weighted imaging; DWI, diffusion-weighted imaging.

a false-negative eHCC detection had a more frequent history of HCC treatment (P = 0.014) and underwent liver transplantation more frequently than resection (P = 0.008), compared to those without. In addition, the multiplicity of both total (P = 0.003) and early (P = 0.014) HCCs was greater in patients with a false-negative detection. Most patients with eHCCs had progressed HCCs (82/119, 69%) in addition to eHCC, but the presence of progressed HCCs did not differ significantly between patients with and without a false negative detection of eHCC (P = 0.742). Liver function, determined by the Child-Pugh score, ALBI grade, and laboratory findings, did not differ significantly between the groups (Ps ≥ 0.138). Hepatobiliary phase image qualities, determined by EnQS and FLIS, were significantly higher in patients without false-negative detection (P = 0.038 and P = 0.004, respectively). Similarly, the image quality of T2WI were significantly higher in patients without false-negative detection (P = 0.032), but those of dynamic phase and DWI did not differ significantly between the groups (P = 0.464 and P = 0.130, respectively).

Interobserver agreement of MRI quality was good to excellent (EnQS, κ = 0.757 [95% confidence interval (95% CI), 0.644-0.870]; ExQS, κ = 0.824 [0.699-0.950]; PVsQS, κ = 0.834 [0.705-0.962]; dynamic phase, κ = 0.849 [0.770-0.928]; T2WI, κ = 0.675 [0.556-0.795]; and DWI, κ = 0.730 [0.632-0.829]).

Magnetic resonance imaging findings

The imaging features of eHCCs on EOB-MRI and DWI are presented in Table 2 and Figs. 2-4. The imaging features of undetected eHCCs (n = 38) were regarded to show negative findings or isointense SI. Fatty change was noted in 29% of detected (n = 135) and 23% of total (n = 173) eHCCs. Most eHCCs showed hypointensity on HBP (90% and 71% of detected and total eHCCs, respectively), while most detected eHCCs showed isointensity on T1WI (59%) and T2WI (66%). Arterial phase hyperenhancement was present in 50% and 39% of detected and total eHCCs, respectively. Washout and capsule appearance in the dynamic phase were observed in 59% and 8% of detected eHCCs, and 46% and 6% of total eHCCs, respectively. Diffusion restriction was observed in 22% and 17% of detected and total eHCCs, respectively. Among the 30 eHCCs showing diffusion restriction, 29 (97%) showed APHE. The interobserver agreement of MRI findings was good to excellent (κ, 0.716-0.894).

Factors associated with the false-negative detection of early hepatocellular carcinoma

Factors affecting the detection of eHCCs are given in Table 3. Univariate analysis showed that history of HCC treatment, type of surgery, number of total HCCs and eHCCs, EnQS, FLIS, and quality of T2WI were significant factors affecting the detection of eHCCs. Multivariate analysis revealed that history of HCC treatment (odds ratio, 0.34 [95% CI, 0.31-0.92], number of total HCCs (≥ 2; odds ratio, 0.08 [0.01-0.66]), and poor FLIS (< 4; odds ratio, 0.13 [0.04-0.51]) were independent factors negatively affecting the detection of eHCCs.

Discussion

Our results showed per-patient and per-lesion sensitivities for the detection of eHCCs of 66% and 68% on the prospective interpretation and 77% and 78% on the retrospective analysis of EOB-MRI. Early HCC on retrospectively analysis was most commonly depicted by HBP hypointensity (90%), with more common presentation of APHE (50%) and washout appearance (59%) than fatty change (29%), diffusion restriction (22%), and capsule appearance (8%). False-negative detection of eHCCs was associated with lesion size, history of HCC treatment, number of HCCs, and the degree of hepatobiliary enhancement.

Our study demonstrates the usefulness of HBP of EOB-MRI for detecting eHCCs as hypointensity. In our series, 90% and 71% of identifiable and total eHCCs showed HBP hypointensity, respectively; comparable with Sano et al. (15) and Kim et al. (17) (97% and 76%, respectively). The high sensitivity of HBP hypointensity for detecting eHCC may be explained by the decrease in OATP8 expression occurring prior to hemodynamic alteration, such as neoarterialization or reduced portal blood flow (15, 17, 32).

Interestingly, in our series, 50% and 39% of detected and total eHCCs showed APHE, compared to just 29% and 13% of total eHCCs reported by Kim et al. (17) and Sano et al. (15), respectively. Additionally, fatty change was less common (29%) in our study than reported by

Table 2. Magnetic resonance imaging findings of early hepatocellular carcinoma

	Group		Interobserver agreement**	
	Detected eHCC (n = 135)	Total eHCC* (n = 173)	Kappa	95% CI
Fat			0.811	0.699-0.923
No	96 (71)	134 (77)		
Yes	39 (29)	39 (23)		
Pre-contrast T1WI			0.801	0.717-0.885
Hypointense	32 (24)	32 (18)		
Isointense	80 (59)	118 (68)		
Hyperintense	23 (17)	23 (13)		
APHE			0.894	0.832-0.957
No	67 (50)	105 (61)		
Yes	68 (50)	68 (39)		
Washout			0.783	0.692-0.874
No	56 (41)	94 (54)		
Yes	79 (59)	79 (46)		
Capsule (conventional)			0.716	0.409-1.000
No	124 (92)	162 (94)		
Yes	11 (8)	11 (6)		
Capsule (HBP)			0.761	0.578-0.944
No	107 (79)	145 (84)		
Yes	28 (21)	28 (16)		
T2WI			0.721	0.583-0.858
Hypointense	14 (10)	14 (8)		
Isointense	89 (66)	127 (73)		
Hyperintense	32 (24)	32 (18)		
DWI restriction			0.894	0.803-0.985
No	105 (78)	143 (83)		
Yes	30 (22)	30 (17)		
HBP			0.829	0.644-1.000
Hypointense	122 (90)	122 (71)		
Isointense	10 (7)	48 (28)		
Hyperintense	3 (2)	3 (2)		

The data in parentheses for imaging features are percentages. Percentages may not sum to 100% because of rounding.

*Total eHCC: Undetected eHCC was regarded as having negative findings or isointensity.

**Interobserver agreement for the analysis of detected eHCC

eHCC, early hepatocellular carcinoma; CI, confidence interval; T1WI, T1-weighted imaging; APHE, arterial phase hyperenhancement; HBP, hepatobiliary phase; DWI, diffusion-weighted imaging.

Sano et al (53%) (15). This discrepancy may be attributed to the different diagnostic criteria applied by pathologists across institutions. We only included the surgically resected lesions determined as eHCC by an expert pathologist, based on the established histological criteria (6, 26). Therefore, our results indicate that eHCCs may also show hypervascularization detectable on EOB-MRI. In our experience, EOB-MRI may be advantageous for identifying APHE in eHCCs, by demonstrating HBP hypointensity, making it easier to match small arterially hyperenhancing lesions with true lesions. Conversely, on CT or extracellular agent-enhanced MRI, subtle hyperenhancing lesions may

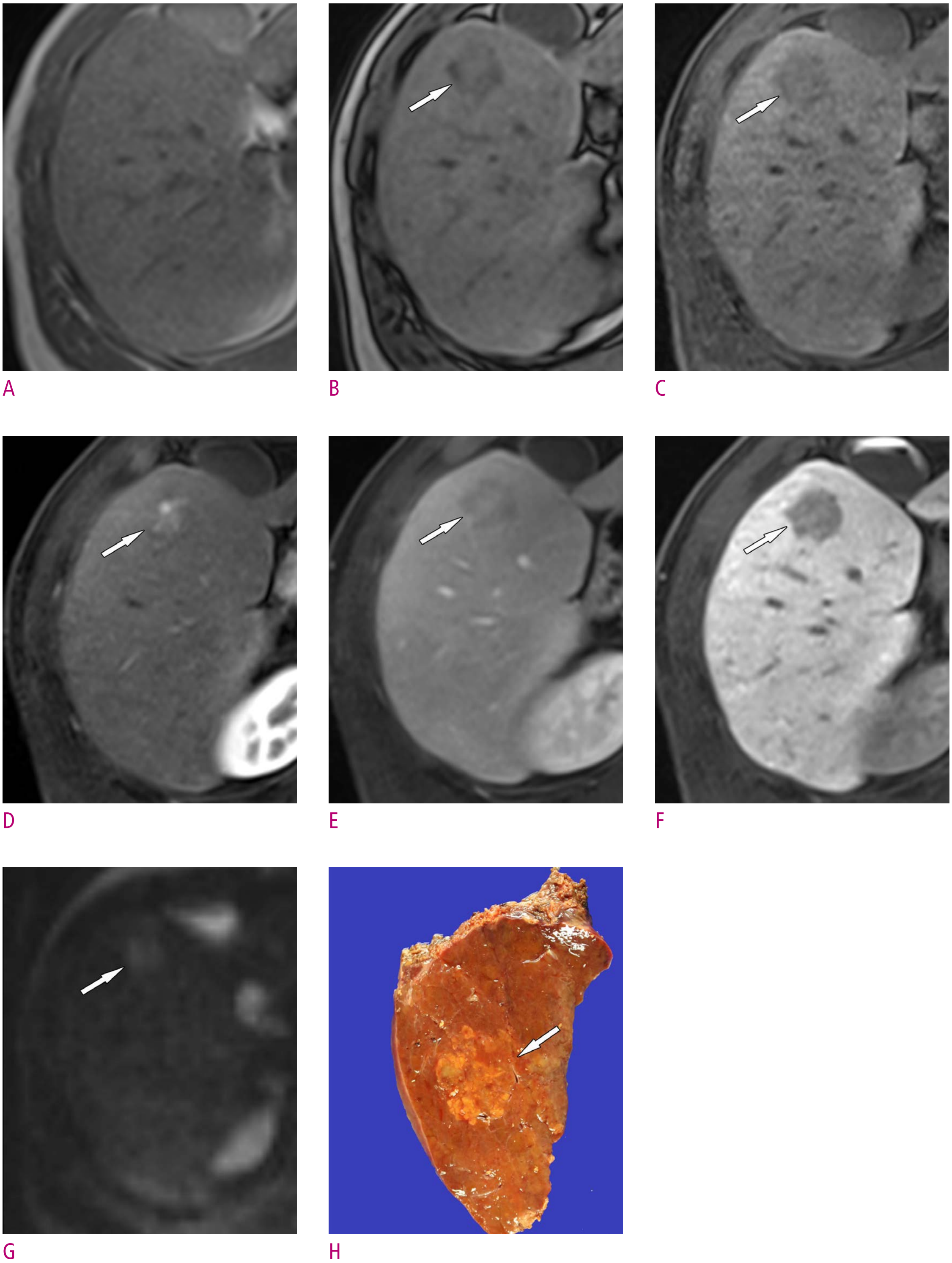

Fig. 2. Magnetic resonance images of an early hepatocellular carcinoma lesion in a 44-year-old man who underwent hepatic resection. (A) The in-phase and (B) opposed-phase T1-weighted magnetic resonance images show fatty change within the tumor (arrow) in segment V. (C) The pre-contrast T1-weighted image shows hypointensity of the tumor (arrow). (D) The hepatic arterial phase image shows hyperenhancement (arrow), and (E) the portal venous phase image reveals washout of the tumor (arrow). (F) The hepatobiliary phase image shows avid hypointensity of the tumor (arrow). (G) The mass shows mild hyperintensity (arrow) on the diffusion-weighted image (b = 800 sec/mm^2). (H) The gross surgical specimen shows a 2.2-cm early hepatocellular carcinoma lesion (arrow).

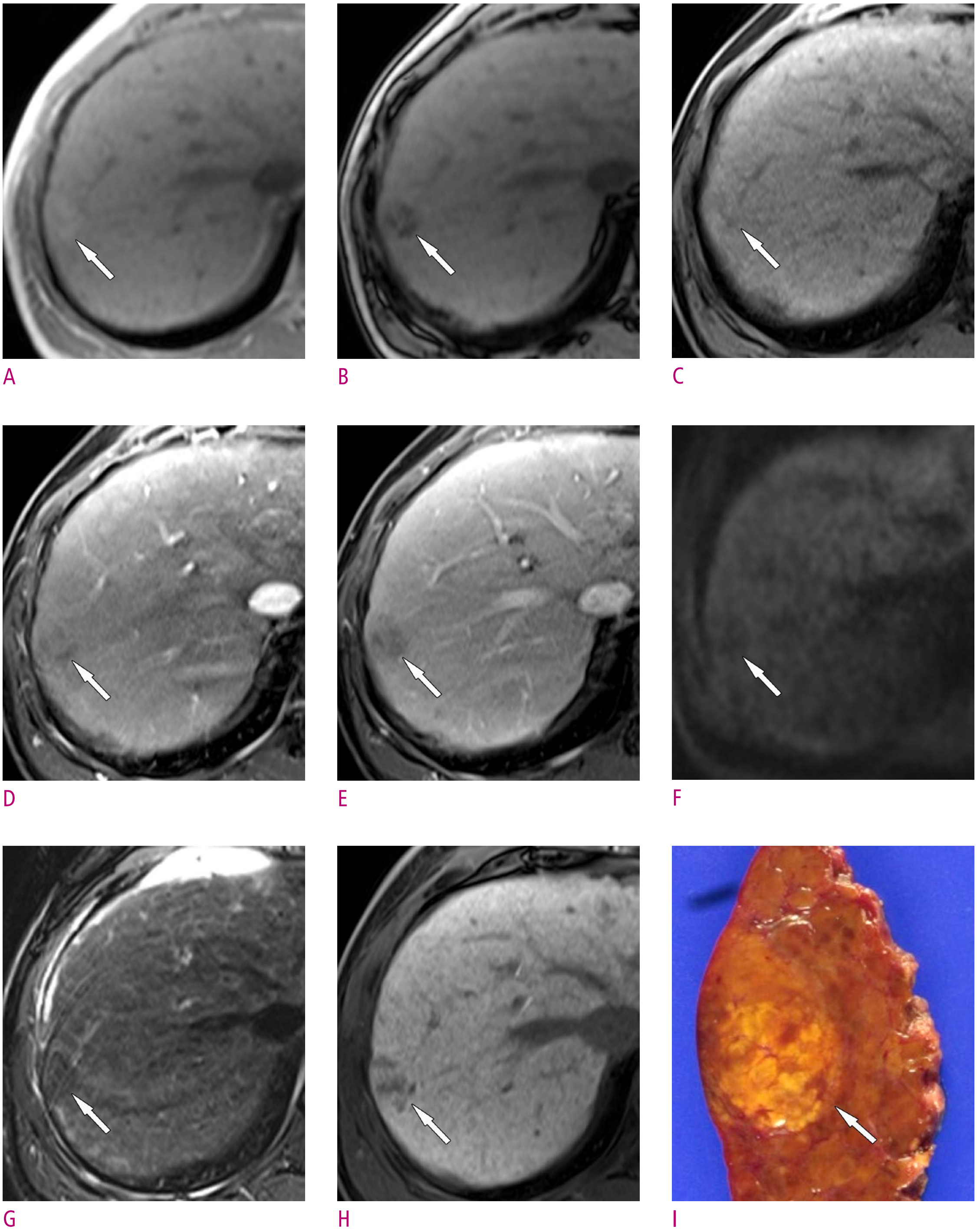

Fig. 3. Magnetic resonance images of an early hepatocellular carcinoma lesion in a 57-year-old woman who underwent hepatic resection. (A) The in-phase and (B) opposed-phase T1-weighted magnetic resonance images show fatty change within the tumor (arrows). Compared with (C) the pre-contrast T1-weighted image, the tumor shows no definite hyperenhancement (arrow) on (D) the hepatic arterial phase image. (E) The portal venous phase demonstrates hypointensity of the tumor (arrow). The tumor shows hypointensity (arrows) on (F) the diffusion-weighted image ($b = 800$ sec/mm^2) and (G) T2-weighted image. (H) The hepatobiliary phase image shows hypointensity of the tumor (arrow). (I) The gross surgical specimen shows a 2.2-cm early hepatocellular carcinoma lesion (arrow).

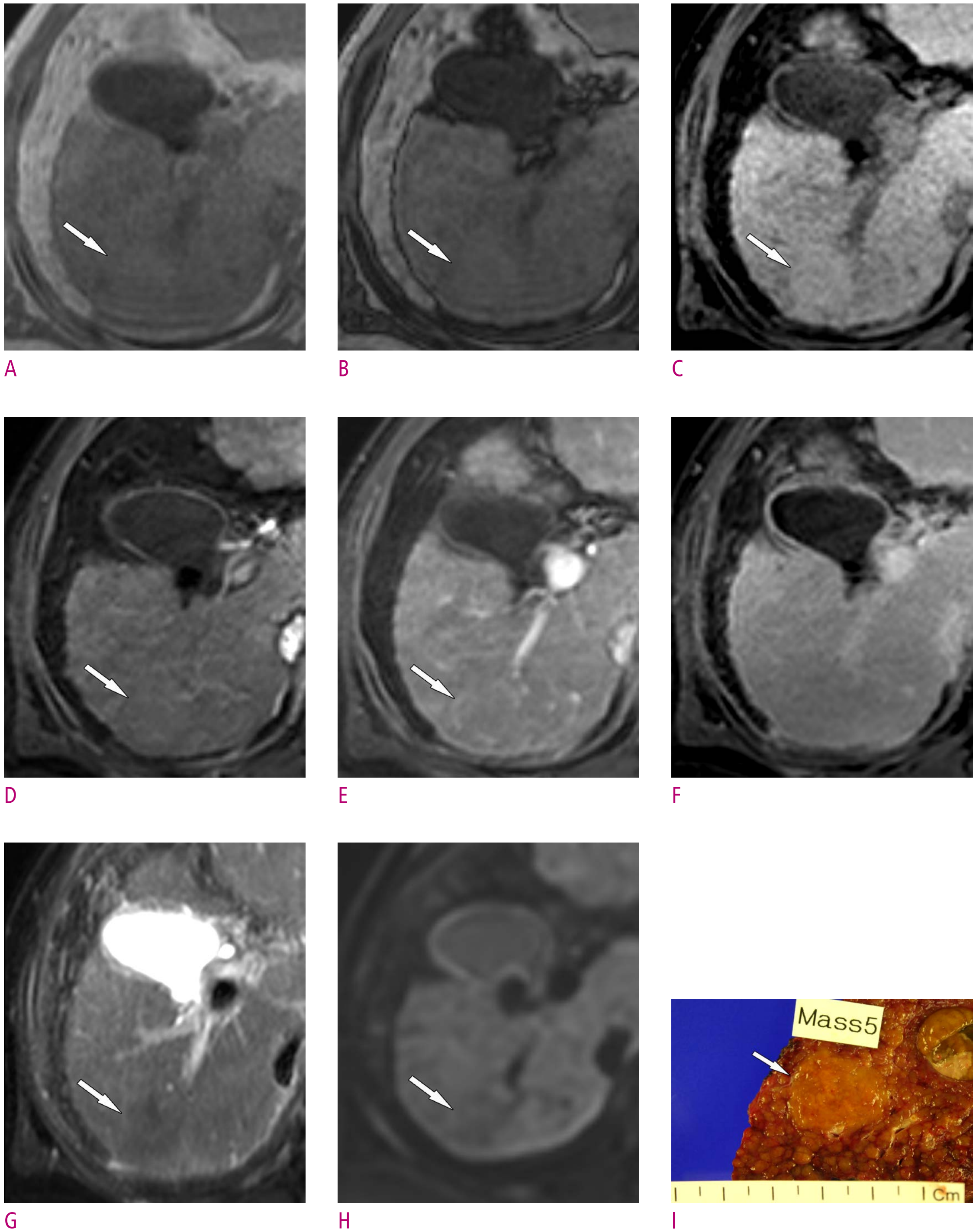

Fig. 4. Magnetic resonance images of an early hepatocellular carcinoma lesion in a 54-year-old woman who underwent liver transplantation. This lesion was not prospectively detected on a radiologic report, but was identified after retrospective review. (A) The in-phase and (B) opposed-phase T1-weighted images show no fatty change within the tumor (arrow). (C) The pre-contrast T1-weighted image shows mild hyperintensity of the tumor (arrow). (D) The hepatic arterial phase image and (E) portal venous phase demonstrate no arterial phase hyperenhancement or washout of the tumor (arrows). The tumor shows isointensity on (F) the hepatobiliary phase. Note that the quality of the hepatobiliary phase was poor, with a functional liver imaging score of 0. The tumor shows hypointensity (arrows) on (G) the T2-weighted image and (H) diffusion-weighted image (b = 800 sec/mm^2). (I) The gross surgical specimen shows a 2-cm early hepatocellular carcinoma lesion (arrow).

Table 3. Factors associated with the false-negative detection of early hepatocellular carcinoma: Per-patient analysis

	Univariate Analysis			Multivariate Analysis		
	Odds ratio	95% CI	P value	Odds ratio	95% CI	P value
Age	0.95	0.89-1.00	0.062			
History of HCC						
No						
Yes	0.33	0.13-0.82	0.016	0.34	0.13-0.92	0.033
Type of surgery						
Resection						
LT	0.32	0.13-0.76	0.010			
Pathologic cirrhosis						
No						
Yes	0.30	0.08-1.08	0.065			
No. of HCC						
One						
Two or more	0.09	0.01-0.68	0.020	0.08	0.01-0.66	0.020
No. of eHCC						
One						
Two or more	0.30	0.12-0.75	0.009			
Presence of progressed HCC						
No						
Yes	0.86	0.34-2.17	0.742			
Child-Pugh score						
A			0.204			
B	0.61	0.21-1.80	0.374			
C	0.13	0.01-1.53	0.105			
ALBI grade						
1			0.636			
2	0.96	0.37-2.49	0.594			
3	0.56	0.16-1.91	0.354			
Hepatobiliary phase						
EnQS						
0			0.041			
1	4.17	0.66-26.29	0.129			
2	6.84	1.50-31.18	0.013			
ExQS						
0			0.319			
1	2.00	0.20-19.91	0.554			
2	3.68	0.49-27.64	0.205			
PVsQS						
0			0.204			
1	1.83	0.20-16.51	0.589			
2	3.90	0.52-29.42	0.187			

Continued

Table 3. Continued

	Univariate Analysis			Multivariate Analysis		
	Odds ratio	95% CI	P value	Odds ratio	95% CI	P value
FLIS						
0-3	0.18	0.06-0.57	0.004	0.13	0.04-0.51	0.003
4-6						
Dynamic phase						
Poor-fair						
Good-excellent	1.50	0.52-4.36	0.457			
T2WI						
Poor-fair						
Good-excellent	4.73	1.17-19.04	0.029			
DWI						
Poor-fair						
Good-excellent	2.42	0.84-7.02	0.102			

CI, confidence interval; HCC, hepatocellular carcinoma; eHCC, early HCC; LT, liver transplantation; ALBI, albumin-bilirubin; EnQS, enhancement quality score; ExQS, excretion quality score; PVsQS, portal vein sign quality score; FLIS, functional liver imaging score; T2WI, T2-weighted imaging; DWI, diffusion-weighted imaging.

be considered pseudolesions, because they frequently show isoattenuation or isointensity on late dynamic images.

Our results showed diffusion restriction in just 22% of the detected lesions, comparable with 21% in a study by Kim et al. (17). Moreover, diffusion restriction was seen in only one eHCC without APHE, suggesting that there is limited additional value in using DWI for detecting eHCC. Notably, in our series, capsule appearance was present in 8% of eHCCs, similar to a previous report (9.5%, 4/42) (17). The presence of capsule appearance on EOB-MRI might be extraordinary because eHCCs are, histologically, vaguely nodular tumors with indistinct margins, lacking a tumor capsule (33). However, in the setting of advanced cirrhosis such as explanted livers, eHCC may show a more distinctly nodular appearance because of surrounding cirrhotic septa, not tumor capsule (3, 34, 35). Therefore, the capsule appearance on EOB-MRI may be indicative of a pseudocapsule, caused by the retention of contrast material at lesion margins(30). In addition, eHCCs frequently showed well-defined margins on MRI, especially on HBP images, probably because of the higher tissue contrast on these images.

Strengths of our study include both the prospective and retrospective evaluation of eHCC detection sensitivity. In the prospectively acquired data from preoperative MRI reports, approximately 10% (17/173) of lesions were missed compared with that in retrospective review, which may reflect more realistic data. The retrospective per-lesion detection sensitivity (78%) in our study was comparable to that in a recent study by Kim et al. (71-79%) based on retrospective analysis (17).

We also evaluated factors related to the failure of preoperative detection. First, as expected, false-negative detection was affected by lesion size; eHCCs < 1 cm (21/56 [37%]) were not preoperatively identified, comprising 55% (21/38) of the total false-negative results. Comparatively, only 3% (1/38) of false-negative detection occurred in eHCCs ≥ 2 cm. Second, a history of HCC treatment increased the false-negative detection of eHCCs, probably due to hemodynamic alteration or parenchymal architectural distortion of the liver associated with treatment. Third, the higher false-negative detection rate in patients with multiple HCCs may be attributed to the satisfaction of search error (36, 37). Finally, the quality of HBP enhancement (determined by FLIS) was independently associated with the false-negative detection of eHCCs. Given that the most sensitive imaging feature for the detection of eHCCs was HBP hypointensity, it may be expected that poor HBP quality leads to false-negative detection. Conversely, other laboratory or clinical parameters of hepatic function (including Child-Pugh class or ALBI grade), image quality of T2WI, DWI, and dynamic imaging were not independent factors associated with the false-negative detection of eHCCs on multivariate analysis.

This study also has limitations. First, it may have inherent selection bias due to the retrospective design. For example, as we only included patients who underwent surgical resection, their hepatic function was relatively good, possibly limiting evaluation of the association between hepatic function and false-negative detection. Second, calculation of prospective eHCC detection sensitivity was based on original radiological reports; however, this approach may have provided more realistic results compared to those based on just retrospective review. Third, although the whole liver was available as a reference standard in transplanted patients, the remnant liver in the resection group could not be evaluated. Finally, despite extensive efforts to correlate preoperative MRI with pathological specimens, accurate lesion-by-lesion matching was occasionally difficult, especially for explanted livers.

In conclusion, our study showed that histologically defined eHCCs are most commonly seen as HBP hypointensity. Arterial phase hyperenhancement and washout appearance are seen more frequently than fatty change, diffusion restriction, and capsule appearance. Detection sensitivity may be affected by lesion size, history of HCC treatment, number of HCCs, and hepatobiliary enhancement.

ORCID: Nieun Seo: https://orcid.org/0000-0001-8745-6454; Myeong-Jin Kim: https://orcid.org/0000-0001-7949-5402; Young Nyun Park: https://orcid.org/0000-0003-0357-7967; Mi-Suk Park: https://orcid.org/0000-0001-5817-2444; Jin-Young Choi: https://orcid.org/0000-0002-9025-6274; Yong Eun Chung: https://orcid.org/0000-0003-0811-9578

References

1. Tang A, Hallouch O, Chernyak V, Kamaya A, Sirlin CB. Epidemiology of hepatocellular carcinoma: target population for surveillance and diagnosis. Abdom Radiol (NY) 2018;43:13-25.
2. Zech CJ, Ba-Ssalamah A, Berg T, Chandarana H, Chau GY, Grazioli L, et al. Consensus report from the 8th International Forum for Liver Magnetic Resonance Imaging. Eur Radiol 2020;30:370-382.
3. Park YN. Update on precursor and early lesions of hepatocellular carcinomas. Arch Pathol Lab Med 2011;135:704-715.
4. Oikawa T, Ojima H, Yamasaki S, Takayama T, Hirohashi S, Sakamoto M. Multistep and multicentric development of hepatocellular carcinoma: histological analysis of 980 resected nodules. J Hepatol 2005;42:225-229.
5. Kojiro M. Pathology of early hepatocellular carcinoma: progression from early to advanced. Hepatogastroenterology 1998;45 Suppl 3:1203-1205.
6. International Consensus Group for Hepatocellular NeoplasiaThe International Consensus Group for Hepatocellular N. Pathologic diagnosis of early hepatocellular carcinoma: a report of the international consensus group for hepatocellular neoplasia. Hepatology 2009;49:658-664.
7. Takayama T, Makuuchi M, Hirohashi S, Sakamoto M, Yamamoto J, Shimada K, et al. Early hepatocellular carcinoma as an entity with a high rate of surgical cure. Hepatology 1998;28:1241-1246.
8. Inoue K, Takayama T, Higaki T, Watanabe Y, Makuuchi M. Clinical significance of early hepatocellular carcinoma. Liver Transpl 2004;10:S16-19.
9. Kudo M. Early hepatocellular carcinoma: definition and diagnosis. Liver Cancer 2013;2:69-72.
10. An C, Choi GH, Lee HS, Kim MJ. Assessment of preoperative magnetic resonance imaging staging in patients with hepatocellular carcinoma undergoing resection compared with the seventh American Joint Committee on Cancer System. Invest Radiol 2012;47:634-641.
11. Rhee H, Kim MJ, Park MS, Kim KA. Differentiation of early hepatocellular carcinoma from benign hepatocellular nodules on gadoxetic acid-enhanced MRI. Br J Radiol 2012;85:e837-844.
12. Chon YE, Jung KS, Kim MJ, Choi JY, An C, Park JY, et al. Predictors of failure to detect early hepatocellular carcinoma in patients with chronic hepatitis B who received regular surveillance. Aliment Pharmacol Ther 2018;47:1201-1212.
13. Tsuboyama T, Onishi H, Kim T, Akita H, Hori M, Tatsumi M, et al. Hepatocellular carcinoma: hepatocyte-selective enhancement at gadoxetic acid-enhanced MR imaging--correlation with expression of sinusoidal and canalicular transporters and bile accumulation. Radiology 2010;255:824-833.
14. Hwang GJ, Kim MJ, Yoo HS, Lee JT. Nodular hepatocellular carcinomas: detection with arterial-, portal-, and delayed-

phase images at spiral CT. Radiology 1997;202:383-388.
15. Sano K, Ichikawa T, Motosugi U, Sou H, Muhi AM, Matsuda M, et al. Imaging study of early hepatocellular carcinoma: usefulness of gadoxetic acid-enhanced MR imaging. Radiology 2011;261:834-844.
16. Rhee H, Kim MJ, Park YN, Choi JS, Kim KS. Gadoxetic acid-enhanced MRI findings of early hepatocellular carcinoma as defined by new histologic criteria. J Magn Reson Imaging 2012;35:393-398.
17. Kim BR, Lee JM, Lee DH, Yoon JH, Hur BY, Suh KS, et al. Diagnostic Performance of Gadoxetic Acid-enhanced Liver MR Imaging versus Multidetector CT in the Detection of Dysplastic Nodules and Early Hepatocellular Carcinoma. Radiology 2017;285:134-146.
18. Ichikawa T, Sano K, Morisaka H. Diagnosis of Pathologically Early HCC with EOB-MRI: Experiences and Current Consensus. Liver Cancer 2014;3:97-107.
19. Kim YY, An C, Kim S, Kim MJ. Diagnostic accuracy of prospective application of the Liver Imaging Reporting and Data System (LI-RADS) in gadoxetate-enhanced MRI. Eur Radiol 2018;28:2038-2046.
20. Piana G, Trinquart L, Meskine N, Barrau V, Beers BV, Vilgrain V. New MR imaging criteria with a diffusion-weighted sequence for the diagnosis of hepatocellular carcinoma in chronic liver diseases. J Hepatol 2011;55:126-132.
21. Park MS, Kim S, Patel J, Hajdu CH, Do RK, Mannelli L, et al. Hepatocellular carcinoma: detection with diffusion-weighted versus contrast-enhanced magnetic resonance imaging in pretransplant patients. Hepatology 2012;56:140-148.
22. Renzulli M, Biselli M, Brocchi S, Granito A, Vasuri F, Tovoli F, et al. New hallmark of hepatocellular carcinoma, early hepatocellular carcinoma and high-grade dysplastic nodules on Gd-EOB-DTPA MRI in patients with cirrhosis: a new diagnostic algorithm. Gut 2018;67:1674-1682.
23. Child CG, Turcotte JG. Surgery and portal hypertension. Major Probl Clin Surg 1964;1:1-85.
24. Pugh RN, Murray-Lyon IM, Dawson JL, Pietroni MC, Williams R. Transection of the oesophagus for bleeding oesophageal varices. Br J Surg 1973;60:646-649.
25. Johnson PJ, Berhane S, Kagebayashi C, Satomura S, Teng M, Reeves HL, et al. Assessment of liver function in patients with hepatocellular carcinoma: a new evidence-based approach-the ALBI grade. J Clin Oncol 2015;33:550-558.
26. Roskams T, Kojiro M. Pathology of early hepatocellular carcinoma: conventional and molecular diagnosis. Semin Liver Dis 2010;30:17-25.
27. Bastati N, Wibmer A, Tamandl D, Einspieler H, Hodge JC, Poetter-Lang S, et al. Assessment of Orthotopic Liver Transplant Graft Survival on Gadoxetic Acid-Enhanced Magnetic Resonance Imaging Using Qualitative and Quantitative Parameters. Invest Radiol 2016;51:728-734.
28. American College of Radiology. Liver imaging reporting and data system (LI-RADS). American College of Radiology. Web site. https://www.acr.org/Clinical-Resources/Reporting-and-Data-Systems/LI-RADS/CT-MRI-LI-RADS-v2017. Accessed June 1, 2017.
29. An C, Rhee H, Han K, Choi JY, Park YN, Park MS, et al. Added value of smooth hypointense rim in the hepatobiliary phase of gadoxetic acid-enhanced MRI in identifying tumour capsule and diagnosing hepatocellular carcinoma. Eur Radiol 2017;27:2610-2618.
30. Ishigami K, Yoshimitsu K, Nishihara Y, Irie H, Asayama Y, Tajima T, et al. Hepatocellular carcinoma with a pseudocapsule on gadolinium-enhanced MR images: correlation with histopathologic findings. Radiology 2009;250:435-443.
31. Landis JR, Koch GG. The measurement of observer agreement for categorical data. Biometrics 1977;33:159-174.
32. Kitao A, Matsui O, Yoneda N, Kozaka K, Shinmura R, Koda W, et al. The uptake transporter OATP8 expression decreases during multistep hepatocarcinogenesis: correlation with gadoxetic acid enhanced MR imaging. Eur Radiol 2011;21:2056-2066.
33. Desmet VJ. East-West pathology agreement on precancerous liver lesions and early hepatocellular carcinoma. Hepatology 2009;49:355-357.
34. Roncalli M, Park YN, Di Tommaso L. Histopathological classification of hepatocellular carcinoma. Dig Liver Dis 2010;42 Suppl 3:S228-234.
35. Theise ND, Park YN, Kojiro M. Dysplastic nodules and hepatocarcinogenesis. Clin Liver Dis 2002;6:497-512.
36. Waite S, Scott J, Gale B, Fuchs T, Kolla S, Reede D. Interpretive Error in Radiology. AJR Am J Roentgenol 2017;208:739-749.
37. Degnan AJ, Ghobadi EH, Hardy P, Krupinski E, Scali EP, Stratchko L, et al. Perceptual and Interpretive Error in Diagnostic Radiology-Causes and Potential Solutions. Acad Radiol 2019;26:833-845.

조직학적 조기 간세포암의 가도세틱산 조영증강영상과 확산강조 자기공명영상 소견

서니은[1], 김명진[1], 박영년[2], 박미숙[1], 최진영[1], 정용은[1]

[1]*연세대학교 의과대학 세브란스병원 영상의학과*

[2]*연세대학교 의과대학 세브란스병원 병리과*

목 적: 조직학적 조기 간세포암의 가도세틱산 조영증강 영상과 확산강조 자기공명영상 소견을 살펴보고자 한다.

대상과 방법: 2006년 1월부터 2017년 9월까지 가도세틱산 조영증강 영상과 확산강조 자기공명영상을 시행 후 수술로 조기 간세포암으로 진단된 환자 119명의 173개의 병변이 연구대상으로 포함되었다. 수술 전 발견된 조기 간세포암의 영상 소견을 2명의 영상의학과 전문의가 후향적으로 분석하였다. 조기 간세포암의 가음성 진단과 관련된 임상적, 영상의학적 요인을 평가하였다.

결 과: 119명의 173개 조기 간세포암 중에서 78명의 118개 (68%)의 조기 간세포암이 수술 전 영상에서 판독되었다. 후향적 리뷰 후에 13명의 17개 조기 간세포암이 추가로 발견되었으며, 병변별 진단 민감도는 78% (135/173)였다. 따라서 91명 환자의 135개의 조기 간세포암의 영상소견이 분석되었다. 대부분의 조기 간세포암은 간담도기 저신호강도를 보였다 (90%, 122/135). 동맥기 과조영증강, 씻김 현상 (washout), 캡슐 양상은 각각 68 (50%), 79 (59%), and 11 (8%)개 병변에서 관찰되었다. 확산 제한과 지방 변화는 30 (22%), 39 (29%)개에서 관찰되었다. 대부분의 조기 간세포암은 T1 및 T2 강조영상에서 동일 신호강도를 보였다 (80 [59%], 89 [66%]). 가음성 진단은 작은 병변 크기 (< 1 cm), 간세포암 치료 기왕력 (odds ratio, 0.34 [95% 신뢰구간, 0.13-0.92]), 간세포암 개수 (≥ 2; odds ratio, 0.08 [0.01-0.66]), 낮은 간기능영상 점수 (< 4; odds ratio, 0.13 [0.04-0.51])와 유의한 관련이 있었다.

결 론: 조직학적 조기 간세포암은 전형적으로 간담도기 영상 저신호강도를 보인다. 조기 간세포암의 진단 민감도는 병변의 크기, 간세포암 치료 기왕력, 간세포암 개수, 그리고 간담도기 조영증강에 영향을 받을 수 있다.

www.e-kjar.org
https://doi.org/10.52668/kjar.2021.00059

pISSN 2586-1719 / eISSN 2799-3299

Korean J Abdom Radiol 2021;5:32-41

Original Article

Effect of Different Iterative Reconstruction Algorithms on Ultra-Low Dose CT of Inflammatory Bowel Disease in a Rabbit Model

Cheong-Il Shin[1,2], Se Hyung Kim[1,2,4], Mi Hye Yu[3], Ijin Joo[1,2], Joon Koo Han[1,2,4]

[1] *Department of Radiology, Seoul National University Hospital, Seoul, Korea*
[2] *Department of Radiology, Seoul National University College of Medicine, Seoul, Korea*
[3] *Department of Radiolgy, Konkuk University Medical Center, Seoul, Korea*
[4] *Institute of Radiation Medicine, Seoul National University Medical Research Center, Seoul, Korea*

Purpose: To evaluate the feasibility of ultra-low dose 80 kVp CT for the evaluation of inflammatory bowel disease (IBD) in a rabbit model and to investigate the effect of two different iterative reconstruction (IR) algorithms on 80 kVp CT in terms of image quality and diagnostic performance in comparison with same session conventional 120 kVp images.

Materials and Methods: This study was approved by the Animal Care and Use Committee of our hospital. Twenty-eight New Zealand white rabbits were randomly divided into two groups: IBD group (n=18) and a control group (n=10). To create an acute IBD model, 3mL of a 5% w/v tri-nitrobenzene sulfonic acid solution was administered to the sigmoid colon of the rabbits. CT was performed at 80 kVp and 120 kVp and was reconstructed using filtered back projection (FBP), hybrid statistic-based IR, and full IR algorithms for 80 kVp and using FBP only for 120 kVp. Effective radiation dose, image noise, image quality, and diagnostic performance by two reviewers were recorded and compared using repeated measure analysis of variance, McNemar test, and receiver operating curve (ROC) analysis.

Results: Mean effective radiation dose of 80 kVp CT (0.05 mSv) was significantly lower than that (0.285 mSv) of 120 kVp CT. Mean image noise was highest in the 80 kVp FBP setting (60.36) but significantly decreased with IR algorithms (47.02 with hybrid IR and 12.92 with full IR) ($P<0.0001$). Mean overall image quality score was lowest in the 80 kVp FBP setting (1.57 and 1.46 for reviewers 1 and 2, respectively) but significantly improved with IR algorithms (2.43 and 2.25 for hybrid IR and 4.79 and 4.93 for full IR) ($P<0.0001$). Sensitivity and area under the curve (AUC) for differentiating a normal bowel from IBD was lowest with 80 kVp FBP (61.1% and 83.3%; 0.883 and 0.967) but improved with IR algorithms (83.3%~100%; 0.992~1), to similar levels as the 120 kVp FBP setting (100% and 1). Differences in sensitivity and AUC between 80 kVp FBP and 80 kVp IR algorithms were statistically significant in reviewer 1.

Conclusions: Ultra-low dose 80 kVp CT in a rabbit IBD model is not feasible using the standard FBP algorithm.

Received: June 9, 2021 **Revised:** June 25, 2021 **Accepted:** June 26, 2021
Correspondence: Se Hyung Kim, MD
Department of Radiology and the Institute of Radiation Medicine, Seoul National University Hospital, 101 Daehangno, Jongno-gu, Seoul 03080, Korea
Tel: +82-2-2072-2057 Fax: +82-2-743-6385 E-mail: shkim7071@gmail.com

However, with the application of IR algorithms, diagnostic performance of 80 kVp CT was acceptable and on par with that at conventional 120 kVp FBP.

Keywords: CT; Ultra-low dose; Iterative reconstruction; Animal model; Inflammatory bowel disease

---

Introduction

CT is widely regarded as the imaging modality of choice for the evaluation of patients with known or suspected small-bowel disease (1, 2). Yet, despite the known utility of CT in assessing patients with inflammatory bowel disease (IBD), radiation exposure remains a major concern in this particular population as patients with IBD are more likely to be younger and to be imaged multiple times leading to increased cumulative radiation exposure over their lifetimes (3). Among the several dose reduction approaches used in CT, reduction of the tube voltage from conventional 120 kVp to 80 kVp has been highlighted as it can potentially reduce organ dosage by up to 65% while providing the added advantage of increased iodine attenuation by a factor of 1.7 as the k-edge of iodine is closer to the reduced tube voltage (4, 5). However, a main limitation of low tube voltage CT for abdominal applications is the concern of image quality loss owing to increased image noise and higher susceptibility to beam-hardening artifacts (6).

Recently, the development of newer image reconstruction algorithms has demonstrated the potential to overcome the increased noise that comes with low tube voltage CT techniques by generating images with less noise than those reconstructed with the standard filtered back projection (FBP) algorithm (7-14). Among them, adaptive statistical iterative reconstruction (ASIR) is an algorithm which repeats successive iterative transformations of the measured value of each pixel to a new estimated pixel value while comparing it to the ideal value that the noise model predicts until the final estimated and ideal pixel values converge (8-11). A more recent model-based iterative reconstruction (MBIR) product in the market, Veo, uses real 3-dimensional system optics instead of idealized system optics, directly weighing each measured projection point, thereby leading to improved overall image quality while reducing more noise than ASIR (9-11).

There has been one previous report showing the effectiveness of 80 kVp CT using these IR algorithms for small bowel diseases, however, the study was retrospectively designed and compared 80 kVp CT with 120 kVp CT in different patient groups (8). In addition, although both 80 kVp CT and 120 kVp CT were imaged in the same patient in some cases, there was a time gap between the two images in which disease activity may have been significantly different between the two CT datasets, making a direct side-by-side comparison between conventional 120 kVp and 80 kVp CT images impossible (8).

Therefore, the purpose of our study is to evaluate the feasibility of ultra-low dose 80 kVp CT for the evaluation of IBD in a rabbit model and to investigate the effect of two different IR algorithms at 80 kVp CT on image quality and diagnostic performance in comparison to same session conventional 120 kVp images.

Materials and Methods

This study was carried out in strict accordance with the recommendations in the Guide for the Care and Use of Laboratory Animals of. The protocol was approved by the Animal Care and Use Committee of Seoul National University Hospital (Permit Number: 14-0154-S1A2). The institutional review board waived the need to obtain informed consent because this study was an animal study.

Animals

Twenty-eight male New Zealand white rabbits weighing 2.5-3.0 kg were randomly divided into two groups: 18 in the IBD group and 10 in the control group. Prior to the procedures, the rabbits were anesthetized with an intramuscular injection of a mixture of zolazepam (5 mg/kg, Zoletil®; Virbac, Carros Cedex, France) and xylazine (10 mg/kg, Rompun®; Bayer-Schering Pharma, Berlin, Germany).

Rabbit Model of Inflammatory Bowel Disease

After the rabbit was anesthetized, an enema was done with 100 ml of saline to remove the feces in the rectosigmoid colon. After the enema, a Foley catheter (12 Fr, Yushin medical, Korea) was inserted via the anus placing the tip at the iliac artery bifurcation level under the guidance of ultrasonography (Accuvix XQ, Samsung Medison, Korea) using a 5-12 MHx linear probe. Ballooning was done with 2 mL of normal saline not to spill out the solution. To induce colitis, 3 mL of 5% weight/volume 2, 4, 6 tri-nitrobenzene sulfonic acid (TNBSA) solved in methanol (Pierce Biotechnology, IL, USA) was administrated via the Foley catheter. To ensure the distribution of the TNBSA solution in the sigmoid colon, all rabbits were carefully maintained at a 30° head down position for 10 minutes and then returned to their cages.

CT Acquisition

All 28 CT examinations were performed on a 64-row MDCT scanner (Discovery CT750 HD, GE Healthcare, USA). Neutral oral or rectal contrast material was not used in any of the animals. All rabbits received 6 mL of nonionic iodinated contrast material with an iodine concentration of 350 mg/mL (iohexol; Iobrix 350, TaeJoon Pharm, Korea) followed by a 5 mL saline flush at a rate of 1.2 mL/s injected with a mechanical power injector. Each rabbit was scanned at 80 kVp first, followed by 120 kVp, after a default delay. The first 80 kVp scanning was initiated in the portal venous phase 40 seconds after the administration of the contrast bolus and ranged from the dome of the diaphragm to the perineum. In all 80 and 120 kVp examinations, the following imaging parameters were utilized: scan type, helical; gantry rotation time, 0.5 seconds; detector configuration, 0.625 mm × 64; pitch, 0.984; and speed, 79 mm/s. The tube currents utilized were 10 mA (5 mAs) and 20 mA (10 mAs) at 80kVp and 120 kVp, respectively. The FBP algorithm was used for image reconstruction of all 80 kVp and 120 kVp examinations and 50% ASIR and MBIR were additionally used for image reconstruction of 80 kVp examinations. Thus, four CT datasets (80 kVp FBP, 80 kVp 50% ASIR, 80 kVp MBIR, 120 kVp FBP) for each of the 28 rabbits yielded a total of 112 image sets. All images were reconstructed with axial 1.25 mm slice thickness at 1.25 mm intervals.

Effective Dose Estimation

Scanner-generated volume CT dose index ($CTDI_{vol}$) and dose length product (DLP) were recorded for each examination. Effective dose (ED) for the examination was calculated by multiplying the DLP by a factor of 0.015, which is the dose conversion factor for CT of the abdomen and pelvis according to the guidelines provided in Publication 60 of the International Commission on Radiological Protection (15).

Quantitative Image Analysis

Quantitative analysis was performed on picture archiving and communication system (PACS) workstations (PacsViewer, Infinitt, Seoul, Korea) using high-resolution monitors (2048x2560, Barco, Belgium). An abdominal radiologist with 11 years of experience (C.I.S.) measured image noise by recording the standard deviation (SD) of attenuation in Hounsfield units within a 0.3-cm^2 region of interest (ROI) placed in both the paraspinal muscles and in retroperitoneal fat at the level of the second lumbar vertebral body. All of the ROIs were placed in the same location for each of the reconstructed datasets using the copy and paste function of the PACS software. The average SD of the three measurements was recorded as the image noise.

Qualitative Image Analysis

Two board-certified abdominal radiologists (S.H.K. and C.I.S. with 18 and 11 years of experience, respectively), blinded to the scan technique, independently reviewed the axial CT images on a workstation in random order. In their review, four characteristics of each examination as described below were evaluated according to a previously described method on a 5-point scale, with 1 being the lowest and 5 the best (1 = poor, 2 = acceptable, 3 = good, 4 = very good, 5 = excellent): The first characteristic was the adequacy of the examination for bowel imaging, in which the reviewers evaluated their ability to identify fold patterns in a distended loop bowel and to differentiate normal from abnormal bowel loops in patients with suspected bowel disease. The second characteristic was the visibility of mesenteric vessels, in which the reviewers evaluated their ability to identify vessels in the adjacent mesentery within 1 cm of the bowel wall. The third characteristic was the evaluation of the liver, in which the reviewers assessed whether there was preservation of a sharp outline of the liver and portal venous branches and assessed the level of parenchymal noise. Finally, the fourth characteristic was the overall quality of the study, in which reviewers assessed whether the examination was adequate for interpretation and whether there was image noise that might obscure pathologic findings.

Evaluation for Diagnostic Performance

To evaluate the diagnostic performance of the 80 kVp CT technique in comparison with the 120 kVp, two different abdominal radiologists (M.H.Y. and I.J. with 8 years of experience) evaluated all 112 CT examinations in random order in a separate reading session. They were blinded to the final diagnosis for the presence or absence of IBD and to which segments of the bowel were involved in cases of disease. The presence or absence of IBD was recorded on a 5-point scale: 1, definitely normal; 2, probably normal; 3, possibly IBD; 4, probably IBD; 5, definitely IBD. Animals with recorded grades of 3-5 were grouped as having IBD while those with grades of 1 and 2 were considered to be normal and without bowel disease.

Statistical Analysis

All statistical analyses were performed using SPSS statistical software version 21.0 (IBM, Armonk, NY, USA) and Graphad Prism version 6 (GraphPad Software, La Jolla, CA, USA). The paired t test was used to assess statistically significant differences in $\mathrm{CTDI}_{\mathrm{vol}}$, DLP, and ED between the 80 kVp and 120 kVp settings. Image noise and subjective scores of image quality parameters of the four image datasets were compared using repeated measure analysis of variance. A p value of < 0.05 was considered to indicate a statistically significant difference. For evaluation of the diagnostic performance in differentiating a normal bowel from IBD, sensitivity, specificity, and areas under the curve (AUCs) of the image datasets were calculated and compared using the McNemar test and receiver operating characteristics (ROC) analysis.

Results

Radiation Dose

The paired t test revealed that mean CTDIvol, DLP, and ED at the 80 kVp setting (0.13 mGy, 3.30 mGy-cm, 0.050 mSv) were significantly lower than those at the 120 kVp setting (0.77 mGy, 19.02 mGy-cm, 0.285 mSv) (P < 0.0001) (Table 1), resulting in a dose reduction of 82.5% at 80 kVp compared to the 120 kVp setting.

Quantitative Image Analysis: Image Noise

The results of quantitative analysis are summarized in Table 2. Among the four settings, mean image noise was highest at 80 kVp with FBP reconstruction, followed by 80 kVp ASIR, 120 kVp FBP, and 80 kVp MBIR in descending order (mean ± standard deviation; 60.36 ± 8.01, 47.02 ± 6.33, 23.48 ± 1.92, and 12.92 ± 1.25, respectively). With FBP reconstruction, the mean image noise of the 80 kVp setting was significantly higher than that of the 120 kVp setting (60.36 vs. 12.92; P < 0.0001). In the 80 kVp setting, image noise was significantly reduced by 22.1% (13.34/60.36) and 78.6% (47.44/60.36) with ASIR and MBIR reconstruction, respectively (P < 0.0001), compared to that using standard FBP reconstruction. Representative images are presented in Figure 1.

Qualitative Image Analysis

In terms of image quality, both reviewers recorded their highest scores at 80 kVp MBIR, followed by 120 kVp FBP, 80 kVp ASIR and 80 kVp FBP for all four characteristics (Table 2 and Fig. 2). There were significant differences in image quality scores among the four datasets in terms of the four characteristics (P < 0.0001). On post-hoc analysis, all comparisons of the image quality characteristics among the four datasets also showed statistical differences with P values < 0.0001 except for the comparisons between 120 kVp FBP and 80 kVp MBIR for bowel wall evaluation

Table 1. Radiation Dose at 80 and 120 kVp CT for Evaluation of Inflammatory Bowel Disease in a Rabbit Model

	80 kVp	120 kVp	P value[‡]
Volume CT Dose Index ($\mathrm{CTDI}_{\mathrm{vol}}$, mGy)	0.13	0.77	
Dose Length Product (DLP, mGy·cm)*	3.30 ± 0.58	19.02 ± 0.24	<0.0001
Effective dose (ED, mSv)*[†]	0.050 ± 0.009	0.285 ± 0.004	<0.0001

*Values are expressed as means ± standard deviations. [†]Effective radiation dose was estimated by multiplying DLP by a conversion factor of 0.015. [‡]P values were obtained using the paired t-test.

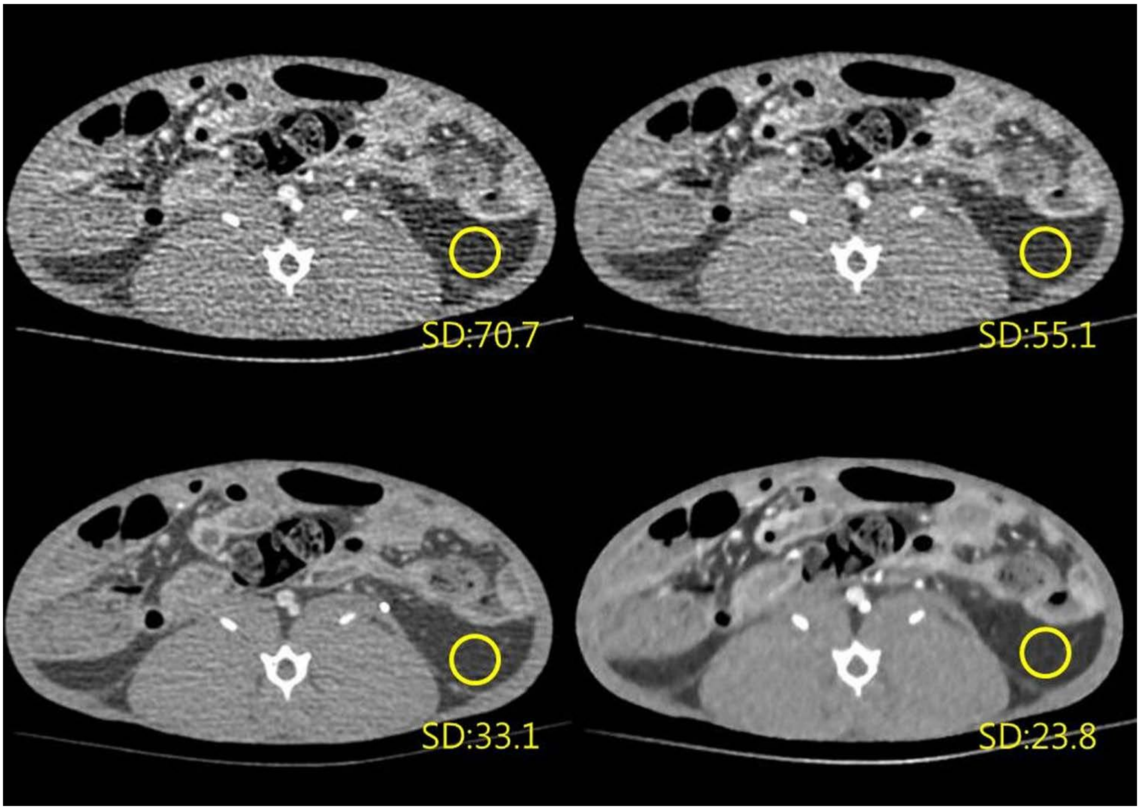

Fig. 1. 80 and 120 kVp CT images using various reconstruction algorithms. Image noise was the highest at 80 kVp with FBP reconstruction (70.7, upper left), followed by 80 kVp 50% ASIR (55.1, upper right), 120 kVp FBP (33.1, lower left), and 80 kVp MBIR (23.8, lower right).

Table 2. Image Noise and Image Quality Scores for Four Characteristics Assessed by Two Reviewers

Category Evaluated by Reviewers	Image Noise and Image Quality Score* (Mean ± Standard Deviation)				
	80 kVp FBP	80 kVp ASIR	120 kVp FBP	80 kVp MBIR	P value[†]
Image Noise					
	60.36 ± 80.1	47.02 ± 6.33	23.48 ± 1.92	12.92 ± 1.25	<0.0001
Reviewer 1					
Bowel wall	1.43 ± 0.50	2.25 ± 0.70	4.21 ± 0.50	4.71 ± 0.46	< 0.0001
Mesenteric vessels	1.96 ± 0.79	2.50 ± 0.64	3.93 ± 0.38	4.82 ± 0.39	< 0.0001
Liver	1.64 ± 0.62	2.34 ± 0.74	3.96 ± 0.19	4.86 ± 0.36	< 0.0001
Overall image adequacy	1.57 ± 0.50	2.43 ± 0.63	4.14 ± 0.36	4.79 ± 0.42	< 0.0001
Reviewer 2					
Bowel wall	1.29 ± 0.46	2.04 ± 0.69	4.21 ± 0.50	4.71 ± 0.46	< 0.0001
Mesenteric vessels	1.71 ± 0.71	2.11 ± 0.57	4.11 ± 0.32	4.93 ± 0.26	< 0.0001
Liver	1.71 ± 0.60	2.29 ± 0.53	3.93 ± 0.26	5.00 ± 0.00	< 0.0001
Overall image adequacy	1.46 ± 0.58	2.25 ± 0.65	4.04 ± 0.19	4.93 ± 0.26	< 0.0001

*Image scores range from 1 to 5: 1, poor; 2, acceptable; 3, good; 4, very good; 5, excellent. [†]P values were obtained using the repeated measure ANOVA. FBP=filtered back projection, ASIR=adaptive statistical iterative reconstruction, MBIR=model-based iterative reconstruction

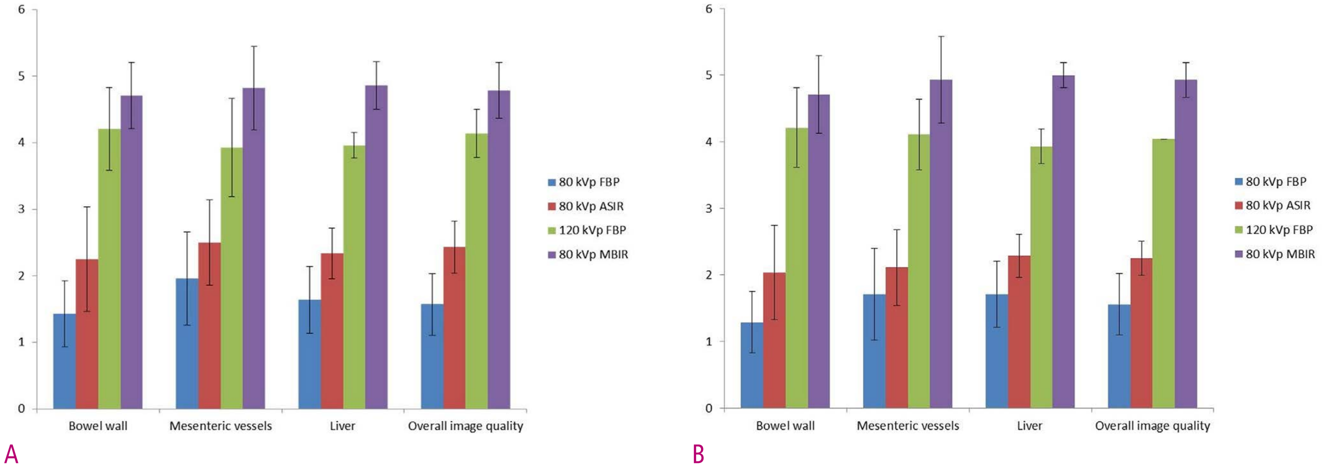

Fig. 2. Bar graphs showing the mean and standard deviation of image quality for the four image quality characteristics by the two reviewers. A. Results of reviewer 1. B. Results of reviewer 2. Regardless of the reviewers or image characteristics, the mean image quality was lowest at 80 kVp FBP, significantly improved with statistic-based IR (ASIR), and further improved with full knowledge-based IR (MBIR) (P<0.0001).

Table 3. Diagnostic Performance for the Differentiation between Normal Bowels and Inflammatory Bowel Disease

	Reviewers	80 kVp FBP	80 kVp ASIR	120 kVp FBP	80 kVp MBIR
Area under the curve	Reviewer 1*	0.883	0.992	1	1
	Reviewer 2	0.967	0.997	1	1
Sensitivity	Reviewer 1[†]	61.1%	83.3%	100%	100%
	Reviewer 2	83.3%	94.4%	100%	100%
Specificity	Reviewer 1	100%	100%	100%	100%
	Reviewer 2	100%	100%	100%	100%

*Significant differences were found in the area under the curve between 80 kVp FBP and the other three settings by reviewer 1. [†]Sensitivity at the 80 kVp FBP setting was significantly lower than those at the 120 kVp FBP and 80 kVp MBIR settings. FBP=filtered back projection, ASIR=adaptive statistical iterative reconstruction, MBIR=model-based iterative reconstruction

by both reviewers (P = 0.019 for reviewer 1, P = 0.028 for reviewer 2) and between 80 kVp FBP and 80 kVp ASIR for mesenteric vessel evaluation by reviewer 2 (P = 0.002).

Diagnostic Performance

Table 3 and Figure 3 demonstrate the individual performances of the two radiologists for the differentiation between normal bowels and IBD. Areas under the curve were highest at 120 kVp FBP (1 for both reviewers) and 80 kVp MBIR settings (1 for both reviewers), followed by 80 kVp ASIR (0.992 and 0.997 for readers 1 and 2, respectively) and the 80 kVp FBP settings (0.883 and 0.967). The difference between 80 kVp FBP and the other three settings was statistically significant for reviewer 1 (P = 0.0143 ~ 0.0163). Sensitivity for differentiation was also highest at 120 kVp FBP (100% for both reviewers) and 80 kVp MBIR settings (100% for both reviewers), followed by 80 kVp ASIR (83.3% and 94.4%) and 80 kVp FBP settings (61.1% and 83.3%). The difference was statistically significant between 80 kVp FBP and 120 kVp FBP and between 80 kVp FBP and 80 kVp MBIR for reviewer 1 (P = 0.0156). Specificity was 100% in all four settings for both reviewers. Representative images are presented in Figure 4.

Discussion

In our study, we found that ultra-low dose 80 kVp/5 mAs CT was not feasible using the standard FBP algorithm owing to severe image noise, poor image quality, and low diagnostic performance. The AUC (0.883) and sensitivity (61.1%) of 80 kVp images reconstructed with

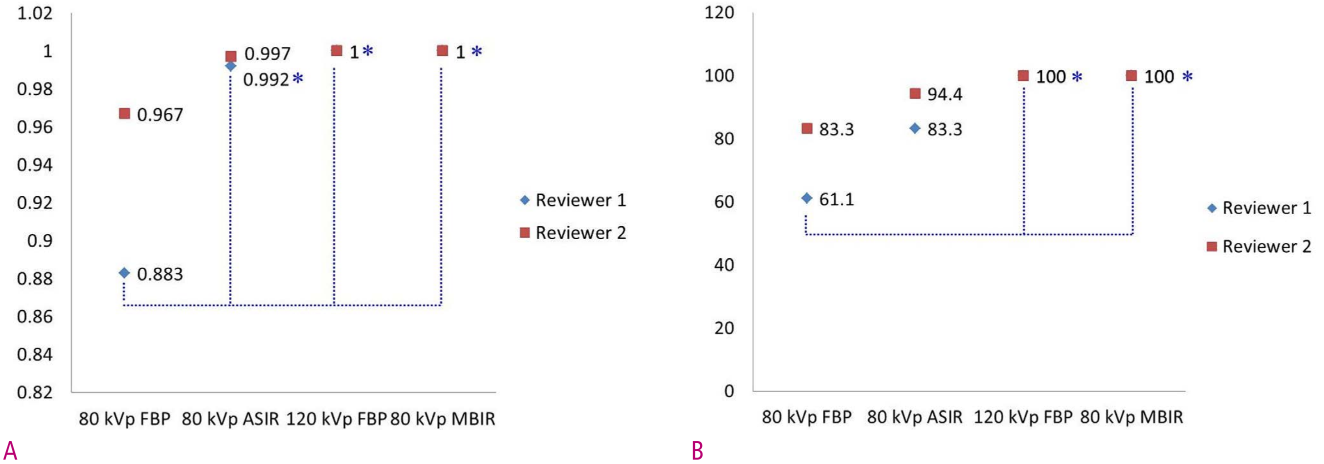

Fig. 3. Dot graphs showing the diagnostic performance in differentiating normal bowels from inflammatory bowel disease in 28 rabbits.
A. Areas under the curve (AUCs) of the two reviewers: The AUC (0.883 and 0.967) of 80 kVp CT reconstructed with the FBP algorithm was the lowest. However, with the application of statistic-based IR (ASIR) and full IR (MBIR) algorithms, AUC on 80 kVp CT improved to 0.992~1, which was not significantly different from that (1) found at the conventional 120 kVp FBP setting. The difference was significant in reviewer 1.
B. Sensitivity of the two reviewers: Sensitivity (61.1% and 83.3%) of 80 kVp CT reconstructed with the FBP algorithm was the lowest. However, with the application of statistic-based IR (ASIR) and full IR (MBIR) algorithms, sensitivity on 80 kVp CT improved to 83.3%~100%, respectively, which was not significantly different from that (100%) found at the conventional 120 kVp FBP setting. The difference was significant in reviewer 1. Significant differences between the settings are shown with dotted lines and *.

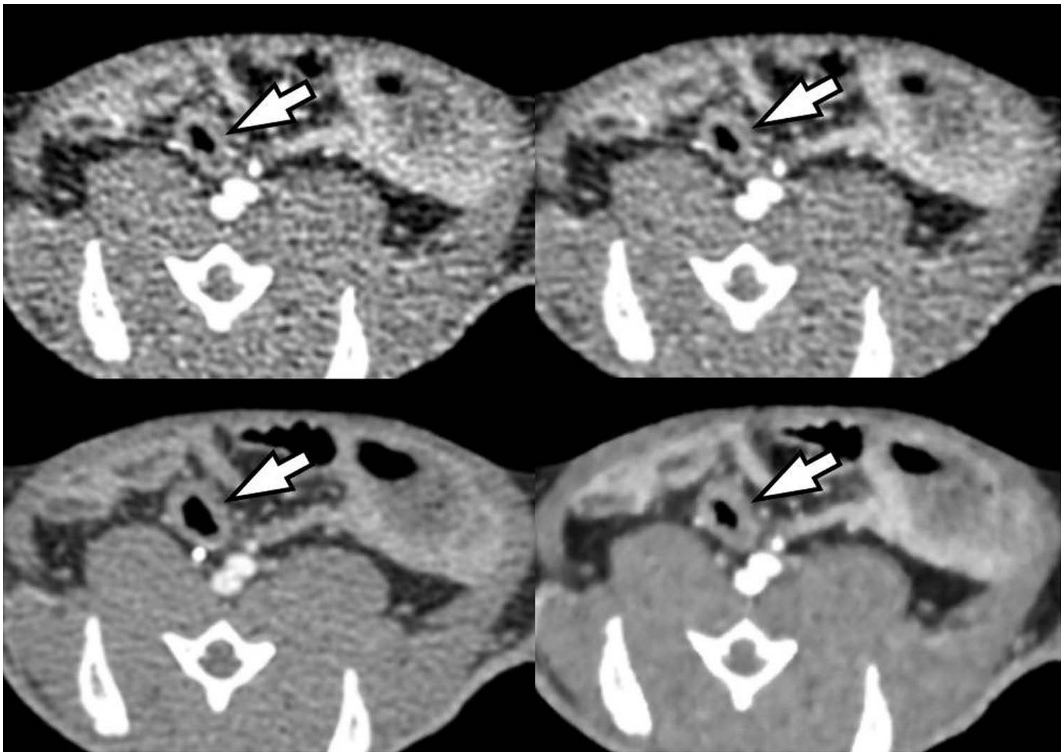

Fig. 4. CT image of acute colitis in a rabbit model. Image noise was the highest at 80 kVp CT with FBP reconstruction (upper left), followed by 80 kVp 50% ASIR (upper right), 120 kVp FBP (lower left), and 80 kVp MBIR (lower right). Due to severe image noise, the two reviewers misinterpreted the thickened inflamed bowel (arrows) as a normal bowel at the 80 kVp FBP setting (upper left). With the other three settings, the two reviewers correctly diagnosed the inflammatory bowel disease.

the FBP algorithm provided the lowest values and was not deemed acceptable for one reviewer (reviewer 1). However, with the application of hybrid IR (ASIR) and full IR (MBIR) algorithms, the AUC and sensitivity of 80 kVp CT improved to 0.992~1 and 83.3%~100%, respectively, which was not significantly different from those found at the conventional 120 kVp FBP setting (1 and 100%). Our observation is of practical importance because we demonstrated that 80 kVp CT using IR algorithms may decrease the risk of radiation exposure while maintaining the quality of diagnostic information, especially in young IBD patients subject to repeated CT examinations. Indeed, the mean effective radiation dose of 80 kVp CT was only 0.05 mSv which is significantly lower than that (0.285 mSv) of conventional 120 kVp CT. Thus, with the application of IR algorithms, we can markedly reduce radiation dose by 82.5% while maintaining diagnostic performance. Although the results of this animal study cannot be directly applicable to those of a human study, our results suggest that low kVp CT at 80 kVp and 5 mAs may be feasible with the aid of IR algorithms on CT.

The superior performance of IR algorithms in comparison with FBP reconstruction can be explained by its effectiveness in noise reduction and prevention of artifacts related to the low tube potential. Indeed, we observed a completely opposite trend between image noise and image quality for all four characteristics in both reviewers. The highest image noise was measured at 80 kVp FBP (60.36), followed by 80 kVp ASIR (47.02), 120 kVp FBP (23.48), and 80 kVp MBIR (12.92), in descending order. Accordingly, the lowest image quality score was achieved at 80 kVp FBP (1.29~1.96), followed by 80 kVp ASIR (2.04~2.50), 120 kVp FBP (3.93~4.21), and 80 kVp MBIR (4.71~5). A similar trend was also observed between image noise and diagnostic performance. The lowest sensitivity and AUC was achieved at 80 kVp FBP (61.1% and 83.3%; 0.883 and 0.967, for readers 1 and 2, respectively), followed by 80 kVp ASIR (83.3% and 94.4%; 0.992 and 0.997), 120 kVp FBP (100%; 1), and 80 kVp MBIR (100%; 1). From these observations, we can deduce that the reduction in image noise may directly reflect the improvement in image quality measured by qualitative scoring as well as by sensitivity and AUC.

In addition to the reduction in image noise, the higher attenuation of iodine at 80 kVp than at 120 kVp may also have been responsible for the highest image quality of 80 kVp MBIR. Reducing the tube voltage from 120 to 80 kVp has the advantage of increasing iodine attenuation by a factor of 1.7 as the k-edge of iodine is closer to the reduced tube voltage (4, 5). This increased attenuation of iodine, in turn, can lead to the increased contrast of vascular structures such as mesenteric vessels and enhanced organs such as the bowel wall and liver. In addition, the increased image contrast obtained at the low kVp setting can be beneficial in evaluating subjects with suspected IBD as changes in the active disease, such as mucosal enhancement and mesenteric hypervascularity, would be readily apparent if the image noise is adequately suppressed (8). Thus, the high image quality and diagnostic performance observed at the 80 kVp MBIR setting in our study may be due to both increased image contrast as well as more effective noise reduction.

In our study, we used both hybrid, statistic-based IR (ASIR) and full knowledge-based IR (MBIR) algorithms to help compensate for the increased image noise in 80 kVp scanning. Although the hybrid IR technique was also able to significantly reduce the image noise on CT compared with FBP reconstruction, a certain amount of image noise and artifacts remained. Such remnant image noise may have been responsible for the intermediate image quality observed with the 80 kVp ASIR setting. On the other hand, full IR was observed to further decrease image noise, generating virtually noise-free images. Knowledge-based full IR is a new algorithm, which unlike previous IR algorithms, does not involve blending with FBP images, and although it may be mathematically more complex, it is also more accurate (9-11). The knowledge-based approach accurately determines data, image statistics, and system models, which depict the geometry and physical characteristics of the CT scanner. Owing to its computational complexity, the full IR algorithm requires somewhat longer reconstruction times (9-11), however, with continued rapid improvement in computer hardware, a reduction in reconstruction times can be expected. With the superior results demonstrated with MBIR in this study as well as in previous studies (9-11), removing this limitation of reconstruction time may eventually enable the replacement of ASIR with knowledge-based IR in the near future.

Our study has several limitations. First, while the TNBSA-induced IBD model is advantageous in terms of its high success rate, it does not fully reflect all disease states from acute to chronic in patients with IBD. However, as we had initially planned to establish an acute IBD model, establishing the full disease spectrum was beyond the scope of our current study. In addition, although our purpose was to examine IBD, inflammation is limited to the colon and does not model small bowel involvement. However, since the mechanism of acute inflammation is mediated through the same cascade in different organs, we can expect similar results for small bowel inflammation imaging. Second, an animal study cannot truly represent a human study with different body sizes and body compositions. Considering that radiation dose is highly dependent on body habitus, our study results cannot be directly applicable to human subjects. Third, we only analyzed CT images obtained from a single-vendor CT scanner whose IR algorithms may not be the same as those of other CT scanners available from different vendors. According to a recent article by Löve et al. (12), although most IR algorithms have been shown to improve image quality and reduce image noise, different IR algorithms by different CT vendors have their own strengths and weaknesses. Therefore, our results may not be directly applicable to other IR algorithms of different CT scanners.

In conclusion, ultra-low dose 80 kVp CT is not feasible using the standard FBP algorithm. However, with the application of IR algorithms, the diagnostic performance of 80 kVp CT was acceptable in a rabbit IBD model and on par with that reconstructed with conventional 120 kVp FBP.

ORCID: Cheong-Il Shin: https://orcid.org/0000-0002-5457-4523; Se Hyung Kim: https://orcid.org/0000-0001-8664-0356; Mi Hye Yu: https://orcid.org/0000-0003-0519-7853; Ijin Joo: https://orcid.org/0000-0002-1341-4072; Joon Koo Han: https://orcid.org/0000-0001-5916-5545

Acknowledgments

This study was supported by the Basic Science Research Program through the National Research Foundation of Korea (NRF) funded by the Ministry of Science, ICT & Future Planning (NRF-2021R1F1A1046393)

References

1. Paulsen SR, Huprich JE, Fletcher JG, Booya F, Young BM, Fidler JL, et al. CT enterography as a diagnostic tool in evaluating small bowel disorders: review of clinical experience with over 700 cases. Radiographics 2006;26:641-57.
2. Hara AK, Swartz PG. CT enterography of Crohn's disease. Abdom Imaging 2009;34:289-95.
3. Brenner DJ. Should computed tomography be the modality of choice for imaging Crohn's disease in children? The radiation risk perspective. Gut 2008;57:1489-90.
4. Reid J, Gamberoni J, Dong F, Davros W. Optimization of kVp and mAs for pediatric low-dose simulated abdominal CT: is it best to base parameter selection on object circumference? AJR Am J Roentgenol 2010;195:1015-20.
5. Kalva SP, Sahani DV, Hahn PF, Saini S. Using the K-edge to improve contrast conspicuity and to lower radiation dose with a 16-MDCT: a phantom and human study. J Comput Assist Tomogr 2006;30:391-7.
6. Nakayama Y, Awai K, Funama Y, Hatemura M, Imuta M, Nakaura T, et al. Abdominal CT with low tube voltage: preliminary observations about radiation dose, contrast enhancement, image quality, and noise. Radiology 2005;237:945-51.
7. Hur S, Lee JM, Kim SJ, Park JH, Han JK, Choi BI. 80-kVp CT using Iterative Reconstruction in Image Space algorithm for the detection of hypervascular hepatocellular carcinoma: phantom and initial clinical experience. Korean J Radiol 2012;13:152-64.
8. Kaza RK, Platt JF, Al-Hawary MM, Wasnik A, Liu PS, Pandya A. CT enterography at 80 kVp with adaptive statistical iterative reconstruction versus at 120 kVp with standard reconstruction: image quality, diagnostic adequacy, and dose reduction. AJR Am J Roentgenol 2012;198:1084-92.
9. Pickhardt PJ, Lubner MG, Kim DH, Tang J, Ruma JA, del Rio AM, et al. Abdominal CT with model-based iterative reconstruction (MBIR): initial results of a prospective trial comparing ultralow-dose with standard-dose imaging. AJR Am J Roentgenol 2012;199:1266-74.
10. Yoon MA, Kim SH, Lee JM, Woo HS, Lee ES, Ahn SJ, et al. Adaptive statistical iterative reconstruction and Veo: assessment of image quality and diagnostic performance in CT colonography at various radiation doses. J Comput Assist

Tomogr 2012;36:596-601.
11. Lee ES, Kim SH, Im JP, Kim SG, Shin CI, Han JK, et al. Effect of different reconstruction algorithms on computer-aided diagnosis (CAD) performance in ultra-low dose CT colonography. Eur J Radiol 2015;84:547-54.
12. Löve A, Olsson ML, Siemund R, Stålhammar F, Björkman-Burtscher IM, Söderberg M. Six iterative reconstruction algorithms in brain CT: a phantom study on image quality at different radiation dose levels. Br J Radiol 2013;86:20130388.
13. Shin CI, Kim SH, Lee ES, Lee DH, Hwang EJ, Chung SY, et al. Ultra-low peak voltage CT colonography: effect of iterative reconstruction algorithms on performance of radiologists who use anthropomorphic colonic phantoms. Radiology 2014;273:759-71.
14. Kim M, Lee JM, Yoon JH, Son H, Choi JW, Han JK, et al. Adaptive iterative dose reduction algorithm in CT: effect on image quality compared with filtered back projection in body phantoms of different sizes. Korean J Radiol 2014;15:195-204.
15. ICRP. 1990 Recommendations of the International Commission on Radiological Protection. ICRP Publication 60. Ann ICRP 1991;21.

초저선량 CT를 이용한 염증성 장질환 평가에서 서로 다른 반복재구성 기법의 효과: 토끼 모델을 이용한 실험적 연구

신청일[1,2], 김세형[1,2,4], 유미혜[3], 주이진[1,2], 한준구[1,2,4]
[1]서울대학교병원 영상의학과
[2]서울대학교 의과대학 영상의학교실
[3]건국대학교병원 영상의학과
[4]서울대학교 의학연구원 방사선의학연구소

목 적: 토끼 염증성 장질환 모델에서 초저선량 CT가 적합한지를 평가하고, 두 개의 다른 반복재구성 알고리즘의 효과를 규명하고자 한다.
방 법: 28마리의 토끼를 염증성 장질환 군 (18 마리)과 대조군 (10 마리) 두 그룹으로 무작위로 나눈다. 염증성 장질환 모델을 구축하기 위해 5% tri-nitrobenzene sulfonic acid 용액 3 ml를 토끼의 S자 결장에 삽입한다. 80 kVp와 120 kVp를 이용하여 CT를 촬영하고, 80 kVp CT는 여과중첩재구성법, 하이브리드 반복재구성기법, 및 완전 반복재구성기법을 이용하여 재구성하고, 120 kVp CT 영상은 여과중첩재구성법을 이용하여 재구성한다. 유효방사선량, 영상잡음, 영상의 질, 및 두 영상의학과 의사의 진단능을 비교한다.
결 과: 80 kVp CT의 평균 유효방사선량은 0.05 mSv로 120 kVp CT의 평균 유효방사선량 0.285 mSv에 비해 유의하게 낮았다. 여과중첩재구성법 80 kVp CT의 평균 영상 잡음 (60.36)은 두 반복재구성기법 (하이브리드 반복재구성기법: 47.02, 완전 반복재구성기법: 12.92)에 비해 유의하게 높았다 ($P<0.0001$). 평균 영상의 질은 여과중첩재구성법 80 kVp CT에서 가장 낮았고, 두 반복재구성기법을 적용했을 때 유의하게 향상되었다 ($P<0.0001$). 정상 소장과 염증성 장질환이 이환된 소장을 감별하는 민감도와 수신자 조작 특성 곡선하 면적값은 여과중첩재구성법 80 kVp CT 영상에서 가장 낮았고 (61.1%, 83.3%; 0.883, 0.967), 두 반복재구성기법을 적용했을 때 유의하게 향상되었으며 (83.3%~100%; 0.992~1) ($P<0.0001$), 여과중첩재구성법 120 kVp CT 값과 비슷한 수준이었다 (100% and 1).
결 론: 염증성 장질환 토끼 모델에서 초저선량 80 kVp CT는 적합하지 않았다. 그러나, 반복재구성기법을 이용하여 재구성한 경우, 초저선량 80 kVp CT 영상의 진단능은 여과중첩재구성법 120 kVp CT 영상과 비슷하며 만족할 만한 수준이었다.

www.e-kjar.org
https://doi.org/10.52668/kjar.2021.00080

pISSN 2586-1719 / eISSN 2799-3299

Korean J Abdom Radiol 2021;5:42-52

Original Article

Determination of Gallstone Composition using Dual-Energy Computed Tomography: An *Ex-vivo* Study

Seonghyun Wee[2], Young Hwan Lee[1], Youe Ree Kim[1], Kwon Ha Yoon[1], Dong-Eun Park[3]

[1]*Department of Radiology, Wonkwang University School of Medicine and Hospital, Iksan, Korea*
[2]*Department of Radiology, Design Hospital, Jeonju, Korea*
[3]*Department of Hepatobiliary Surgery, Wonkwang University School of Medicine and Hospital, Iksan, Korea*

Purpose: This study aimed to investigate whether *ex-vivo* gallstones are distinguishable by type using dual-energy computed tomography (DECT).
Materials and Methods: A total of 124 gallstones from 65 patients with acute or chronic calculous cholecystitis were evaluated using DECT. The extracted gallstones were submerged in distilled water in an acrylic container and scanned at tube voltages of 80/140 kVp and 100/140 kVp. The images were grouped into three sets: 80, 100, and 140 kVp. Qualitative analyses of DECT sensitivity and attenuation patterns in each image set were performed, and quantitative analyses included calculation of mean attenuation values and measurement of the gallstone size. Semi-quantitative Fourier transform infrared (FTIR) spectroscopy was used as the reference standard to confirm the chemical composition of the gallstones.
Results: FTIR spectroscopy identified 66 gallstones from 33 patients as cholesterol gallstones and 58 gallstones from 32 patients as pigment gallstones. Qualitative analysis indicated that DECT sensitivity for cholesterol gallstones was greatest at 80 kVp. Most cholesterol gallstones (79%) showed low attenuation at 80 kVp and high attenuation (65%) at 140 kVp. Pigment gallstones demonstrated high attenuation at all image sets. On quantitative analysis, the mean calculated attenuation values of cholesterol gallstones were -17 ± 50 Hounsfield Units (HU), -5.1 ± 43 HU, and 19.2 ± 39 HU at 80, 100, and 140 kVp, respectively, and 342 ± 173 HU, 286 ± 116 HU, and 195 ± 91 HU, respectively, for pigment stones.
Conclusions: *Ex-vivo* gallstones were distinguishable as cholesterol or pigment gallstones by using DECT.

Keywords: Gallstones; Computed tomography; Cholecystitis; Cholesterol; Calcium; Fourier transform infrared spectroscopy

Introduction

Gallstone disease is an important problem that causes considerable expense in healthcare systems worldwide. Gallstones are not only responsible for cholecystitis but also 30~75% of cases of pancreatitis as well as biliary

Received: June 18, 2021 **Revised:** June 29, 2021 **Accepted:** July 1, 2021
Correspondence: Young Hwan Lee, MD, PhD
Department of Radiology, Wonkwang University School of Medicine and Hospital, 895, Muwang-ro, Iksan-si, Jeonbuk 54538, Korea
Tel: +82-63-859-1927 Fax: +82-63-851-4749 E-mail: yjyh@wonkwang.ac.kr

obstruction and cholangitis. In the United States alone, 500,000~600,000 cholecystectomies are performed annually (1). When gallstone disease presents as acute cholecystitis, complete recovery can be expected after successful cholecystectomy. However, not all patients are suitable for surgical intervention due to individual preoperative risk factors and many serious gallstone diseases such as cholangitis and pancreatitis, can be treated by non-surgical removal of gallstones.

Gallstones are classified as cholesterol or pigment. About two-thirds of gallstones are cholesterol gallstones, the remaining are pigment stones that contain less than 30% cholesterol. Cholesterol gallstones can contain as much as 30% calcium bilirubinate and are sometimes called 'mixed' stones. Pigment gallstones are classified descriptively as 'black' or 'brown'. They are composed mostly of calcium hydrogen bilirubinate, which is polymerized and oxidized in 'black' stones but remains unpolymerized in 'brown' stones. So it is important to identify the composition of gallstones, because cholesterol gallstones may be treatable by non-surgical means (2-9), including oral bile salts therapy, extracorporeal shock wave lithotripsy (ESWL) (10, 11) and contact dissolution therapy with methyl tert-butyl ether (MTBE) (12).

For these reasons, an accurate and reliable means of detection and characterization of gallstones that may be eligible for non-surgical treatment modalities has been a topic of great interest. Moreover, it is not always possible to detect gallstones on conventional computed tomography (CT). Recently, dual-energy computed tomography (DECT) has become available for clinical use. Certain materials will show characteristic changes in attenuation value (Hounsfield Units; HU) on DECT based on the X-ray spectrum to which they are exposed (the dual-energy effect) (13). Based on this physical background, it is theoretically possible to distinguish the composition of tissues on DECT. DECT can obtain higher and lower kilovoltage peak (kVp) datasets using two tubes simultaneously during a single scan, with acceptable image noise (14-16). In practice, 80 kVp, 100 kVp and 140 kVp datasets on DECT were commonly used in South Korea according to the various clinical conditions considering image quality, radiation dose and iodine contrast agent dosage.

Many recent studies have shown the clinical applications of DECT including differentiation of urinary stones (uric acid versus calcium stones) (17-20) and have examined the sensitivity of DECT at different kVp images for detection and compositional analysis of gallstones (high percentage of cholesterol components versus calcium components) (21). Thus, using DECT, it should be possible to distinguish cholesterol and pigment gallstones by analyzing specific absorption characteristics of the constituent materials at different tube voltages (15, 22, 23). There was no published report about differentiation of gallstones from living patients in clinical setting of cholecystitis using DECT. The purpose of this study was to investigate whether *ex-vivo* gallstones from living patients in a clinical setting could be distinguished by type using DECT with both qualitative and quantitative analyses of gallstone attenuation.

Materials and Methods

Patients

This study was approved by the ethics committee of our hospital. Patients who underwent cholecystectomy because of clinically suspected acute or chronic calculous cholecystitis from September 2013 to April 2015 (about 20 months) were retrospectively reviewed on electronic medical record and were enrolled in this study. Patients who met the following criteria were selected: (1) cholecystectomy performed at the department of hepatobiliary surgery of our hospital; (2) preoperative dual energy computed tomography (DECT) performed during detailed clinical evaluation for patients suspected of acute cholecystitis with symptom of biliary colic or chronic cholecystitis before possible surgery, regardless of using preoperative US; (3) gallstones measuring 5 mm or longer on gross examination after surgical extraction; (4) no pathologically proven coexistent biliary diseases, such as gallbladder polyp or malignancy. Preoperative clinical DECT using 140 kVp and 100 kVp tube voltage was performed for detailed evaluation of clinical settings by surgeon's decision, not an extra preoperative step for participation in this experiment, to rule out other surgical or nonsurgical conditions in addition to gallstone diseases. In this experiment, the role of clinical DECT was limited to measure gallstone size and prepare the future study to correlate the clinical DECT results with FTIR results.

In total, one hundred sixty two patients who underwent cholecystectomy were included. First, fifty two patients who did not undergo DECT on clinical settings were excluded. Next, ten patients who did not have measurable gallstones on gross examination and twenty patients who had gallstones measuring 5 mm or smaller were excluded. Immediately after collection, the gallstones were placed in an acrylic container 30 cm wide × 20 cm long and 20 cm high (produced at our department; Fig. 1A) in order of size for DECT scan. Fifteen patients, whose gallstones were shattered or unsinkable in the acrylic container filled with distilled water, were also excluded. Finally, 124 gallstones from 65 patients were eligible for inclusion in this study.

Gallstone size

The mean diameter of all visible gallstones was 10 mm (range, 5 to 44 mm). The mean diameter of the 66 cholesterol gallstones was 11.4 mm (range, 5 to 44 mm) and the mean diameter of the 58 pigment gallstones was 8.7 mm (range, 5 to 16 mm); the size difference between the cholesterol and pigment gallstones was statistically significant ($P < 0.018$).

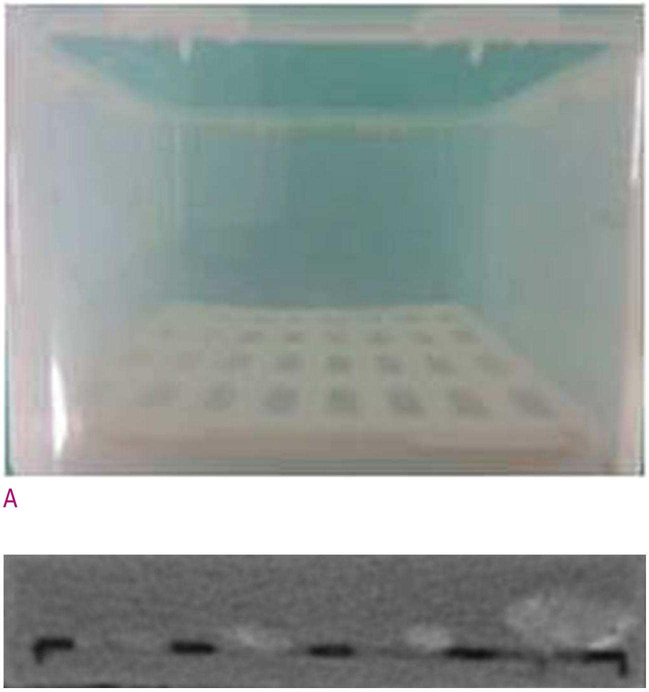

Fig. 1. Gallstone phantom model for DECT
A. Rectangular acrylic container, 30 cm wide × 20 cm long and 20 cm high. B. For each coronal DECT scan, phantoms with a maximum of 3 pieces of gallstone arranged in order of size were placed at the center of the scanner.

Scan protocol of DECT

The gallstones were placed in an acrylic container 30 cm wide × 20 cm long and 20 cm high (produced at our department; Fig. 1A). A maximum of 3 largest pieces of uncrushed sinkable gallstones were selected randomly and placed at the center of the container in order of size (Fig. 1B). The composition of 3 pieces of stones were not known in advance. This process was performed by the internship doctor without having any idea what its purpose was. The container was then filled with distilled water at room temperature and scanned with DECT. We used a SOMATOM Definition Flash dual-source MDCT scanner (Siemens Healthcare, Forchheim, Germany) in this study. Two CT scans of the collected gallstones were performed with the dual-source CT system using a dual-energy protocol. For scan 1, tube voltage/current were 140 kVp/135 mA on tube A and 80 kVp/350 mA on tube B, with the following parameters: configuration, 64 × 0.6 mm; rotation time, 0.33 second; and pitch, 0.6. For scan 2, tube voltage/current were 140 kVp/135 mA on tube A and 100 kVp/300 mA on tube B, with the same parameters. The reason why 100kVp scan was used was to evaluate that 100 kVp scan could be helpful to detect gallstones and differentiate the gallstone composition compared to 80 kVp scan. Three image sets (80, 100, and 140 kVp, respectively) were obtained and images were reconstructed at a slice thickness of 5 mm in a standard abdomen window setting (width 300 HU, center 40 HU).

Image interpretation of DECT

Two abdominal radiologists with experience of 3, 20 years respectively read all DECT images in consensus. All image sets were displayed, respectively, side-by-side in regular sequence in CT scans. The readers knew that all image sets included stones and were not blinded as to which images represented the 80, 100, and 140 kVp image sets. The reader was blinded to which postop stones corresponded to which preop scans. Both readers interpreted the images of the gallstones removed by cholecystectomy together. Preoperative clinical DECT scan was interpreted by 3-year-experienced reader. Window settings could be freely adjusted at all kVp image sets.

Qualitative and quantitative analyses were performed for each image set (Fig. 3). For qualitative analysis, gallstone detection was rated according to a 4-point scale, where 1 indicated definite absence of stone, 2 indicated probable absence of stone, 3 indicated probable presence of stone, and 4 indicated definite presence of stone. For the qualitative assessment of gallstone attenuation, the gallstones were classified during the visual exam as hypodense, isodense, hyperdense, or mixed, according to their CT attenuation patterns compared to the surrounding distilled water.

On quantitative analysis, attenuation values of gallstones were measured using a circular region of interest (ROI) tool at each kVp image set. ROI cursors were situated at the same Z-axis position on all image sets to avoid misregistration. For gallstones displaying homogenous attenuation patterns, the largest possible ROI was measured. For the gallstones that displayed heterogeneous attenuation patterns (e.g., core-and-shell and target appearance), ROI measurements were performed in the major sectors of the gallstones by correlation with FTIR spectroscopy results. Each ROI measurement was performed 3 times to minimize the effect of measurement errors, and the mean attenuation values of the gallstones were calculated. The corresponding attenuation values of gallstones were plotted in a diagram for each group. Additionally, the maximum diameter of each gallstone was measured and the mean sizes of the gallstones were calculated.

Fourier transform infrared spectroscopy

After DECT scanning and interpretating the images, the gallstones were subsequently analyzed with Fourier transform infrared (FTIR; IFS 28, Bruker, Karlsruhe, Germany) spectroscopy (Fig. 2). FTIR spectroscopy was performed by the pathologic investigators with over 5 year experience. On FTIR spectroscopy, the sample to be analyzed was mounted in a solvent (potassium bromide; KBr) and passed through a known infrared (IR) spectrum, where emission and absorption of specified wavelengths were measured in order to determine the chemical compositions of the samples based on the emission/absorption characteristics (24).

Preparation of the gallstone samples was performed without the reference to the DECT images. The gallstones were ground in toto, mounted in the KBr solvent, and analyzed regardless of the CT attenuation patterns. The FTIR spectroscopy measurements were determined with the support of computer-based libraries for reference spectra. The results were described semi-quantitatively.

Statistical analysis

Statistical analyses were performed using dedicated software (SPSS 21.0 for Windows statistical software). For qualitative analysis, sensitivity values for gallstone detection were calculated at all kVp image sets for each group of gallstones (cholesterol gallstones and pigment gallstones), respectively. Visual assessment of the gallstone attenuation was displayed at each group and compared at corresponding kVp image sets (80-100, 80-140, 100-140 kVp image sets) using the x^2 test. For quantitative analysis, the mean attenuation values of gallstones were calculated in each group and compared at corresponding kVp image sets using the paired t test.

Results

Qualitative analysis of gallstones by DECT and correlation with spectroscopy results

Gallstone detection

Gallstones with peak concordance of >80% possibility of cholesterol on FTIR spectroscopy were identified as cholesterol gallstones and those identified as 100% calcium bilirubinate were defined as pigment gallstones (Fig. 2). With these FTIR spectroscopy results as the reference standard, 64 of 66 (97%) cholesterol gallstones were detected by 80 kVp DECT, and this setting demonstrated the highest sensitivity for detection of cholesterol gallstones (Table 1). 100 kVp scan (86%) represented the lower sensitivity to 80 kVp scan. Fifty seven of 58 (98%) pigment gallstones were detected by DECT at all three settings, and the sensitivity for detection of pigment gallstones was equal at all three settings (Table 1). On preoperative clinical DECT exams, 46 of 66 cholesterol (70%) gallstones were detected, and 57 of 58 (98%) pigment gallstones were detected.

Visual assessment of gallstone attenuation

At 80 kVp, 52 of 66 (79%) cholesterol gallstones showed low attenuation and 14 of 66 (21%) cholesterol gallstones showed iso- or high attenuation (P = 0.041), while at 140 kVp, 43 of 66 (65%) cholesterol gallstones had high attenuation and 23 of 66 (35%) demonstrated iso- or low attenuation (P < 0.001) (Table 2, Fig. 3). Moreover, of the 52 cholesterol gallstones that demonstrated low attenuation at 80 kVp, 46 (88%) had iso- or high attenuation at 140 kVp. In contrast, all the pigment gallstones detected by DECT demonstrated high attenuation across all kVp settings (Table 2, Fig. 3). At 100

Table 1. Sensitivity of gallstones by dual-energy computed tomography and correlation with spectroscopy results

Type of Gallstone	80 kVp n = 121	100 kVp n = 114	140 kVp n = 114	P-value		
				80/140	100/140	80/100
Total gallstone n = 124	121 (98)	114 (92)	117 (94)	-	-	-
Pigment gallstone n = 58	57 (98)	57 (98)	57 (98)	-	-	-
Cholesterol gallstone n = 66	64 (97)	57 (86)	60 (91)	0.382	0.344	0.076

Note__kVp, Peak kilovoltage, Numbers of parenthesis are percentage

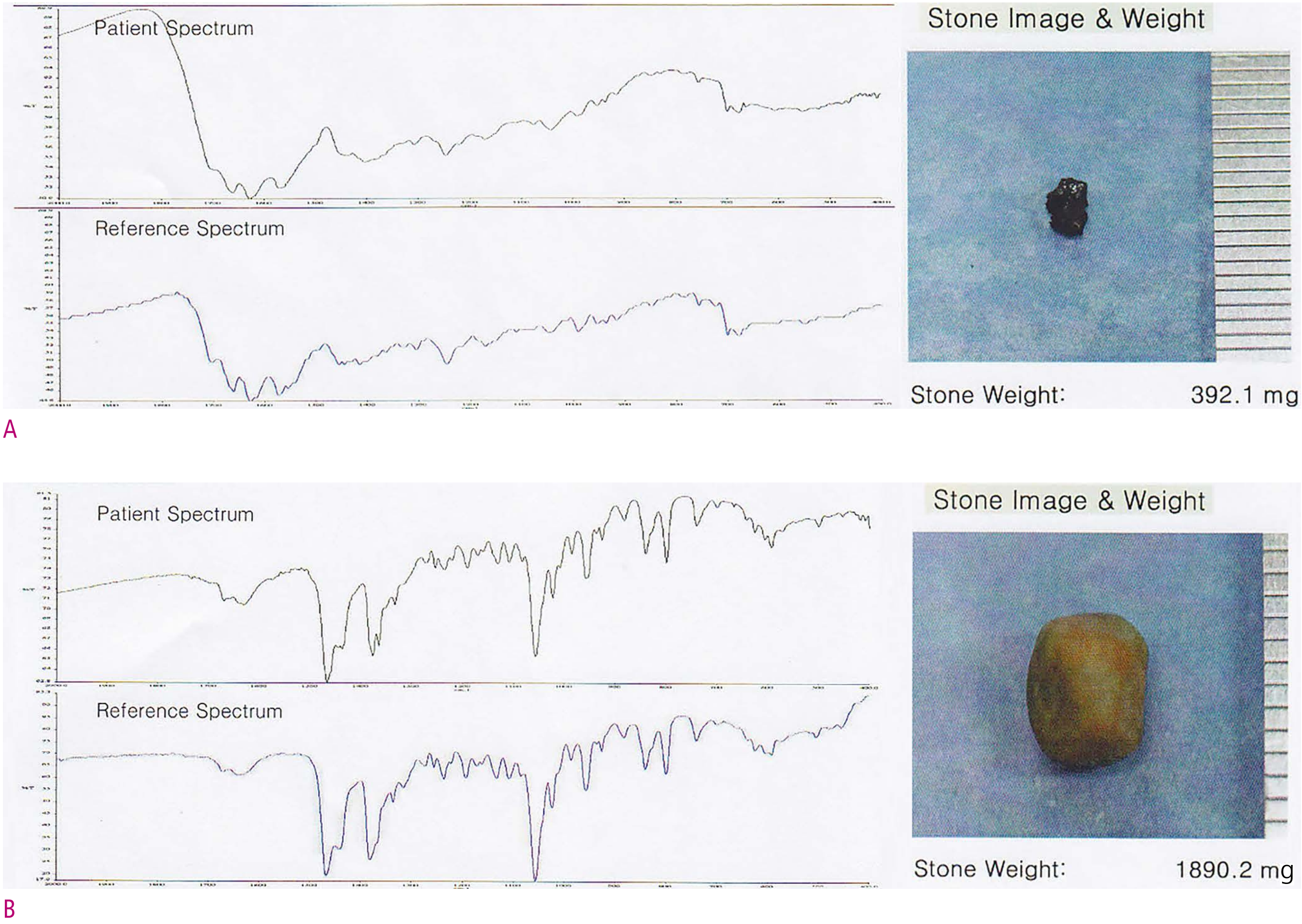

Fig. 2. FTIR spectroscopy

A, B. 45-year-old woman with acute cholecystitis (A) and 63-year-old man with acute cholecystitis (B). On FTIR spectroscopy, the components of 124 gallstones were identified as cholesterol, bilirubin, carbonates, phosphates, and/or protein. The bilirubin turned out to be modified calcium bilirubinate. Phosphates were also accompanied with calcium as a counter ion, and FTIR spectroscopy therefore identified 58 gallstones as 100% calcium bilirubinate (A) and 66 gallstones as >80% possibility (peak concordance) of cholesterol (B).

Table 2. Attenuation patterns of gallstones by dual-energy computed tomography and correlation with spectroscopy results

Type of Gallstone		80 kVp	100 kVp	140 kVp	P-value		
					80/140	100/140	80/100
Pigment gallstone n = 58	Isodense	1 (2)	1 (2)	1 (2)	-	-	-
	Hyperdense	57 (98)	57 (98)	57 (98)	-	-	-
Cholesterol gallstone n = 66	Hypodense	52 (79)	27 (41)	16 (24)	<.001	.041	<.001
	Isodense	7 (10.5)	32 (48)	7 (11)	-	<.001	<.001
	Hyperdense	7 (10.5)	7 (11)	43 (65)	<.001	<.001	-

Note__ kVp, Peak kilovoltage, Numbers of parenthesis area percentage

Table 3. Quantitative analysis of gallstones by dual-energy computed tomography and correlation with spectroscopy results

Mean attenuation value	80kVp	100kVp	140kVp	P-value		
				80/140	100/140	80/100
Pigment gallstone (mean ± SD, HU)	342 ± 173	286 ± 116	195 ± 91	<.001	<.001	<.001
Cholesterol gallstone (mean ± SD, HU)	-17 ± 50	-5 ± 43	19 ± 39	<.001	<.001	<.001

Note__ kVp, Peak kilovoltage, SD, standard deviation, HU, Hounsfield unit

kVp scan, the percentage of cholesterol stones showing isodense attenuation was increased, and the percentage of cholesterol stones showing hypodense attenuation was decreased, compared to 80 kVp scan. But, pigment stones did not show visual attenuation difference between the two kVp scans.

Quantitative analysis of gallstones by DECT and correlation with spectroscopy results

Calculated attenuation values

Because the sensitivity for gallstone detection was highest at 80 kVp, ROI measurements were made using the 80-kVp image set. The results of the ROI measurements are shown in Figure 3.

The mean calculated attenuation values (mean ± standard deviation, SD) of the cholesterol gallstones were -17 ± 50 HU, -5.1 ± 43 HU, and 19.2 ± 39 HU at 80, 100, and 140 kVp, respectively (Table 3). These results were statistically significant for all comparative kVp analyses ($P < 0.001$) and they indicate that the attenuation values of cholesterol gallstones tend to be higher at 140 kVp than at 80 kVp.

The mean calculated attenuation values of the pigment stones were 342 ± 173 HU, 286 ± 116 HU, and 195 ± 91 HU at 80, 100, and 140 kVp, respectively (Table 3). These results were statistically significant at all comparative kVp analyses ($P = 0.001$) and they indicate that the attenuation values of pigment gallstones tend to be higher at 80 kVp than at 140 kVp.

Discussion

CT is an important imaging technique in the detailed evaluation of gallstone diseases. Acute or chronic cholecystitis can be generally treated by cholecystectomy. However, not all patients with gallstones can tolerate cholecystectomy, and not all gallstone diseases can be treated by cholecystectomy. There are nonsurgical options for treatment of gallstones, among them oral bile salts, extracorporeal shockwave lithotripsy, and contact dissolution therapy with methyl tert-butyl ether (MTBE). The principal non-surgical medical treatment for cholesterol gallstones is oral litholysis with bile salts (13). Ursodeoxycholic acid (UDCA) is the most widely used agent of medical treatments for gallstone disease by oral lithotysis but practically devoid of side-effects (14). Because the success of these therapies depends on the composition of the gallstones, it is important to distinguish cholesterol gallstones from pigment gallstones (2-9). This may be possible with DECT.

Many recent studies have shown the clinical applications of DECT including differentiation of urinary stones (uric acid versus calcium stones) (17-20) and have examined the

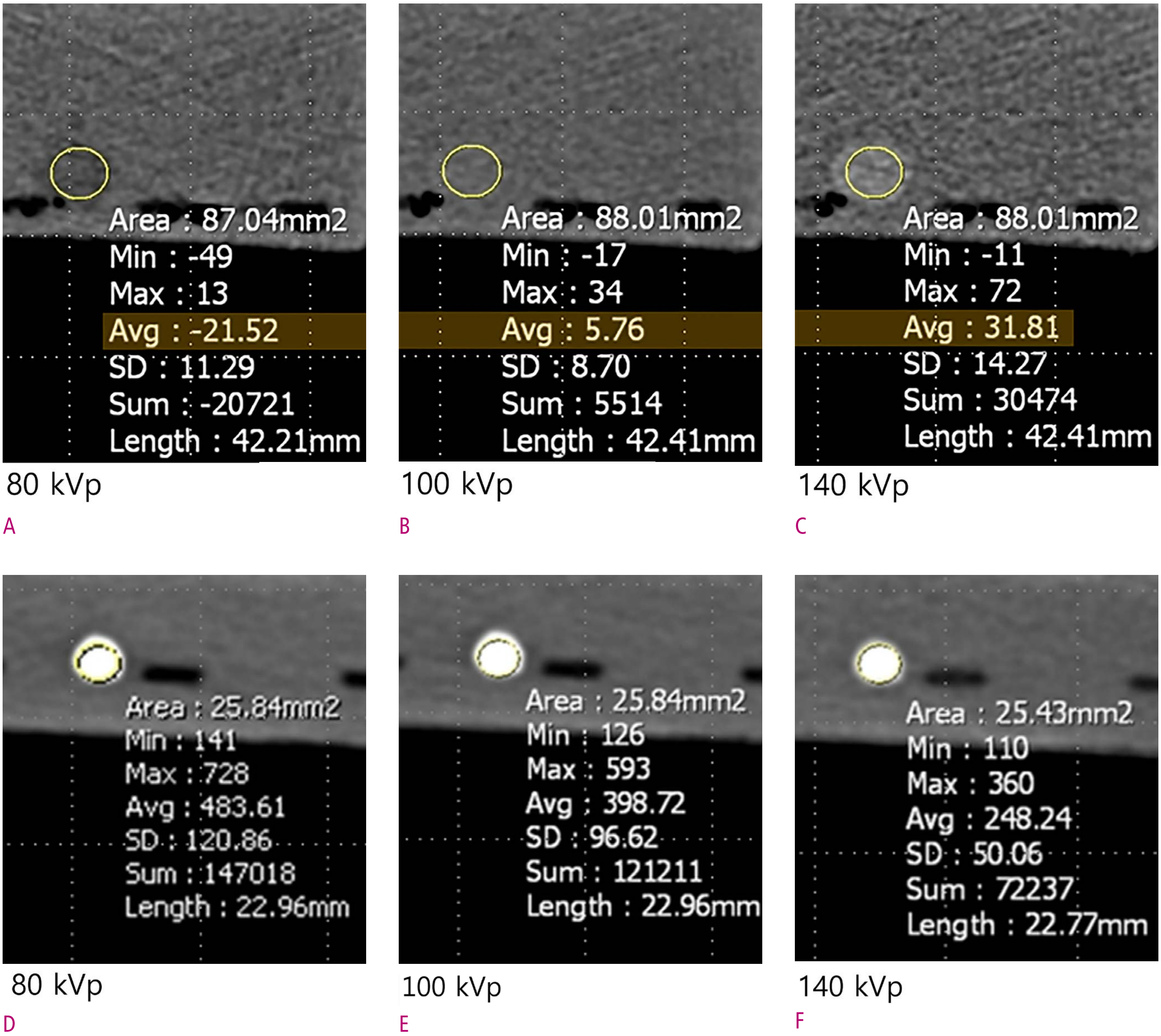

Fig. 3. Gallstone components at DECT

A, B, C. 63-year-old man with cholesterol gallstones. Fifty-two of 66 cholesterol gallstones were identified (79%). The majority showed low attenuation at 80 kVp and high attenuation at 140 kVp. D, E, F. 45-year-old woman with pigment gallstones. Fifty-seven of 58 calcium bilirubinate gallstones (98%) were detected on DECT; all demonstrated high attenuation in all image sets.

sensitivity of DECT at different kVp images for detection and compositional analysis of gallstones (high percentage of cholesterol components versus calcium components) (21). DECT has made it possible to distinguish cholesterol gallstones from pigment gallstones by analyzing specific absorption properties of the materials at different tube voltages using postprocessing algorithms (15, 22, 23).

In this study, *ex-vivo* gallstones were distinguishable as cholesterol gallstones or pigment gallstones on DECT. The gallstones showed characteristic attenuation patterns, with cholesterol gallstones having significantly lower attenuation patterns on low kVp (80 kVp) versus high kVp (140 kVp) image sets ($P = 0.041$), as confirmed by calculated mean attenuation values ($P < 0.001$), and the pigment gallstones showing higher attenuation values at low kVp versus high kVp image sets ($P < 0.001$).

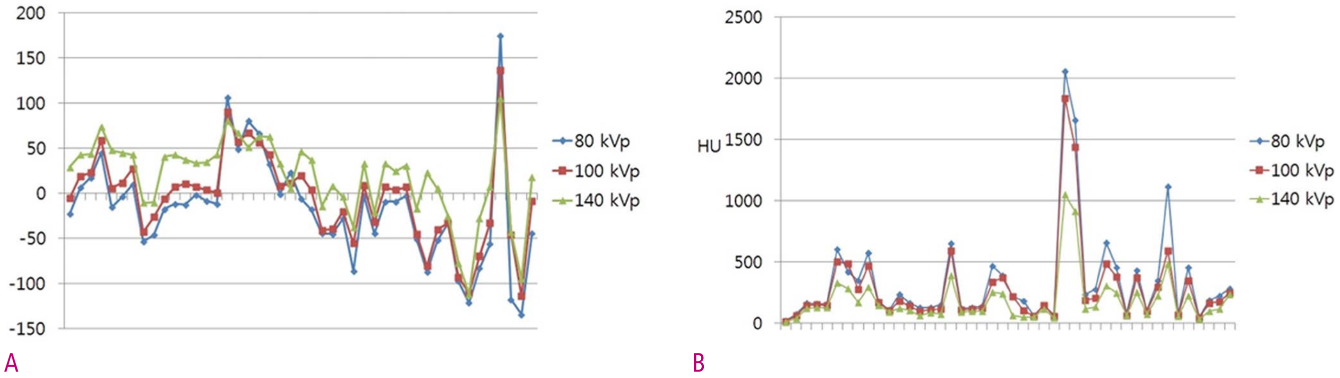

Fig. 4. ROI measurements

ROI measurements and further analyses were based on the 80-kVp image set. The mean calculated attenuation value of cholesterol (A) tended to be higher on the high kVp versus the low kVp image set, while the mean attenuation value of pigment gallstones (B) tended to be higher at the low kVp than at the high kVp image set.

Cholesterol is a lipid consisting of four linked hydrocarbon rings forming a bulky steroid structure. At higher energies, fat has a somewhat higher Compton mass attenuation coefficient than other body tissues (24). Because hydrogen contributes a larger proportion of the mass in fat than it does in soft tissue and bone, fats have a larger electron density than other tissues. This becomes particularly important at higher energies, where Compton interactions dominate attenuation as it contributes to the high attenuation of fats at higher energies of CT.

Chan et al. (25) reported that the mean CT attenuation of cholesterol gallstones was significantly lower than that of pigment gallstones at four voltage settings (80, 100, 120, and 140 kVp) of single-energy CT. This was similar to the result in the present study. However, they suggested that single-energy CT attenuation measurements were not useful for determination of gallstone composition because there was extensive overlap in the CT attenuation values between the two types of gallstones. In our study, cholesterol gallstones were distinguished from pigment gallstones by visual assessment and ROI measurement of attenuation in three kVp image sets at DECT, indicating that dual-energy CT attenuation measurements are useful for determination of gallstone composition.

There was a report about *in-vitro* results for differentiation of gallstone components using DECT (26). That report stated that DECT had poor sensitivity but good specificity for the identification of cholesterol gallstones, and the authors found that DECT was able to correctly classify gallstones according to a reference standard based on visual assessment of the gallstones by a single pathologist. The findings were similar in the present study, and they were based on an FTIR chemical analysis as the reference standard. Moreover, in the present study, we have quantified mean attenuation values and ranges for two types of gallstones.

Another recent study sought to distinguish cholesterol gallstones from pigment or mixed gallstones with DECT by defining reliable attenuation values for autopsy specimens (21) using FTIR as a reference standard. The authors reported that cholesterol gallstones without calcium components showed typically low attenuation at 80 kVp and high attenuation at 140 kVp. There was not an extensive overlap in the attenuation values between the two types of gallstones. Their results were very similar to those reported here, although in the present study, the gallstones were obtained from living patients at cholecystectomy and were placed in the distilled water for DECT analysis, as opposed to formalin, which may have influenced the CT attenuation characteristics of the gallstones (27).

To our knowledge, the present study is the first to perform both qualitative and semiquantitative analyses of gallstone attenuation in DECT, not single energy CT, by using gallstones from living patients, not autopsy specimens, in a clinical setting of cholecystitis and with FTIR results as an objective reference standard. There are no reports performed in living patients with gallstones by DECT. Furthermore, distilled water used as a covering solution would not be expected to influence the attenuation value of the gallstones.

Infrared (IR) or Fourier transform infrared (FTIR) spectroscopy has a large range of applications, from the analysis of small molecules or molecular complexes to the analysis of cells or tissues (24). In this study, FTIR spectroscopy measurements were verified with the help of computer-based libraries for reference spectra. Results were displayed semi-quantitatively so that gallstone components could be described by percent.

This study has several limitations. First, we did not completely correlate gallstone compositions at DECT with the FTIR results because the results of FTIR were reported semi-quantitatively. FTIR results didn't mean the percentage of stone compositions, but they mean how the stone spectra are matched with computer-based libraries for reference spectra. FTIR results of 58 pigment gallstones were identified with 100% possibility (peak concordance) of calcium bilirubinate and phosphates, it meaned they were completely concorded with the reference spectra. But the results of 66 cholesterol gallstones were identified with >80% possibility (peak concordance) of cholesterol, it meaned they were not completely concorded with the reference spectra. In practice, the 124 stones contained many kinds of components in addition to cholesterol and calcium. They were identified as cholesterol, bilirubin, carbonates, phosphates, and/or protein. The bilirubin turned out to be modified calcium bilirubinate. Phosphates were also accompanied with calcium as a counter ion.

Second, this study was non-blinded. The two readers already knew the gallstone composition by correlation with FTIR spectroscopy before they read the DECT images. Therefore, the measured portions of the gallstones were selected as the sectors that correlated with the composition reported at FTIR spectroscopy. They knew that all image sets included stones, the inclusion of "1-definite absence of stone" in the qualitative rating scale is counterintuitive and there is a bias toward higher grading for detectability. And 124 *ex-vivo* gallstones represented a relatively small sample size. Lastly, this study did not compare in vivo and in vitro imaging, and thus limits applicability of this work to clinical radiology.

In conclusion, *ex vivo* gallstones were distinguishable as cholesterol gallstones or pigment gallstones at DECT. Unlike cholesterol stones which increase with increasing kVp, pigment stones decrease in attenuation value within increasing kVp. This, along with overall higher attenuation values in general, will likely allow *in vivo* composition discrimination. In clinical settings, DECT would be expected to verify the results of this study and their reproducibility for routine use.

ORCID: Seonghyun Wee: https://orcid.org/0000-0003-3573-4824; Young Hwan Lee: https://orcid.org/0000-0001-5893-6571; Youe Ree Kim: https://orcid.org/0000-0001-5615-9721; Kwon Ha Yoon: https://orcid.org/0000-0002-2634-8510; Dong-Eun Park: https://orcid.org/0000-0002-7839-6338

References

1. Shaffer EA. Gallstone disease: Epidemiology of gallbladder stone disease. Best Pract Res Clin Gastroenterol 2006;20:981-996.
2. Wang HH, Portincasa P, Mendez-Sanchez N, Uribe M, Wang DQ. Effect of ezetimibe on the prevention and dissolution of cholesterol gallstones. Gastroenterology 2008;134:2101-2110.
3. Caroli A, Del Favero G, Di Mario F, Spigariol F, Scalon P, Meggiato T, et al. Computed tomography in predicting gall stone solubility: a prospective trial. Gut 1992;33:698-700.
4. Fu XB, Liu JY, Liu GN, Shao XM, Zhou XS. Computed tomography in predicting the efficacy of oral cholelitholysis with bile acids. Chin Med J (Engl) 1993;106:734-738.
5. Hickman MS, Schwesinger WH, Bova JD, Kurtin WE. Computed tomographic analysis of gallstones. An in vitro study. Arch Surg 1986;121:289-291.
6. Pereira SP, Veysey MJ, Kennedy C, Hussaini SH, Murphy GM, Dowling RH. Gallstone dissolution with oral bile acid therapy. Importance of pretreatment CT scanning and reasons for nonresponse. Dig Dis Sci 1997;42:1775-1782.
7. Petroni ML, Jazrawi RP, Pazzi P, Lanzini A, Zuin M, Pigozzi MG, et al. Ursodeoxycholic acid alone or with chenodeoxycholic acid for dissolution of cholesterol gallstones: a randomized multicentre trial. The British-Italian Gallstone Study group. Aliment Pharmacol Ther 2001;15:123-128.
8. Polverosi R, Sbeghen R, Zambelli C, Caracciolo F, Spigariol F, Caroli A. [Role of computerized tomography in the densitometric assessment of lithiasis of the gallbladder]. Radiol Med 1992;84:387-392.

9. Tuncer I, Harman M, Mercan R, Ozturk M, Arslan I, Meral C, et al. The effects of ursodeoxycholic acid alone and ursodeoxycholic acid plus low-dose acetylsalicylic acid on radiolucent gallstones. Turk J Gastroenterol 2003;14:91-96.
10. Carrilho-Ribeiro L, Pinto-Correia A, Velosa J, Carneiro De Moura M. A ten-year prospective study on gallbladder stone recurrence after successful extracorporeal shock-wave lithotripsy. Scand J Gastroenterol 2006;41:338-342.
11. Rabenstein T, Radespiel-Troger M, Hopfner L, Benninger J, Farnbacher M, Greess H, et al. Ten years experience with piezoelectric extracorporeal shockwave lithotripsy of gallbladder stones. Eur J Gastroenterol Hepatol 2005;17:629-639.
12. Hellstern A, Leuschner U, Benjaminov A, Ackermann H, Heine T, Festi D, et al. Dissolution of gallbladder stones with methyl tert-butyl ether and stone recurrence: a European survey. Dig Dis Sci 1998;43:911-920.
13. Zatz LM. The effect of the kVp level on EMI values. Selective imaging of various materials with different kVp settings. Radiology 1976;119:683-688.
14. Yeh BM, Shepherd JA, Wang ZJ, Teh HS, Hartman RP, Prevrhal S. Dual-energy and low-kVp CT in the abdomen. AJR Am J Roentgenol 2009;193:47-54.
15. Graser A, Johnson TR, Chandarana H, Macari M. Dual energy CT: preliminary observations and potential clinical applications in the abdomen. Eur Radiol 2009;19:13-23.
16. Fletcher JG, Takahashi N, Hartman R, Guimaraes L, Huprich JE, Hough DM, et al. Dual-energy and dual-source CT: is there a role in the abdomen and pelvis? Radiol Clin North Am 2009;47:41-57.
17. Yuh BI, Cohan RH. Different phases of renal enhancement: role in detecting and characterizing renal masses during helical CT. AJR Am J Roentgenol 1999;173:747-755.
18. Baron RL. Role of CT in characterizing gallstones: an unsettled issue. Radiology 1991;178:635-636.
19. Baron RL, Rohrmann CA, Jr., Lee SP, Shuman WP, Teefey SA. CT evaluation of gallstones in vitro: correlation with chemical analysis. AJR Am J Roentgenol 1988;151:1123-1128.
20. Bensid A, Ucar Y, Bendeddouche B, Ozogul F. Effect of the icing with thyme, oregano and clove extracts on quality parameters of gutted and beheaded anchovy (Engraulis encrasicholus) during chilled storage. Food Chem 2014;145C:681-686.
21. Bauer RW, Schulz JR, Zedler B, Graf TG, Vogl TJ. Compound analysis of gallstones using dual energy computed tomography--results in a phantom model. Eur J Radiol 2010;75:e74-80.
22. Coursey CA, Nelson RC, Boll DT, Paulson EK, Ho LM, Neville AM, et al. Dual-energy multidetector CT: how does it work, what can it tell us, and when can we use it in abdominopelvic imaging? Radiographics 2010;30:1037-1055.
23. Johnson TR, Krauss B, Sedlmair M, Grasruck M, Bruder H, Morhard D, et al. Material differentiation by dual energy CT: initial experience. Eur Radiol 2007;17:1510-1517.
24. Berthomieu C, Hienerwadel R. Fourier transform infrared (FTIR) spectroscopy. Photosynth Res 2009;101:157-170.25.
25. Fuentes A, Fernandez-Segovia I, Serra JA, Barat JM. Effect of partial sodium replacement on physicochemical parameters of smoked sea bass during storage. Food Sci Technol Int 2012;18:207-217.
26. Vera Pingitore E, Bru E, Elena Nader-Macias MI. Effect of lyophilization and storage temperature on the activity of salivaricin CRL 1328, a potential bioactive ingredient of a urogenital probiotic product. J Gen Appl Microbiol 2012;58:71-81.
27. Schulte SJ, Baron RL. The effect of storage on the computed tomography attenuation of gallstones. Invest Radiol 1994;29:307-312.

이중 에너지 전산화단층촬영을 이용한 담석 성분 확인: 생체외 연구

위성현[2], 이영환[1], 김유리[1], 윤권하[1], 박동은[3]

[1]원광대학교병원 영상의학과, [2]대자인병원 영상의학과, [3]원광대학교병원 외과

목 적: 이중 에너지 전산화단층촬영 (Dual energy computed tomography)을 이용하여 생체 외 담석을 종류에 따라 구별 가능한 지를 알아보고자 하였다

대상 및 방법: 담석을 동반한 급성 및 만성 담낭염으로 담낭절제술을 시행 받은 65명의 환자를 대상으로 하였다. 담낭절제술 후에 추출된 124개의 담석들을 증류수로 채워진 아크릴로 만든 모형 용기에 넣고 이중 에너지 전산화단층촬영(이하 CT)을 시행하였다. 담석에 대한 이중 에너지 CT는 80/140 kVp, 100/140 kVp의 관 전압을 이용하여 시행하였고, 얻은 영상을 80, 100, 140 kVp의 세 가지 영상 세트 범주로 분류하였다. 각각의 이중 에너지 CT 영상 세트에서 정성분석과 정량분석을 시행하였다. 정성분석으로 각각의 영상 세트에서 담석의 발견 민감도를 크기계산하고 담석의 감쇄 정도를 육안적으로 평가하였다. 정량분석으로 담석의 감쇄 지수와 크기를 측정하였다. 담석의 화학적 성분 분석을 위하여 반정량적 Fourier transform infrared (FTIR) spectroscopy를 시행하였다.

결 과: 반정량적 FTIR spectroscopy 분석상에서 33명의 환자에서 66개의 담석이 콜레스테롤 담석으로 진단되었고, 32명의 환자에서 58개의 담석이 색소 담석으로 진단되었다. 정성분석상에서 콜레스테롤 담석은 낮은 관 전압 영상 세트에서 가장 잘 검출되었다. 콜레스테롤 담석의 79%가 80 kVp 영상에서 낮은 감쇄를 보였고, 21%는 증류수와 같거나 보다 높은 감쇄를 보였다. 140 kVp 영상에서는 65%에서 높은 감쇄를 보였고 35%에서 같거나 낮은 감쇄를 보였다. 색소 담석의 98%는 모든 영상 세트에서 높은 감쇄를 보였다. 정량분석상에서 콜레스테롤 담석의 평균 감쇄 지수는 80, 100, 140 kVp 영상에서 각각 -17 ± 50 HU, -5.1 ± 43 HU, 19.2 ± 39 HU로 계산되었다. 색소 담석의 평균 감쇄 지수는 80, 100, 140 kVp 영상에서 각각 342 ± 373, 286 ± 316 HU, 195 ± 191 HU로 계산되었다.

결 론: 이중 에너지 CT을 이용하여 생체 외 담석을 콜레스테롤 담석 또는 색소 담석으로 구별 가능하였다.

www.e-kjar.org
https://doi.org/10.52668/kjar.2021.00066

pISSN 2586-1719 / eISSN 2799-3299

Korean J Abdom Radiol 2021;5:53-56

Case Report

Primary Malignant Melanoma of the Small Bowel with Hepatic Metastasis: A Case Report

Jei Hee Lee, Jimi Huh
Department of Radiology, Ajou University School of Medicine, Suwon, Korea

Primary intestinal melanoma is extremely rare, whereas metastatic melanoma of the small bowel is common. In this report, we present a rare case of primary small bowel melanoma with hepatic metastasis. A 51-year-old man presented with constipation and CT identified an ileal mass without bowel obstruction. CT and MRI revealed hepatic metastasis. Ileal mass was confirmed on laparotomy and histologically diagnosed as melanoma.

Keywords: Malignant melanoma; Small bowel; Computed tomography; Magnetic resonance

Introduction

Malignant melanomas typically occur in the skin but may rarely occur in the mouth, intestines or eye (uveal melanoma). Malignant melanoma in gastrointestinal (GI) tract is an uncommon entity, most often seen as metastatic disease from cutaneous lesions (1). Primary small bowel melanoma (PSBM) is very rare and only limited cases of PSBM have been reported worldwide. We here report a rare case of primary malignant melanoma of the small bowel with hepatic metastasis.

Case Report

A 51-year-old man visited the authors' institution complaining of constipation for one month and mild fever for a week. No other symptoms, such as abdominal pain or weight loss, were noted. His past medical history was unremarkable, except he had performed cholecystectomy five years ago. On the physical examination, the abdomen was soft and non-tender, and no mass was palpable. Laboratory investigations revealed mild anemia and elevated C-reactive protein level (hemoglobin, 10.1 g/dL; C-reactive protein, 24.4 mg/L). Therefore, abdominal computeted tomography (CT) was performed for evaluation of fever focus and to exclude small bowel bleeding.

CT scan revealed about 9.5 cm size lobulated mass in the ileum with heterogenous contrast enhancement (Fig. 1A). Multiple enlarged lymph nodes around the tumor were noted. There was no evidence of obstruction. Initial assessment based on CT findings was lymphoma. The differential diagnosis included gastrointestinal stromal tumor (GIST) or primary ileal adenocarcinoma. Multiple small nodules are seen in the liver, which were regarded as hepatic lymphoma or metastasis (Fig. 1B).

Received: June 14, 2021 **Revised:** June 22, 2021 **Accepted:** June 22, 2021

Correspondence: Jei Hee Lee, MD
Department of Radiology, Ajou University School of Medicine, 164, World cup-ro, Yeongtong-gu, Suwon-si, Gyeonggi-do 16499, Korea
Tel: +82-31-219-5852 Fax: +82-31-219-5862 E-mail: radljh@ajou.ac.kr

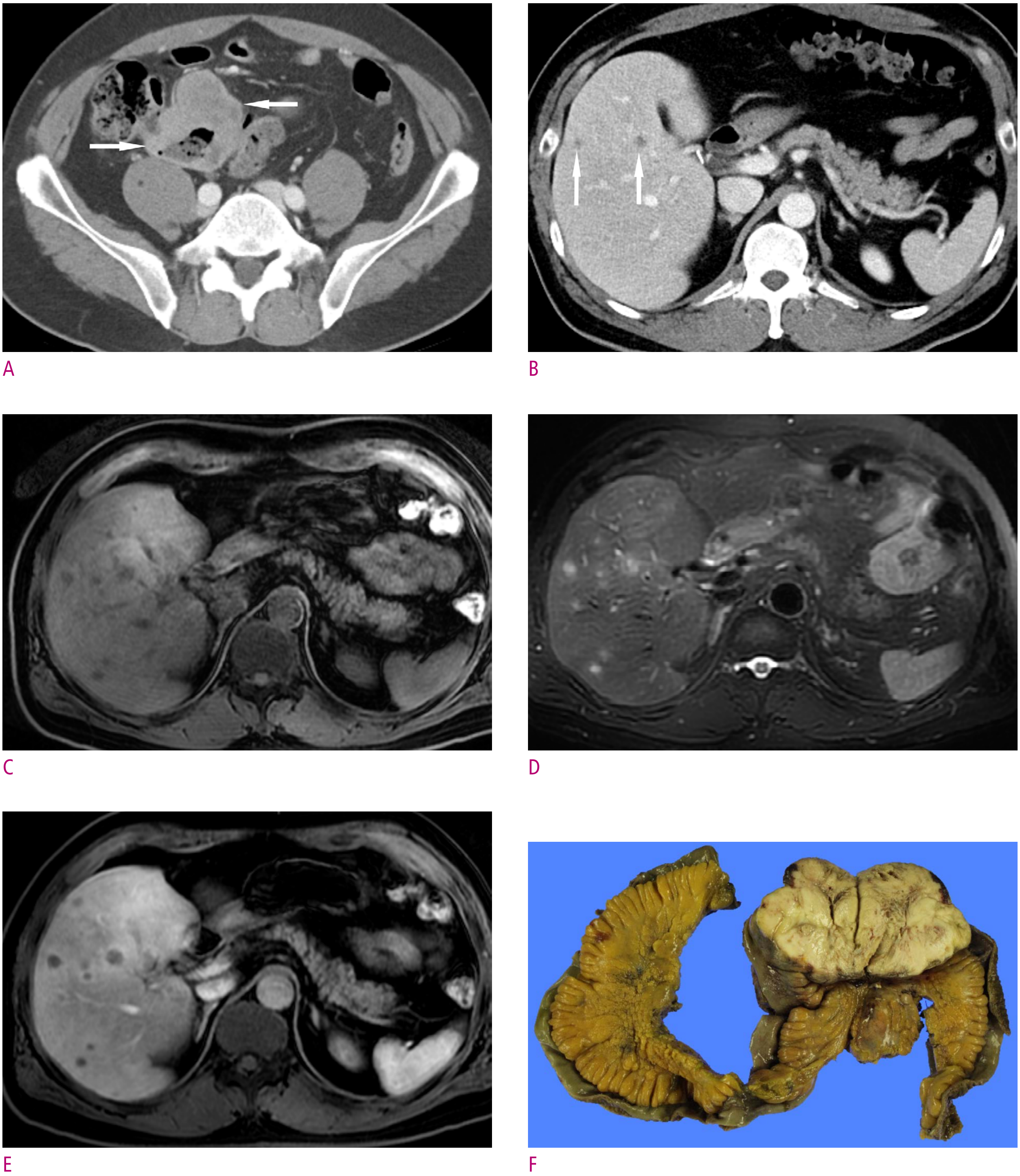

Fig. 1. Primary malignant melanoma of the small bowel in a 51-year-old male patient.
A. CT scan shows about 9.5 cm size lobulated mass (arrows) in the ileum with heterogenous contrast enhancement. B. CT scan shows multiple ill-defined small low density nodules (arrows) in liver. C. T1-weighted liver MR image shows multiple hypointensity hepatic nodules in liver. D. T2-weighted liver MR image shows multiple hyperintensity hepatic nodules in liver. E. T1-weighted image on late arterial phase shows multiple peripheral enhancing target-like nodules in liver. F. Grossly specimen of the mass shows ileum origin whitish mass.

Magnetic resonance (MR) imaging of liver was performed, which revealed more hepatic nodules than CT. And there was size discrepancy between CT and MR. Multiple liver lesions show low signal intensity (SI) on T1 (Fig. 1C), and high SI on T2 (Fig. 1D), and target appearance contrast enhancement of late arterial phase (Fig. 1E). Low signal intensity on hepatobiliary phase and diffusion restriction was noted in the multiple liver lesions. The final assessment was malignant GIST with hepatic metastasis.

The patient underwent segmental resection of the ileum. The mass was located 50 cm above the ileocecal valve. On gross examination, exophytic soft mass was identified in the ileal wall and multiple enlarged lymph nodes are noted in mesentery.

Grossly the mass exhibited whitish mass (Fig. 1F) and microscopic examination revealed infiltration of epithelioid cells with prominent nucleoli. On immunohistochemistry, the tumor cells were negative for c-kit, CD34, DOG-1, Actin, and Melan-A, but the tumor cells were positive for HMB45 and S-100 protein. The final diagnosis was malignant melanoma of the small bowel.

Discussion

Malignant melanomas constitute 1%-3% of all malignant tumors of the GI tract (2). Primary mucosal melanoma can arise at any site within the GI mucosa, but it is most common in anorectal (53.6%) and oropharyngeal (32.8%) regions, whereas esophagus (5.9%), stomach (2.7%), small bowel (2.3%), gallbladder (1.4%), and colon (0.9%) are extremely rare sites of origin (1).

The origin of PSBM remains unknown, because small bowel contains no melanocystes. One potential origin of the primary melanoma of small bowel is melanoblastic cells of the neural crest that migrate to the distal ileum through the omphalomesenteric canal. A second theory suggest that these tumors originate from enteric neuroendocrine noncutaneous tissue in the form of amine precursor uptake decarboxylase cells, which undergo neoplastic transformation (3). Most of malignant melanomas in the small bowel are metastases from primary cutaneous lesions, but a clear distinction between primary intestinal melanoma and intestinal metastasis can be difficult when considering histopathological features alone (3). A primary GI mucosal melanoma is considered in patients with no obvious primary cutaneous melanoma or those with an isolated GI lesion in the absence of other extraintestinal metastases. Blecker et al. (4) suggest the criteria for a diagnosis of primary intestinal melanoma: no evidence of concurrent melanoma or atypical melanocytic lesion of the skin, absence of extraintestinal metastatic spread of melanoma, and presence of intramucosal lesions in the overlying or adjacent intestinal epithelium. Another criteria of Sachs et al. (5), primary small bowel melanoma is a solitary lesion, has no metastatic lesions other than those of regional lymph nodes at diagnosis, and has a disease-free survival period of at least 12 months after diagnosis.

Bender et al. (6) defined four different types of metastatic melanoma of the small bowel: polypoid, cavitary, infiltrating, and exoenteric. Among 32 patients, the polypoid pattern was seen in 20 patients (63%), and the "target lesion," a discrete polypoid mass with a central ulceration, was observed in only three (9%) of the 32 patients. Six of whom showed multiple polypoid lesions (more than 10) referred to as polyposis. Eight patients (25%) demonstrated a cavitary pattern, a circumferential mass with inner marginal necrosis, and five (16%) showed an infiltrating pattern. One patient (3%) had an exoenteric lesion with a fistulous tract. Because primary small bowel melanoma is very rare, there has been no report for imaging features and gross morphologic types (7). Our case can be categorized as exoenteric type according to Bender's categorization, that mimic small bowel lymphoma of GIST.

Hepatic metastasis is a common feature in the advanced stage of malignant melanoma. Detection of hepatic metastases provides valuable prognostic information and critical impact for the therapeutic plan (8). Although CT can provide a limited specificity for the detection of hepatic metastasis in patients with malignant melanoma, but MR imaging was more useful in the detection of hepatic metastasis (8). Typical MR imaging features of hepatic metastasis of malignant melanoma shows shortened T1 and T2 relaxation times and the presence of T1 shortening closely related to the melanin content of the lesion. Although it is rare, we should consider that T1-shortning effects may be caused by extracellular methemoglobin, fat, and high protein content (9). In our study, MR shows higher sensitivity for detection of hepatic metastasis of malignant melanoma than CT. But low to iso-intensity on fat-suppressed T1-weighted images and high intensity on fat-suppressed T2-weighted images were identified in our case of amelantoic melanoma.

In summary, we reported a rare case of primary SBM with hepatic metastasis mimic small bowel lymphoma or GIST. Primary SBM is a rare tumor without a history of melanoma in another organ. For the early detection of primary SBM, clinical examination including imaging studies and pathologic examination is essential.

ORCID: Jei Hee Lee: https://orcid.org/0000-0002-2231-820X; Jimi Huh: https://orcid.org/0000-0002-8832-6165

References

1. Cheung MC, Perez EA, Molina MA, Jin X, Gutierrez JC, Franceschi D, et al. Defining the role of surgery for primary gastrointestinal tract melanoma. J Gastrointest Surg 2008;12:731-738.
2. Atmatzidis KS, Pavlidis TE, Papaziogas BT, Papaziogas TB. Primary malignant melanoma of the small intestine: report of a case. Surg Today 2002;32:831-833.
3. Lens M, Bataille V, Krivokapic Z. Melanoma of the small intestine. Lancet Oncol 2009;10:516-521.
4. Blecker D, Abraham S, Furth EE, Kochman ML. Melanoma in the gastrointestinal tract. Am J Gastroenterol 1999;94:3427-3433.
5. Sachs DL, Lowe L, Chang AE, Carson E, Johnson TM. Do primary small intestinal melanomas exist? Report of a case. J Am Acad Dermatol 1999;41:1042-1044.
6. Bender GN, Maglinte DD, McLarney JH, Rex D, Kelvin FM. Malignant melanoma: patterns of metastasis to the small bowel, reliability of imaging studies, and clinical relevance. Am J Gastroenterol 2001;96:2392-2400.
7. Yang KM, Kim CW, Kim S-W, Lee JL, Yoon YS, Park IJ, et al. Primary malignant melanoma of the small intestine: a report of 2 cases and a review of the literature. Ann Surg Treat Res 2018;94:274-278.
8. Sofue K, Tateishi U, Tsurusaki M, Arai Y, Yamazaki N, Sugimura K. MR imaging of hepatic metastasis in patients with malignant melanoma: evaluation of suspected lesions screened at contrast-enhanced CT. Eur J Radiol 2012;81:714-718.
9. Kelekis NL, Semelka RC, Woosley JT. Malignant lesions of the liver with high signal intensity on T1-weighted MR images. J Magn Reson Imaging 1996;6:291-294.

간전이를 동반한 원발성 소장 흑색종: 증례보고

이제희, 허지미

아주대학교병원 영상의학과

초 록

원발성 장관 흑색종은 매우 드물며, 전이성 소장 흑색종이 가장 흔하다. 이 증례보고는 원발성 소장 흑색종이 간전이를 한 드문 증례이다. 51세 남환이 변이 주소로 내원하였고, CT에서 장 폐쇄가 없는 회장의 종괴가 발견되었다. CT와 MRI에서 간전이가 발견되었다. 회장의 종괴는 개복술을 통하여 확인되었고, 조직학적으로 흑색종으로 진단되었다.

www.e-kjar.org
https://doi.org/10.52668/kjar.2021.00073

pISSN 2586-1719 / eISSN 2799-3299

Korean J Abdom Radiol 2021;5:57-62

Case Report

Granulocyte Colony-Stimulating Factor (G-CSF) Induced Aortitis: A Case Report with Literature Review

Hye-Won Lee, Hong Il Ha
Department of Radiology, Hallym University Sacred Heart Hospital, Anyang-si, Korea

Granulocyte colony-stimulating factor (G-CSF) is widely used as a neutrophil supportive therapy in cancer chemotherapy. Recently, some cases of G-CSF-induced aortitis are reported. Our case patient is a 54-year-old female diagnosed with breast cancer and received adjuvant chemotherapy with prophylactic use of G-CSF. She developed G-CSF-induced aortitis 20 days after the use of G-CSF. The disease was diagnosed with serum markers and radiologic findings. Her symptoms and imaging findings were rapidly improved with high-dose steroid therapy. The rapid improvement of the disease implies that prompt diagnosis with treatment can prevent severe vascular complications.

Keywords: Aortitis; Granulocyte colony-stimulating factor; Computed tomography

Introduction

Granulocyte colony-stimulating factor (G-CSF) is a kind of cytokine that belongs to the hematopoietin family. It regulates the leukocyte growth and maturation in the bone marrow (1). The common cytotoxic agents decrease the production of progenitor cells of the marrow. If the nadir neutrophil count is under 500/uL, the risk of death is markedly increased. G-CSF is broadly used to augment bone marrow production of polymorphonuclear leukocytes and reverse chemotherapeutic agent-induced neutropenia (2). However, recently, some cases have reported G-CSF-induced large vessel vasculitis. It is an infrequent adverse effect of G-CSF, and there are few reviews on published articles. We report a case of G-CSF-induced aortitis in a patient who was on adjuvant chemotherapy for breast cancer, and we thoroughly review this disease entity with published articles and our case.

Case Report

A 54-year-old female, who had been diagnosed with breast cancer, visited the emergency department eleven days after her first adjuvant chemotherapy cycle with doxorubicin and cyclophosphamide. She complains of a fever, and an emergent laboratory exam shows severe neutropenia (absolute neutrophil count: 96/uL). A long-acting glycosylated G-CSF (lenograstim) was initiated with intravenous (IV) antibiotics (tazobactam) to revise the neutropenia. After two days, her fever was subsided, the

Received: June 15, 2021 **Revised:** June 23, 2021 **Accepted:** June 23, 2021
Correspondence: Hong Il Ha, MD, PhD
Department of Radiology, Hallym University Sacred Heart Hospital, 22, Gwanpyeong-ro 170beon-gil, Dongan-gu, Anyang-si, Gyeonggi-do 14068, Korea
Tel: +82-31-380-3880 E-mail: ha.hongil@gmail.com

neutrophil count was increased, and C-reactive protein (CRP) was slightly decreased (66.16 mg/dL). After then, she has discharged.

However, she visited the emergency department four days after discharge for abdominal and back pain. On laboratory exam, an elevated CRP level (98.02 mg/dL) was noted. She underwent abdomen-pelvis computed tomography (CT) for evaluation. Previously, she took baseline abdomen-pelvis CT, 43 days before the onset of symptom, and there was no remarkable finding (Fig. 1A). However, A newly developed soft-tissue density lesion encases the abdominal aorta with mild enhancement (Fig. 1B) at this time. The lesion was extended from the diaphragmatic crura to the bilateral renal vein level. It was suspected of aortitis, but the possible malignancy could not be excluded. She underwent ^{18}F-fluorodeoxyglucose positron emission tomography-computed tomography (^{18}F -FDG-PET/CT) for further evaluation. It revealed a thickening of the suprarenal abdominal aorta wall with strong FDG uptake (Fig. 2A, 2B) without other abnormality. When considering the medical history and radiologic findings, abdominal aortitis induced by G-CSF was strongly suspected. Serum rheumatoid factor and fluorescent antinuclear antibody tests were negative.

The treatment with intravenous steroids was immediately initiated the following day after diagnosis. The CRP levels

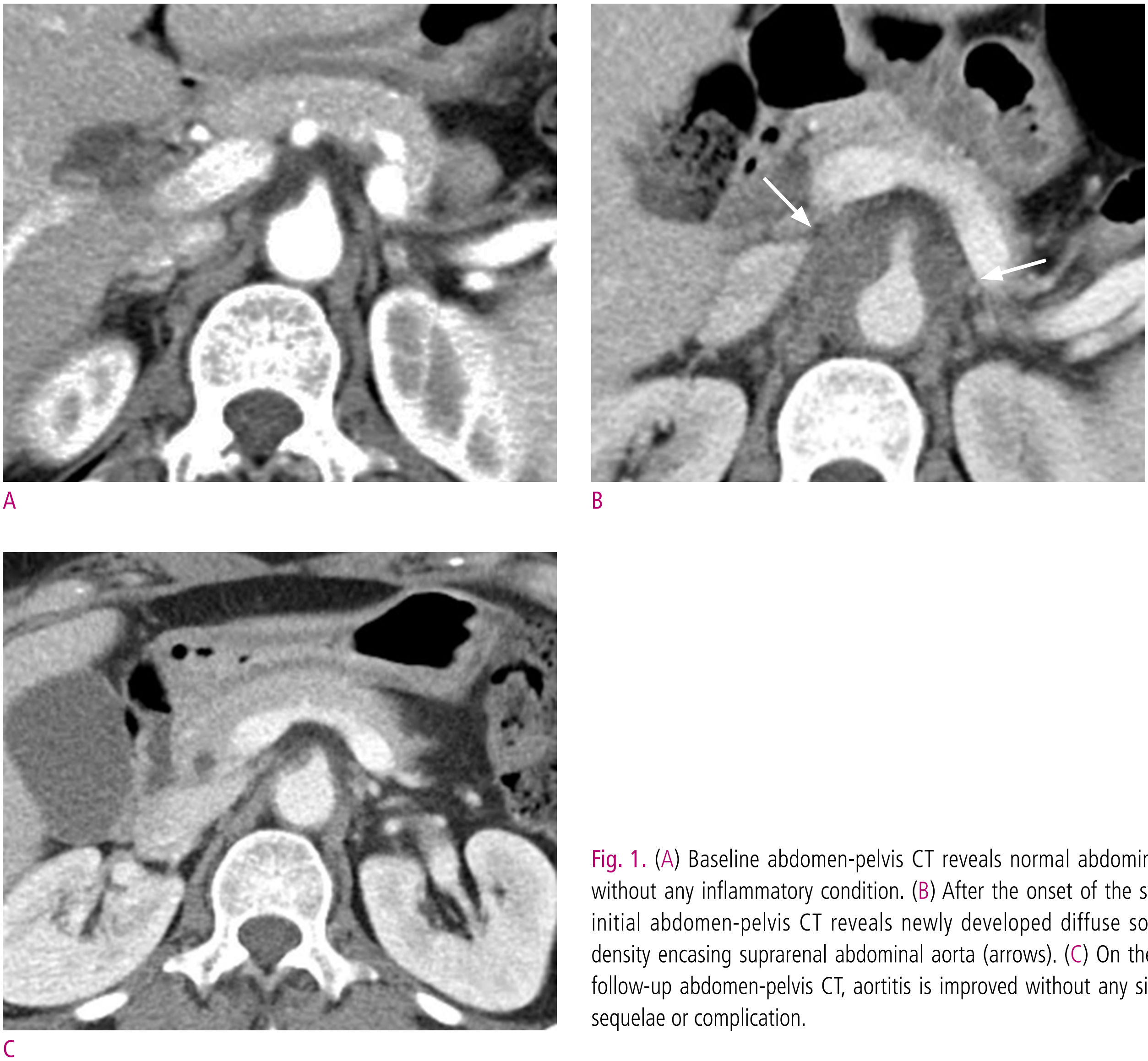

Fig. 1. (A) Baseline abdomen-pelvis CT reveals normal abdominal aorta without any inflammatory condition. (B) After the onset of the symptom, initial abdomen-pelvis CT reveals newly developed diffuse soft tissue density encasing suprarenal abdominal aorta (arrows). (C) On the second follow-up abdomen-pelvis CT, aortitis is improved without any significant sequelae or complication.

decreased rapidly, and the patient was discharged a few days later, following a rapid clinical improvement. After the high-dose steroid therapy, the dose tapering followed. A follow-up abdomen-pelvis CT scan was conducted 18 days after the second admission, and a second follow-up abdomen-pelvis CT scan 16 days after the first follow-up CT show improved aortitis with residual granulation tissue (Fig.1C). Follow-up ^{18}F -FDG-PET/CT shows normalized metabolism in the involved area (Fig. 2C, 2D). The entire disease course is summarized in Figure 3.

The patient restarted the chemotherapy cycle without prophylactic G-CSF, and there was no recurrence of aortitis and no development of any associated complications.

Discussion

There are few reported cases with G-CSF-induced aortitis. When reviewed for previously published articles,

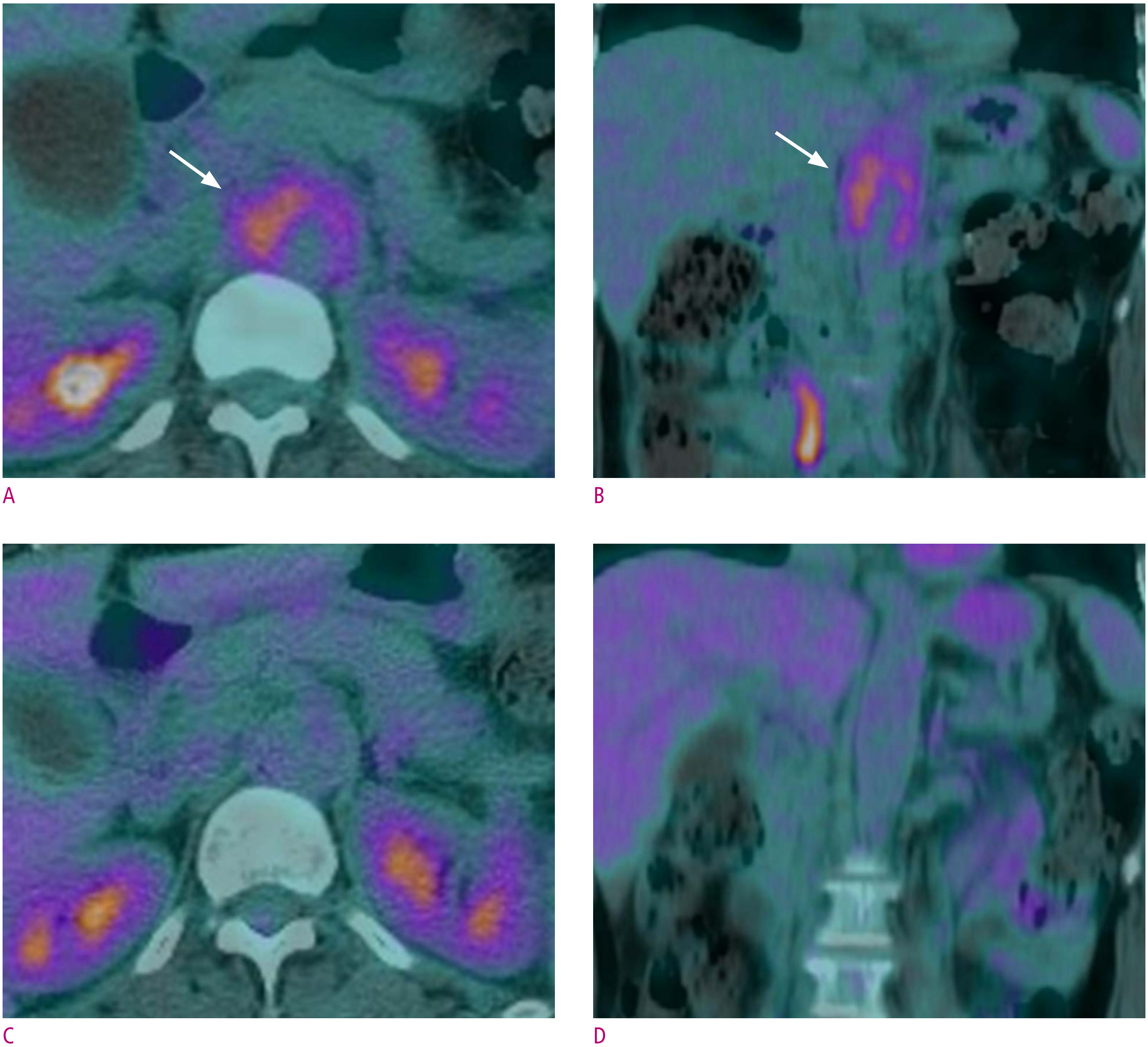

Fig. 2. Disease manifestation on PET/CT. (A), (B) Initial ^{18}F-FDG-PET/CT reveals increased metabolism around the abdominal aorta (arrows). (C), (D) Follow-up ^{18}F-FDG-PET/CT after steroid therapy reveals improvement of aortitis.

except for one male case, most of the patients are women diagnosed with breast cancer who had been initiated chemotherapy with prophylactic G-CSF therapy. Two of the cases are remarkable because they did not have any underlying disease (3, 4). It suggests that some cases of aortitis seem to be caused by the G-CSF use rather than the chemotherapy agent.

Our case patient was diagnosed based on the symptom, medical history, serum markers, and radiologic findings, including abdominal CT and PET-CT. Similarly, reported cases were diagnosed by imaging modalities such as CT, magnetic resonance imaging (MRI), ultrasonography, and PET-CT. The most frequently used diagnostic tool was CT and PET-CT. CT may demonstrate thickening of the aortic wall and periaortic inflammation, although milder degrees of inflammation or wall edema may not be apparent (5). CT is used in the long-term follow-up of patients with treated aortitis, particularly for monitoring the progression of aortic aneurysm. MR angiography also can depict an area of active aortitis that appears as vessel wall edema, enhancement, or wall thickening (6). Recently, the use of ^{18}F-FDG-PET/CT has emerged as a potential tool for the initial diagnosis and assessment of disease activity of aortitis (7). Serum markers, including CRP and erythrocyte sedimentation rate, are easy ways to follow up and determine the endpoint of steroid therapy. Most reported patients have initiated G-CSF agents such as filgrastim or pegylated-filgrastim, but our case patient used G-CSF, which is the first reported case for this agent.

In a large vessel vasculitis, there are many reported complications such as aneurysm, stenosis, dissection, and even rupture (8). Some reported G-CSF-induced vasculitis cases revealed aortic dissection (9), iliac artery aneurysms (4), and left pleural effusion (10). It is recommended for suspected G-CSF-induced aortitis patients to undergo follow-up contrast-enhanced CT to evaluate the subacute or late complications.

G-CSF-induced aortitis is usually resolved spontaneously. However, a case shows long-term involvement of the G-CSF-induced aortitis (4). There is a possibility of developing severe complications like in other large vessel vasculitides (8). Thus, prompt diagnosis and rapid initiation of steroid therapy are essential for G-CSF-induced aortitis. Our case patient was treated based on this regimen

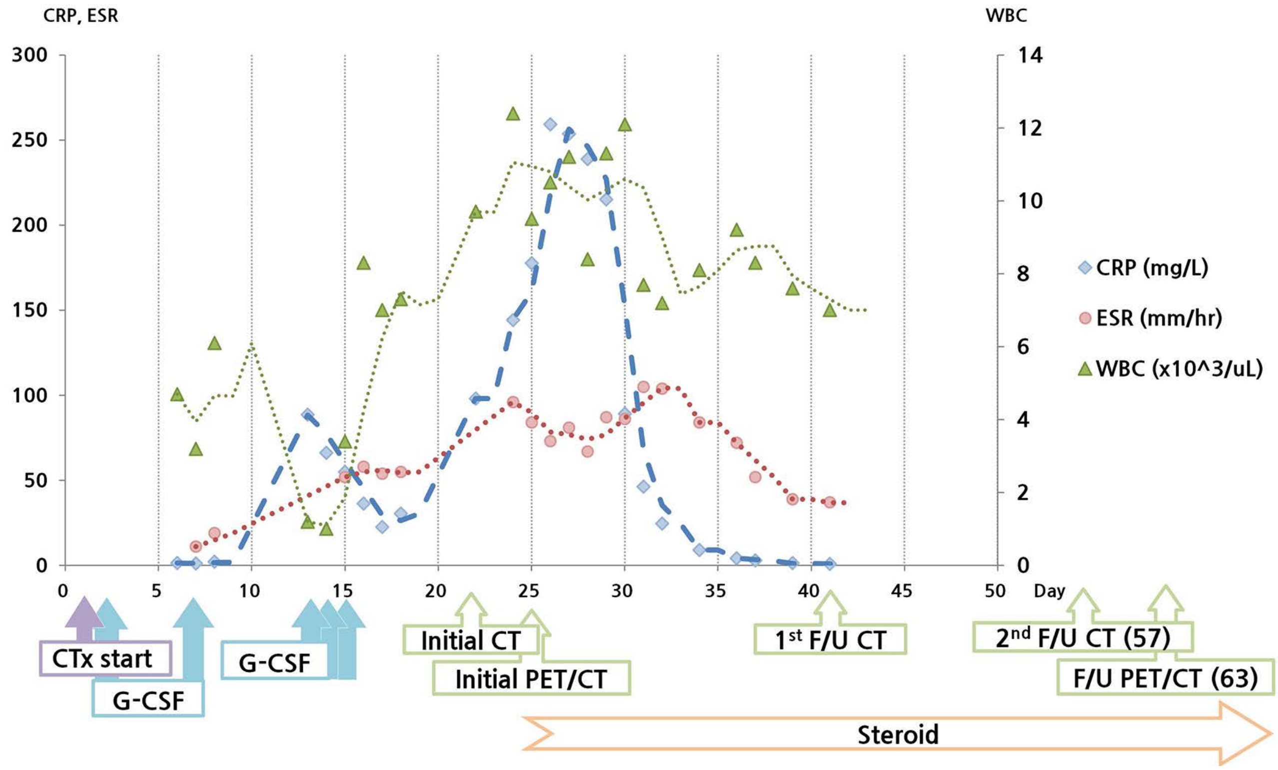

Fig. 3. The schematic visualization of the case patient's disease course.

(11, 12): IV methylprednisolone 500 mg/day for three days, followed by oral prednisolone at 1 mg/kg per day with dose tapering. This regimen was effective, and the patient's serum markers were completely normalized in a week after the initiation of the therapy.

Conclusion

We herein report a case of G-CSF-induced aortitis. This adverse event is scarcely reported, but the concept of G-CSF-induced aortitis is recently emerging. Because it seems to appear any patient who has undergone G-CSF therapy, it should be considered in cases of unexplained fever and no treatment response with antibiotics in case of receiving G-CSF therapy. High-dose steroid therapy seems to shorten the disease-affected period in several reported cases. We suggest that the treatment should be started promptly upon diagnosis. Andcontrast-enhanced CT is recommended for long-term follow-up of patients with treated aortitis, particularly for monitoring the subacute or late complications.

Disclosure statement

The authors report no conflict of interest.

Authors' contributions

Hye-Won Lee: wrote the paper

Hongil Ha: paper's conception, reviewed the paper, and approved the final version of the article

ORCID: Hye-Won Lee: https://orcid.org/0000-0002-6166-2468; Hong Il Ha: https://orcid.org/000-0001-9050-7486

References

1. Holland SM, Gallin JI. Disorders of Granulocytes and Monocytes. In: Jameson JL, Fauci AS, Kasper DL, Hauser SL, Longo DL, Loscalzo J, editors. Harrison's Principles of Internal Medicine, 20e. New York, NY: McGraw-Hill Education; 2018
2. Sausville EA, Longo DL. Principles of Cancer Treatment. In: Jameson JL, Fauci AS, Kasper DL, Hauser SL, Longo DL, Loscalzo J, editors. Harrison's Principles of Internal Medicine, 20e. New York, NY: McGraw-Hill Education; 2018
3. Darie C, Boutalba S, Fichter P, Huret JF, Jaillot P, Deplus F, et al. [Aortitis after G-CSF injections]. Rev Med Interne 2004;25:225-229.
4. Miller EB, Grosu R, Landau Z. Isolated abdominal aortitis following administration of granulocyte colony stimulating factor (G-CSF). Clin Rheumatol 2016;35:1655-1657.
5. Gornik HL, Creager MA. Aortitis. Circulation 2008;117:3039-3051.
6. Tso E, Flamm SD, White RD, Schvartzman PR, Mascha E, Hoffman GS. Takayasu arteritis: utility and limitations of magnetic resonance imaging in diagnosis and treatment. Arthritis Rheum 2002;46:1634-1642.
7. Meller J, Strutz F, Siefker U, Scheel A, Sahlmann CO, Lehmann K, et al. Early diagnosis and follow-up of aortitis with [(18)F]FDG PET and MRI. Eur J Nucl Med Mol Imaging 2003;30:730-736.
8. Creager MA, Loscalzo J. Diseases of the Aorta. In: Jameson JL, Fauci AS, Kasper DL, Hauser SL, Longo DL, Loscalzo J, editors. Harrison's Principles of Internal Medicine, 20e. New York, NY: McGraw-Hill Education; 2018
9. Sato Y, Kaji S, Ueda H, Tomii K. Thoracic aortitis and aortic dissection following pegfilgrastim administration. Eur J Cardiothorac Surg 2017;52:993-994.
10. Hoshina H, Takei H. Granulocyte-colony stimulating factor-associated aortitis in a woman with advanced breast cancer: a case report and review of the literature. BMC Cancer 2019;19:1217.
11. Mukai T, Kubo S, Morita Y, Yamamoto M, Ikeda M. Aortitis which developed after the administration of granulocyte-colony stimulating factor. Mod Rheumatol Case Rep 2020;4:74-78.
12. Parodis I, Dani L, Notarnicola A, Martenhed G, Fernstrom P, Matikas A, et al. G-CSF-induced aortitis: Two cases and review of the literature. Autoimmun Rev 2019;18:615-620.

과립구집락자극인자(G-CSF) 유발 대동맥염: 증례보고 및 문헌고찰

이혜원, 하홍일
한림대학교성심병원 영상의학과

초 록

과립구집락자극인자(G-CSF)는 암환자의 화학요법 치료 중에 발생하는 호중구 감소에 널리 사용된다. 최근 과립구집락자극인자 유발 대동맥염의 증례들이 보고되고 있다. 본 54세 여자 환자는 유방암으로 보조화학요법치료 중에 호중구 감소증이 발생하여 과립구집락자극인자를 투여받았다. 환자는 과립구집락자극인자 사용 20일 후에 급성대동맥염이 발생했으며, 고용량 스테로이드 요법 시행 후 호전되었다. 본 저자들은 영상의학검사를 이용한 진단과 적절한 치료를 통해 과립구집락자극인자 유발 대동맥염의 성공적 치료를 경험하였기에 문헌 고찰과 함께 보고하는 바이다.

www.e-kjar.org
https://doi.org/10.52668/kjar.2021.00031

pISSN 2586-1719 / eISSN 2799-3299

Korean J Abdom Radiol 2021;5:63-66

Case Report

Lymphoepithelial Cyst of the Pancreas: A Case Report

Mi Hye Yu
Department of Radiology, Konkuk University Medical Center, Konkuk University School of Medicine, Seoul, Korea

---

Lymphoepithelial cyst of the pancreas is a rare, non-malignant lesion with a good prognosis. It is filled with keratinized material, lined by squamous epithelium, and surrounded by lymphoid tissue. The imaging appearance of lymphoepithelial cyst varies and sometimes similar to other pancreatic lesions. Therefore, the preoperative imaging diagnosis of the lymphoepithelial cyst is difficult. We present a case of surgically diagnosed lymphoepithelial cyst of the pancreas focused on MR imaging features.

Keywords: Pancreas; Pancreatic cyst; Magnetic resonance imaging; Diffusion-weighted imaging

---

Introduction

Lymphoepithelial cyst of the pancreas is very rare, benign pancreatic cyst (1). Because it has a good prognosis, it is important to differentiate accurately this lesion from other more aggressive pancreatic neoplasm for an appropriate treatment strategy. However, the imaging appearance of lymphoepithelial cyst varies and sometimes similar to other pancreatic lesions (1, 2). Furthermore, studies regarding the imaging appearance of lymphoepithelial cyst are limited to case report or small case series (3-10). Thus, it is difficult to make a definitive diagnosis of lymphoepithelial cyst solely on the findings of preoperative imaging (2). Recently, MRI features including diffusion-weighted imaging (DWI) of the pancreatic lymphoepithelial cyst have been reported in a few case reports (11, 12). Herein, we present a case of surgically confirmed pancreatic lymphoepithelial cyst focused on MR imaging features.

Case Report

A 53-year-old men was referred to our institution for evaluation of incidentally detected pancreas mass. During the preoperative evaluation of the rectal cancer, the pancreatic mass was founded. He had undergone low anterior resection and followed adjuvant chemotherapy for rectal cancer on 2018. Except this medical history, he has no other underlying disease such as diabetes, hypertension. He has no specific symptoms related to the pancreatic lesion.

On pre-operative contrast-enhanced CT which was taken on 2018 April, a 3.3 cm sized, lobulated low-attenuated cystic lesion was found at the upper portion of the pancreas tail (Fig. 1A). The cystic lesion revealed mild rim enhancement and internal septa was suspicious on CT. However, there was no enhancing solid component within the cystic lesion. The remaining pancreas parenchyma demonstrated no swelling, atrophic change, calcification,

Received: May 18, 2021 **Revised:** June 23, 2021 **Accepted:** June 24, 2021
Correspondence: Mi Hye Yu, MD, PhD
Department of Radiology, Konkuk University Medical Center, Konkuk University School of Medicine, 120-1, Neungdong-ro, Gwangjin-gu, Seoul 05030, Korea
Tel: +82-2-2030-7684 Fax: +82-2-2030-5549 E-mail: yumihye@gmail.com

or other abnormal enhancement pattern suggestive of previous pancreatitis.

Biliary-pancreas protocol MRI with MRCP was performed with 3T unit (Skyra, Siemens, Erlangen, Germany) with gadolinium contrast for further evaluation. The pancreatic cyst showed slightly low signal intensity on T2-weighted image (Fig. 1B) and high signal intensity component within the cystic lesion comparison with pure water on T1-weighted image (Fig. 1C). On MRCP, the main pancreatic duct was not dilated. Communication between the pancreatic cyst and main pancreatic duct was not revealed. The cyst showed mild rim-enhancement without enhancing mural nodule or solid component on the dynamic scan (Fig. 1D). On DWI using a respiratory-triggered single-shot spin-echo echo-planar sequence (TR/TE, 6400/54 msec; number of average, 3), the cyst showed hyper signal intensity regardless of different b values (50, 400, and 800 s/mm^2) and the apparent diffusion coefficient (ADC) value of the internal component which was measured about 0.67 x 10^{-3} mm^2/s, while the ADC of background pancreatic parenchymal was 1.13 x 10^{-3} mm^2/s, suggesting the profound restriction of water molecules (Figs, 1E and 1F). There was no area of significant signal drop at the in- and out-of-phase chemical shift imaging. Additionally, ^{18}F-Fluorodeoxyglucose (FDG) PET-CT was performed and the pancreatic cyst did not show significant FDG uptake.

During the follow-up for two years, blood tests performed and carbohydrate antigen (CA) 19-9 was increased from 21 to 68. Therefore, he underwent the distal pancreatectomy. On surgical specimen, well-demarcated yellowish white mass was revealed (Fig. 1G). The cystic lesion was filled with keratinized material and the epithelized cell was surrounded on H&E staining, and was pathologically confirmed as a lymphoepithelial cyst (Fig. 1H).

Discussion

Lymphoepithelial cyst is true pancreatic cyst and it is filled with keratinized material, lined by squamous epithelium, and surrounded by lymphoid tissue (6). The pathogenesis of the pancreatic lymphoepithelial cyst is no fully understood and unclear (1). There were several hypothesis regarding the histopathogenesis of the lymphoepithelial cyst as follows: 1) squamous metaplasia of the pancreatic ducts with subsequent cystic transformation; 2) ectopic pancreatic tissue included in a peripancreatic lymph node; 3) epithelial remnants with peripancreatic lymph nodes; and 4) ectopic remnants of a brachial cleft cyst that are misplaced and fused with the pancreas during embryogenesis (11, 13).

Lymphoepithelial cyst frequently develops in middle-aged and elderly men and occurs to all parts of the pancreas with equal frequency (12, 14). Usually, the cyst is well-defined and exophytic off the pancreatic parenchyma. It could be presented with unilocular or multilocular form (2). Many patients with lymphoepithelial cyst have elevated serum CA19-9 level (15). The contents of the lymphoepithelial cyst may differ from serous to caseous-like depending on the degree of keratin formation

Lymphoepithelial cyst shows uniform non-enhancing low density lesion and it demonstrates wall enhancement and internal septum on CT (3-5). The lesion does not contain the enhancing solid portion within the cyst. On MRI, lymphoepithelial cyst shows a higher intensity than that of free water on T1-weighted image and lower intensity that of free water on T2-weighted image because of the containing keratinized material (11, 12, 16). The pancreatic lymphoepithelial cyst showed higher signal intensity than that of free water on DWI (11). Restricted diffusion within the lymphoepithelial cyst is assumed to be due to the presence of viscos fluid containing keratinized material, like other squamous-lines cysts in other organs (11). Therefore, especially, the cystic lesion shows high signal intensity in the central part and iso- signal intensity in the periphery indicated wall. However, these findings should be interpreted cautiously because other pancreatic cystic neoplasm such as mucinous cystic neoplasm or intraductal papillary mucinous neoplasm can sometimes show similar signal intensity if bleeding into the cyst has occurred (17).

In conclusion, we report a case of the pancreatic lymphoepithelial cyst with imaging features on both CT and MRI. On MRI, lymphoepithelial cyst show slightly high signal intensity on T1-weighted image and slightly low signal intensity on T2-weighted image comparison with pure water, and diffusion restriction on DWI due to the its keratinized material. It is supposed that MRI features may facilitate the differential diagnosis of pancreatic cystic lesions despite the rarity of lymphoepithelial cyst.

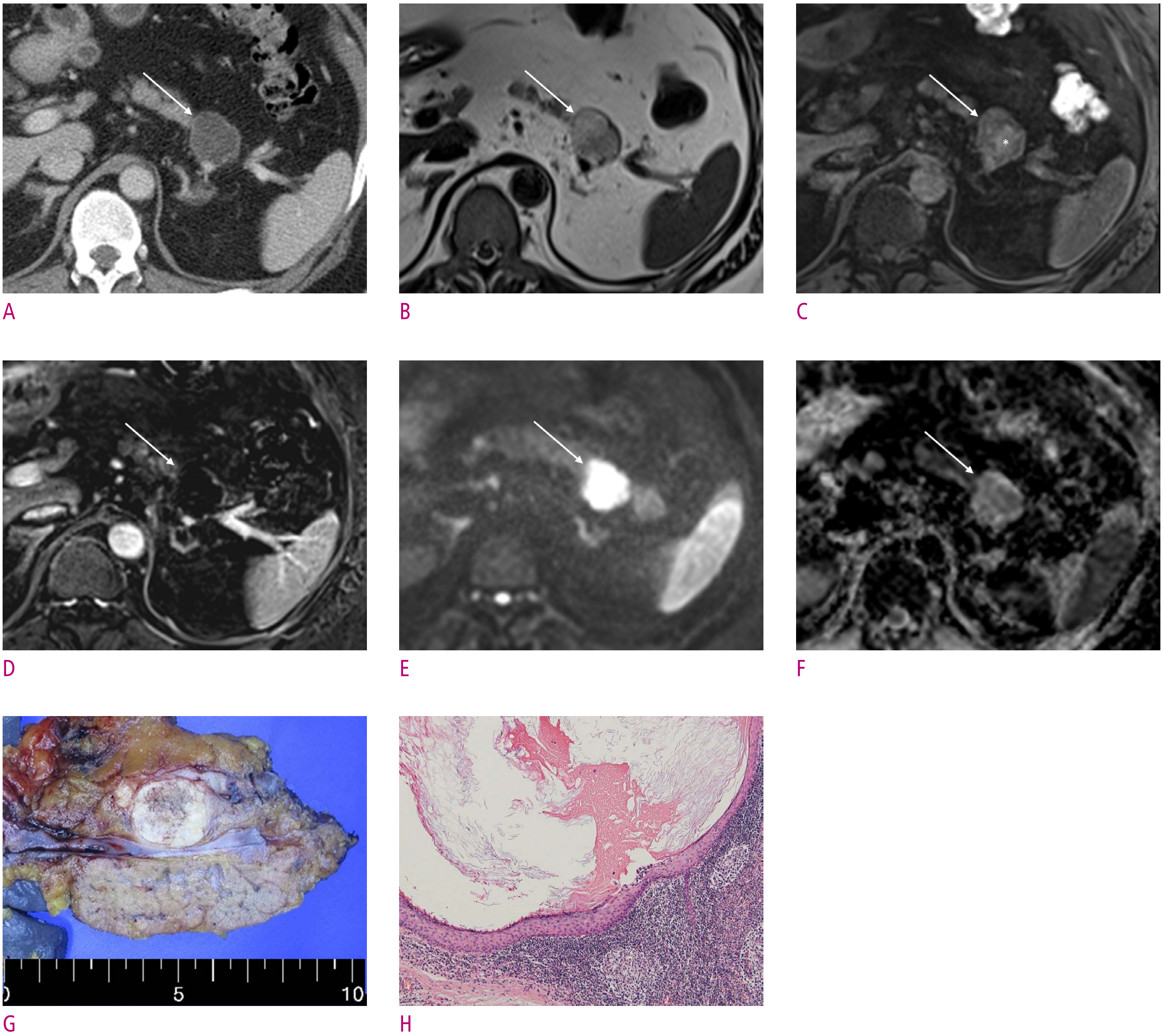

Fig. 1. A lymphoepithelial cyst of the pancreas in a 53-year-old man.
A 3.3 cm sized, lobulated low-attenuated cystic lesion (arrow) is seen at the upper portion of the pancreas tail on contrast-enhanced CT (A). The cystic lesion reveals mild rim-enhancement and suspicious internal septa. On MRI, the pancreatic cyst (arrow) shows slightly low signal intensity on T2-weighted image comparison with pure water (B). Main pancreatic duct is not dilated. The lesion reveals internal high signal intensity component (asterisk) within the cyst (arrow) on T1-weighted image (C). On subtraction image of delayed phase (D), the cyst (arrow) shows mild rim-enhancement. Enhancing mural nodule or solid component is not seen within the cyst. On diffusion-weighted imaging (E and F), the cyst (arrow) demonstrates high signal intensity on high b-value image (b = 800 s/mm^2) and the low apparent diffusion coefficient value of the internal component. After distal pancreatectomy, well-demarcated yellowish white mass is seen on gross specimen (G). The cystic lesion is filled with keratinized material and the squamous epithelium is surrounded on H&E staining (x 100) (H).

ORCID: Mi Hye Yu: https://orcid.org/0000-0003-0519-7853

References

1. Osiro S, Rodriguez JR, Tiwari KJ, Rodriguez, II, Mathenge N, Tubbs RS, et al. Is preoperative diagnosis possible? A clinical

and radiological review of lymphoepithelial cysts of the pancreas. JOP 2013;14:15-20.

2. Kavuturu S, Sarwani NE, Ruggeiro FM, Deshaies I, Kimchi ET, Kaifi JT, et al. Lymphoepithelial cysts of the pancreas. Can preoperative imaging distinguish this benign lesion from malignant or pre-malignant cystic pancreatic lesions? JOP 2013;14:250-255.
3. Koga H, Takayasu K, Mukai K, Muramatsu Y, Mizuguchi Y, Furukawa H, et al. CT of lymphoepithelial cysts of the pancreas. J Comput Assist Tomogr 1995;19:221-224.
4. Kim YH, Auh YH, Kim KW, Lee MG, Kim KS, Park SY. Lymphoepithelial cysts of the pancreas: CT and sonographic findings. Abdom Imaging 1998;23:185-187.
5. Fukukura Y, Inoue H, Miyazono N, Kajiya Y, Fujiyoshi F, Yano T, et al. Lymphoepithelial cysts of the pancreas: demonstration of lipid component using CT and MRI. J Comput Assist Tomogr 1998;22:311-313.
6. Adsay NV, Hasteh F, Cheng JD, Bejarano PA, Lauwers GY, Batts KP, et al. Lymphoepithelial cysts of the pancreas: a report of 12 cases and a review of the literature. Mod Pathol 2002;15:492-501.
7. Idetsu A, Ojima H, Saito K, Hirayama I, Hosouchi Y, Nishida Y, et al. Lymphoepithelial cyst of the pancreas: report of a case. Surg Today 2008;38:68-71.
8. Arumugam P, Fletcher N, Kyriakides C, Mears L, Kocher HM. Lymphoepithelial Cyst of the Pancreas. Case Rep Gastroenterol 2016;10:181-192.
9. Namba Y, Oshita A, Nishisaka T, Namba M, Sasaki T, Matsugu Y, et al. Lymphoepithelial cyst of the pancreas: A case report and summary of imaging features of pancreatic cysts. Int J Surg Case Rep 2019;55:192-195.
10. Matsubayashi H, Aikawa Y, Sugiura T, Sasaki K, Hotta K, Ono H. Pancreatic Lymphoepithelial Cyst Showing Multiple Floating Ball-like Appearances. J Gastrointestin Liver Dis 2016;25:239-242.
11. Nam SJ, Hwang HK, Kim H, Yu JS, Yoon DS, Chung JJ, et al. Lymphoepithelial cysts in the pancreas: MRI of two cases with emphasis of diffusion-weighted imaging characteristics. J Magn Reson Imaging 2010;32:692-696.
12. Terakawa H, Makino I, Nakagawara H, Miyashita T, Tajima H, Kitagawa H, et al. Clinical and radiological feature of lymphoepithelial cyst of the pancreas. World J Gastroenterol 2014;20:17247-17253.
13. Adsay NV, Hasteh F, Cheng JD, Klimstra DS. Squamous-lined cysts of the pancreas: lymphoepithelial cysts, dermoid cysts (teratomas), and accessory-splenic epidermoid cysts. Semin Diagn Pathol 2000;17:56-65.
14. Volkan Adsay N. Cystic lesions of the pancreas. Mod Pathol 2007;20 Suppl 1:S71-93.
15. Yamaguchi T, Takahashi H, Kagawa R, Takeda R, Sakata S, Yamamoto M, et al. Lymphoepithelial cyst of the pancreas associated with elevated CA 19-9 levels. J Hepatobiliary Pancreat Surg 2008;15:652-654.
16. Shinmura R, Gabata T, Matsui O. Lymphoepithelial cyst of the pancreas: case report with special reference to imaging--pathologic correlation. Abdom Imaging 2006;31:106-109.
17. Fukunaga N, Ishikawa M, Minato T, Yamamura Y, Ishikura H, Ichimori T, et al. Lymphoepithelial cyst of the pancreas that was difficult to distinguish from branch duct-type intraductal papillary mucinous neoplasm: report of a case. Surg Today 2009;39:901-904.

췌장의 림프상피낭종: 증례 보고

유미혜

건국대학교 의학전문대학원 건국대학교병원 영상의학과

초 록

췌장의 림프상피낭종은 예후가 좋은, 드문 비악성 병변이다. 이 병변은 각질화된 물질로 채워져 있고, 편평 상피로 둘러싸여 있으며 림프 조직으로 둘러싸여 있다. 림프상피낭종의 영상 소견은 다양하고 때로는 췌장의 다른 병변과 유사하게 보여서, 림프상피낭종의 수술 전 영상 진단은 쉽지 않다. 이 증례 보고에서는 수술을 통해 진단된 췌장의 림프상피낭종의 영상 소견을 자기공명영상 소견에 초점을 맞추어 보고하고자 한다.

www.e-kjar.org
https://doi.org/10.52668/kjar.2021.00045

pISSN 2586-1719 / eISSN 2799-3299

Korean J Abdom Radiol 2021;5:67-71

Case Report

Multiphasic CT and MR Imaging Findings of an Isolated Transverse Colon Hemangioma

Bohyun Kim
Department of Radiology, Seoul St. Mary's Hospital, College of Medicine, The Catholic University of Korea, Seoul, Korea

Colonic hemangiomas are rare benign mesenchymal tumors but can potentially cause a life-threatening bleeding. Although phlebolith on simple radiography or CT scan is a pathognomonic sign of colonic hemangioma, it may not be always present. With wider use of cross-sectional images, it is necessary to know the imaging findings of the colonic hemangiomas on multiphasic scan and MRI for the correct diagnosis and management of the disease.

Keywords: Hemangioma; Colon; Magnetic resonance imaging; Computed tomography

Introduction

Gastrointestinal (GI) tract hemangiomas are rare benign mesenchymal tumors, and may manifest as various degree of hemorrhage ranging from occult to life-threatening bleeding. While surgical resection is regarded as a definitive treatment of the disease, pre-operative biopsy is contraindicated due to the risk of bleeding. Thus, acknowledging the radiologic findings of GI tract hemangiomas may help in diagnosis and patient management. Herein, a rare case of a transverse colon hemangioma is presented focusing on endoscopic findings and imaging features on cross-sectional images.

Case Report

A 63-year-old female patient was referred to our hospital for the evaluation of a colonic mass discovered during a screening colonoscopy. The patient was asymptomatic, and physical examination showed no abnormality. Routine laboratory tests were all within the normal range, including a hemoglobin of 13.3 g/dL. The level of tumor markers were also within the normal range, with carcinoembryonic antigen of 2.28 ng/mL and carbohydrate antigen 19-9 of 3.12 U/mL.

On colonoscopy, there was an approximately 3 cm elevated mass at the distal transverse colon having a purplish red to blue surface and an erythematous central depression (Fig. 1).

Multiphasic CT revealed a 2.7-cm sized lobulated and exophytic mass that rested on the cranial side of the transverse colon (Fig. 2). On noncontrast scan, the mass showed homogeneous attenuation without calcification or hemorrhage. On dynamic enhancement study, the mass

Received: June 6, 2021 **Revised:** June 27, 2021 **Accepted:** June 27, 2021
Correspondence: Bohyun Kim, MD, PhD
Department of Radiology, Seoul St. Mary's Hospital, College of Medicine, The Catholic University of Korea, 222 Banpo-daero, Seocho-gu, Seoul 06591, Korea
Tel: +82-2-2258-5793 Fax: +82-2-599-6771 E-mail: kbh@catholic.ac.kr

showed subtle progressive enhancement from the center to the periphery (Fig. 2). There was no sign of colonic obstruction. There was no remarkable findings in the solid organs. No enlarged lymph node was noticed in the abdomen and pelvis.

MRI more clearly demonstrated lobulated contour of the mass that showed hyperintense T2 signal (Fig. 3). There was no remarkable diffusion restriction in the mass. Similar to the enhanced CT, the central portion of the mass showed more prominent enhancement.

Based on these findings, preliminary diagnosis of colonic hemangioma was given. Because of the risk of bleeding, diagnostic and therapeutic laparoscopic colectomy was planned after a multidisciplinary team discussion. Laparoscopic exploration revealed a 2 cm mass-like lesion

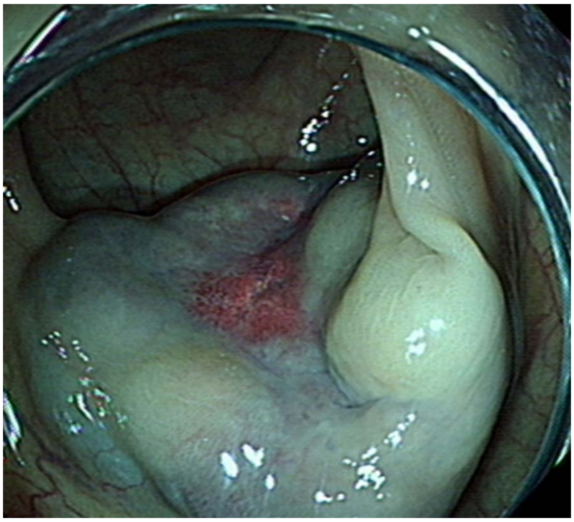

Fig. 1. Colonoscopy shows an elevated mass with a purplish red to blur surface and an erythematous central depression.

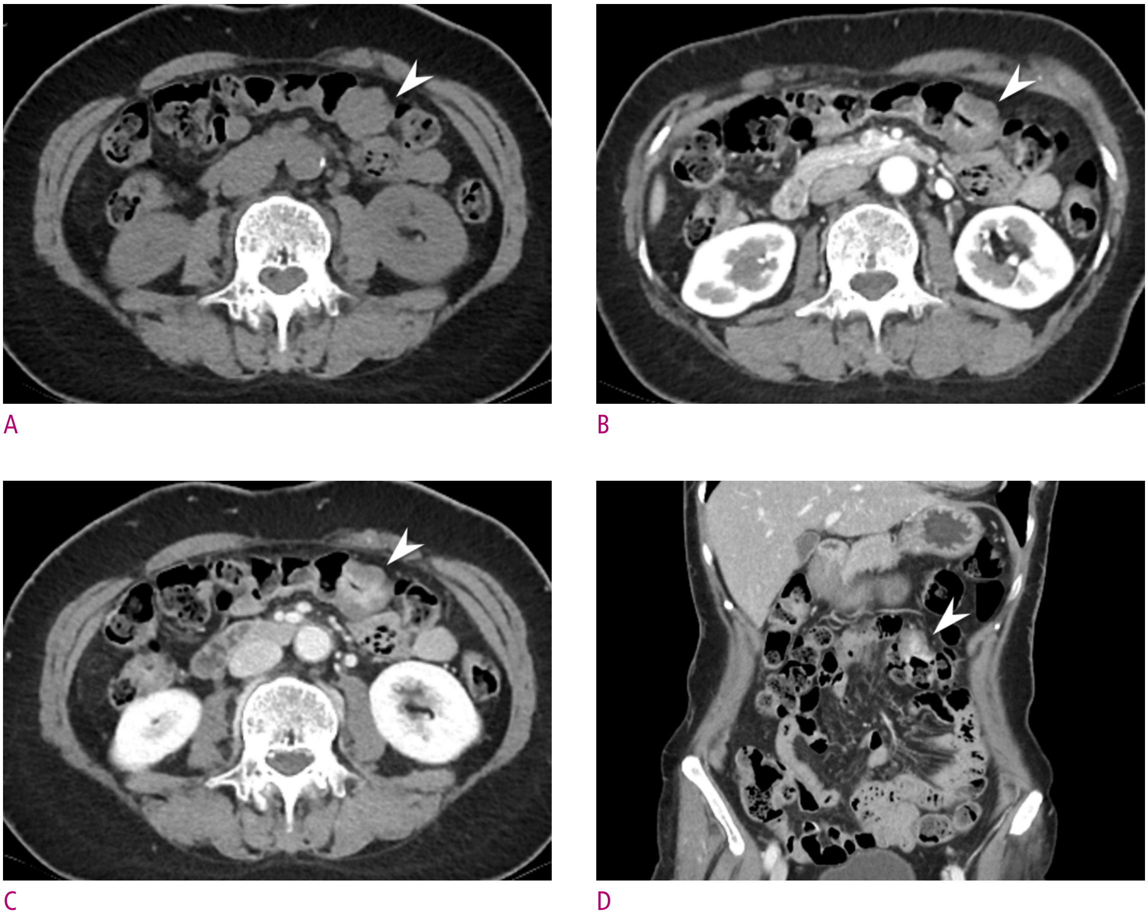

Fig. 2. Multiphasic CT reveals a 2.7 cm mass (arrowheads) in the distal transverse colon. On noncontrast CT scan (A), the mass show homogeneously low attenuation without calcifications or hemorrhage. Arterial (B) and portovenous (C) phases show a subtle and progressive enhancement that begins from the center of the mass. Coronal multiplanar reformation image (D) indicates that the mass is located on the serosal side of the transverse colon and having an exophytic growth.

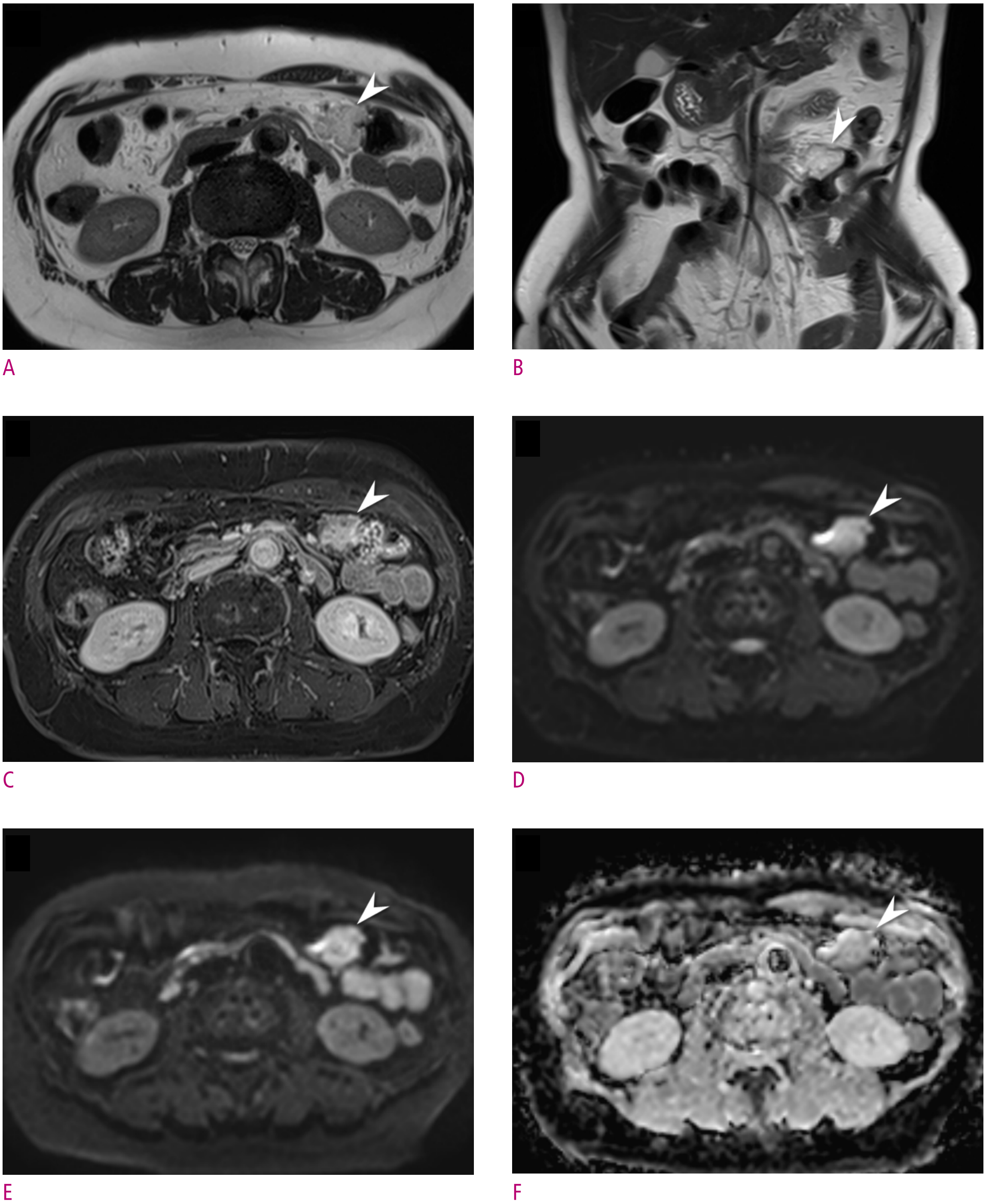

Fig. 3. MR images show a lobulated mass (arrowheads) in the distal transverse colon. Axial (TR, 900 ms; TE, 82 ms) (A) and coronal (TR, 900 ms; TE, 111 ms) (B) T2-weighted HASTE images show a well-defined and lobulated mass with a high T2 signal intensity. Enhanced axial T1-weighted image (C) shows more prominent enhancement in the center of the mass. No remarkable diffusion restriction was noticed on diffusion weighted images with b values of 0 s/mm^2 (D), 800 s/mm^2 (E), and corresponding ADC map (F).

composed of conglomerated and engorged vascular structure at the serosal side of the transverse colon. Approximately 8 cm of the colon that contained the mass was resected without complication, and the patient was discharged on the sixth postoperative day.

Histopathologic examination of the resected specimen

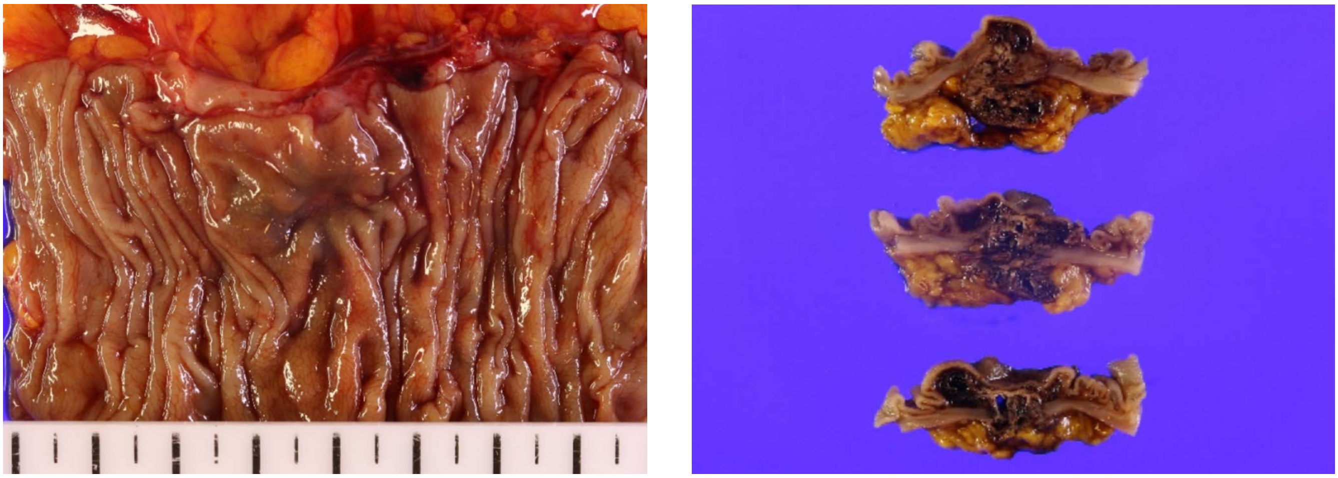

Fig. 4. Surgical and pathologic specimens show a submucosal mass comprised of engorged vascular structure, indicating cavernous hemangioma.

indicated a 2.5 cm spongiotic cavernous hemangioma located in the submucosal layer of the transverse colon (Fig. 4). Immunohistochemical examination excluded possibilities of adenocarcinoma, lymphoma or other mesenchymal tumor.

Discussion

GI tract hemangiomas are rare benign mesenchymal tumors, accounting for 0.3% of all GI tract tumors. GI tract hemangiomas comprise proliferations of lymphatics, capillaries, or veins within the mucosa or submucosa (1). They can occur singly or multiply anywhere from the esophagus to the rectum, but the most common site is the small intestine followed by the rectosigmoid colon (1, 2). Approximately 80% of colonic hemangiomas are cavernous subtype having relatively circumscribed proliferations of large and often dilated thin-walled vessels or blood-filled sinuses which may contain thrombus (1, 3). These features give typically purplish-red to blue surface of the tumor that is soft and compressible on touch on endoscopy (2, 4, 5). Clinically, 60-90% of the patients with GI tract hemangiomas present with occult or life-threatening bleeding, while approximately 10% of the patients can be asymptomatic (3, 6). Other symptoms include anemia from chronic bleeding, abdominal or pelvic pain, and intestinal obstruction (4).

GI tract hemangiomas may show polypoid intraluminal or diffusely infiltrative growths involving both intraluminal and extraserosal sides on gross pathology, and these appearances are readily reflected on cross-sectional imaging studies (2). CT shows wall thickening of the involved segment and phlebolith, which is an important clue to the diagnosis of a GI tract hemangioma (2). Engorgement of adjacent mesenteric vessels and progressive nodular enhancement of the colonic wall are observed on enhanced CT or MRI (6). On T2-weighted MRI images, thickened bowel wall shows high signal intensity from distended vascular spaces (4, 7). Although no prior reports described findings on diffusion weighted images, no remarkable diffusion restriction as have demonstrated in current case may help in distinguishing GI tract hemangiomas from colon cancers or gastrointestinal stromal tumors.

Biopsy prior to surgery may cause severe hemorrhage and is usually not recommended (4, 7). Therefore, surgical resection is performed for the diagnosis and definitive treatment of the GI tract hemangiomas in general. In a rare pedunculated hemangioma, colonoscopic polypectomy can be considered (8). For hemangiomas located in rectosigmoid colon, sphincter preserving low anterior resection or segmental resection is performed. In more proximal lesions, segmental resection or wedge resection is advised (4).

ORCID: Bohyun Kim: https://orcid.org/0000-0003-1157-415X

References

1. Fukayama M, Goldblum JR, Miettinen M, Lazar AJ.

Mesenchymal tumours of the digestive system. In: Klimstra DS, Lam AK, Paradis V, Schimacher P, eds. WHO classification of tumours of the digestive system, 5th ed. Lyon: International Agency for Research on Cancer, 2019:434-498.
2. Levy AD, Abbott RM, Rohrmann CA, Jr., Frazier AA, Kende A. Gastrointestinal hemangiomas: imaging findings with pathologic correlation in pediatric and adult patients. AJR Am J Roentgenol 2001;177:1073-1081.
3. Marinis A, Kairi E, Theodosopoulos T, Kondi-Pafiti A, Smyrniotis V. Right colon and liver hemangiomatosis: a case report and a review of the literature. World J Gastroenterol 2006;12:6405-6407.
4. Yoo S. GI-Associated Hemangiomas and Vascular Malformations. Clin Colon Rectal Surg 2011;24:193-200.
5. Zhang M-G, Lu Z, Wang Y, Redati D, Zheng Z, Wang X. A Rare Case of Transverse Colonic Cavernous Hemangioma: An Ambiguous Preoperative Diagnosis, An Inappropriate Biopsy, A Fortunate Outcome, One Good Lesson and Some Serious Reflections. Medical Case Reports 2018;04.
6. Shen J-D, Chen C-W, Chen T-A, Yueh T-C. Colonic hemangioma, a diagnostic challenge in young adults with lower gastrointestinal tract bleeding. Formosan Journal of Surgery 2016;49:238-241.
7. Kim KH, Kim HK, Lee HK, Shim JC, Lee GJ, Lee KE, et al. Imaging Findings of Cavernous Hemangioma Arising from the Transverse Colon: A Case Report. Journal of the Korean Society of Radiology 2013;69.
8. Ogasawara N, Suzuki M, Adachi K, Yamaguchi Y, Yamamoto S, Hijikata Y, et al. Endoscopic Resection of a Pedunculated Cavernous Hemangioma of the Sigmoid Colon: A Case Report. Case Rep Gastroenterol 2019;13:418-422.

횡행결장 혈관종의 다중시기 조영증강 컴퓨터단층촬영영상과 자기공명영상 검사 소견

김보현

가톨릭대학교 서울성모병원 영상의학과

초 록

대장 혈관종은 드문 양성 중간엽 종양이나 생명을 위협하는 심한 위장관 출혈을 일으킬 수 있다. 대장 혈관종의 주요 영상 소견인 정맥돌 (phlebolith)은 단순 방사선 촬영이나 컴퓨터 단층촬영을 통해 확인 할 수 있으나 항상 있는 것은 아니다. 본 증례는 대장 내시경에서 전형적인 소견을 보여 대장 혈관종으로 강력히 의심했으나 영상검사에서는 정맥돌이 없어 진단에 혼란이 있었던 드문 대장 혈관종의 예이다.

www.e-kjar.org
https://doi.org/10.52668/kjar.2021.00094

pISSN 2586-1719 / eISSN 2799-3299

Korean J Abdom Radiol 2021;5:72-76

Case Report

FDG Uptakes at Unilateral Axillary and Supraclavicular Lymph Nodes and Deltoid Muscle on [^{18}F] FDG PET/CT After COVID-19 Vaccination: A Potential Pitfall for Metastatic Lymph Nodes in Colon Cancer Patient

Jin Sol Choi[1,2], Se Hyung Kim[1,2,3]
[1]Department of Radiology, Seoul National University Hospital, Seoul, Korea
[2]Department of Radiology, Seoul National University College of Medicine, Seoul, Korea
[3]Institute of Radiation Medicine, Seoul National University Medical Research Center, Seoul, Korea

---

Coronavirus disease 2019 (COVID-19), caused by severe acute respiratory syndrome coronavirus 2 (SARS-CoV-2) has caused the ongoing global pandemic. It can manifest a wide range of complications depending upon the severity of infection and comorbidities of the patient. Vaccines are very important measure to provide protection against COVID-19. We report a case of 73-year-old female who underwent [^{18}F]F-2-fluoro-2-deoxy-d-glucose (FDG) positron emission tomography/computed tomography (PET/CT) and contrast-enhanced CT for staging of her rectosigmoid colon cancer and was found to have hypermetabolic uptakes in the deltoid muscle of the left shoulder and hypermetabolic left axillary and supraclavicular lymph nodes due to adenovirus vectored vaccine (ChAdOx1 nCoV-19, AstraZeneca) administrated 18 days ago prior to PET/CT scan.

Keywords: Lymphadenopathy; Positron-emission tomography; Vaccination; Pitfall

---

Introduction

Severe acute respiratory syndrome coronavirus 2 (SARS-CoV-2) is an enveloped RNA beta coronavirus that emerged in Wuhan, China, in December of 2019 (1). It causes the novel coronavirus disease (COVID-19), a global pandemic and has resulted in more than 175 million infections and more than 3.8 million deaths according to the World Health Organization (2).

COVID-19 vaccination drive in Korea began on the 10 February 2021 and vaccines are currently offered to frontline health and social care workers, care home residents and staff, people with chronic conditions, and older adults. As of June 13, 2021, approximately 14 million Korean populations have been inoculated the first round of vaccination. Two-thirds of those populations received AstraZeneca vaccine and the remaining one-third received Pfizer-BioNTech vaccine (3).

Whole-body [^{18}F]F-2-fluoro-2-deoxy-d-glucose (FDG) positron emission tomography/computed tomography

Received: June 23, 2021 **Revised:** June 28, 2021 **Accepted:** June 29, 2021

Correspondence: Se Hyung Kim, MD
Department of Radiology, Seoul National University Hospital, 101 Daehangno, Jongno-gu, Seoul 03080, Korea
Tel: +82-2-2072-2057 Fax: +82-2-743-6385 E-mail: shkim7071@gmail.com

(PET/CT) combines functional and anatomical imaging. It has major roles in oncology for staging and post-treatment follow up of many cancers. Therefore, it is important for the reporting nuclear medicine physicians and radiologists to accurately interpret and recognize potential imaging challenges and pitfalls of false-positive FDG avidity.

Vaccinations and injections are known to cause diagnostic dilemma due to false-positive uptake locally on FDG PET/CT (4, 5). Such dilemma can be critical for oncologic patients who might lose a chance of curative surgery due to false-positive FDG uptake at distant sites. Several case reports of lymphadenopathy post-COVID-19 vaccination have been published recently (5-8). In this case report, we present the case of axillary and supraclavicular lymphadenopathies detected on FDG PET/CT during a staging work-up for rectosigmoid colon cancer.

Case Report

A 73-year-old woman visited our hospital for further work-up of positive stool occult blood test. Colonoscopy revealed a 5cm ulceroinfiltrative mass in the rectosigmoid junction (Fig.1). Biopsy confirmed well-differentiated adenocarcinoma. She underwent contrast-enhanced CT and [^{18}F] FDG PET/CT for staging work-up. On contrast-enhanced CT, there is an enhancing wall thickening in the rectosigmoid junction colon and adjacent pericolic lymph node (LN) enlargement. Left distal ureter was encased by the enlarged LN, leading to left hydronephrosis. On FDG PET/CT images, colon wall thickening and adjacent enlarged LN showed strong FDG uptake suggesting rectosigmoid junction cancer with pericolic metastatic LNs. On FDG PET/CT image at thoracic level, there were several FDG-avid LNs at left axilla area and left supraclavicular area (Fig.1). Nuclear medicine physician initially interpreted these LNs as metastatic LNs. Therefore, palliative chemotherapy was planned. However, after a thorough image review for multi-disciplinary team (MDT) discussion by a dedicated gastrointestinal radiologist, the radiologist circumspectly noticed that there was a FDG avid lesion at left deltoid area and suggested the possibility of reactive FDG uptake after COVID-19 vaccination. After MDT conference, clinicians confirmed that the patient received COVID-19 vaccination using AstraZeneca vaccine 18 days before FDG PET/CT imaging. Therefore, management plan for the patient was changed to radical colon surgery.

Discussion

An identification of potential false-positive results on PET/CT is vital to ensure an accurate interpretation during oncologic image reporting by taking into account the clinical context because many inflammatory and reactive phenomena are known to cause false-positive avidity (9). In our case, FDG-avid LNs at axillary and supraclavicular areas were initially interpreted as distant metastatic LNs. Therefore, clinicians including oncologists and colorectal surgeons planned palliative chemotherapy for the patient as they regarded patients as having stage IV colon cancer. However, our radiologist meticulously observed an elongated FDG uptake at left deltoid muscle and correctly diagnosed FDG-avid LNs at axillary and supraclavicular areas as reactive LNs due to COVID-19 vaccination. Subsequently, the patient did not lose a critical chance of curative resection for rectosigmoid colon cancer.

Vaccination can cause transient inflammation of LNs which demonstrates increased FDG avidity through macrophage accumulation (10). Indeed, vaccine-related increased metabolic activity at injection site, draining LNs, systemic inflammatory response at various sites in different patterns has been reported post-vaccination for COVID-19 vaccines (5-8). According to Schroeder DG et al., positive axillary LN uptake was observed in approximately 10% of patients on FDG PET examinations and extra-axillary LN uptake was observed only in one patient (10). However, the previous study was performed in USA which accepted vaccines only from Pfizer, Moderna, and Yanssen pharmaceutical companies. Therefore, studies regarding FDG PET/CT after vaccination of AstraZeneca company is lacking.

An approach to the performance and interpretation of FDG PET/CT after COVID-19 vaccination should seek to provide accurate interpretations while avoiding treatment delays, additional patient anxiety, excessive follow-up imaging studies, and unnecessary biopsies. Additional imaging and tissue sampling should be cautiously suggested only when necessary. Clues towards reactive LNs include a history of recent vaccination, normal size and benign morphology of LN on CT. Further, a comparison with baseline imaging can also be helpful and if there is

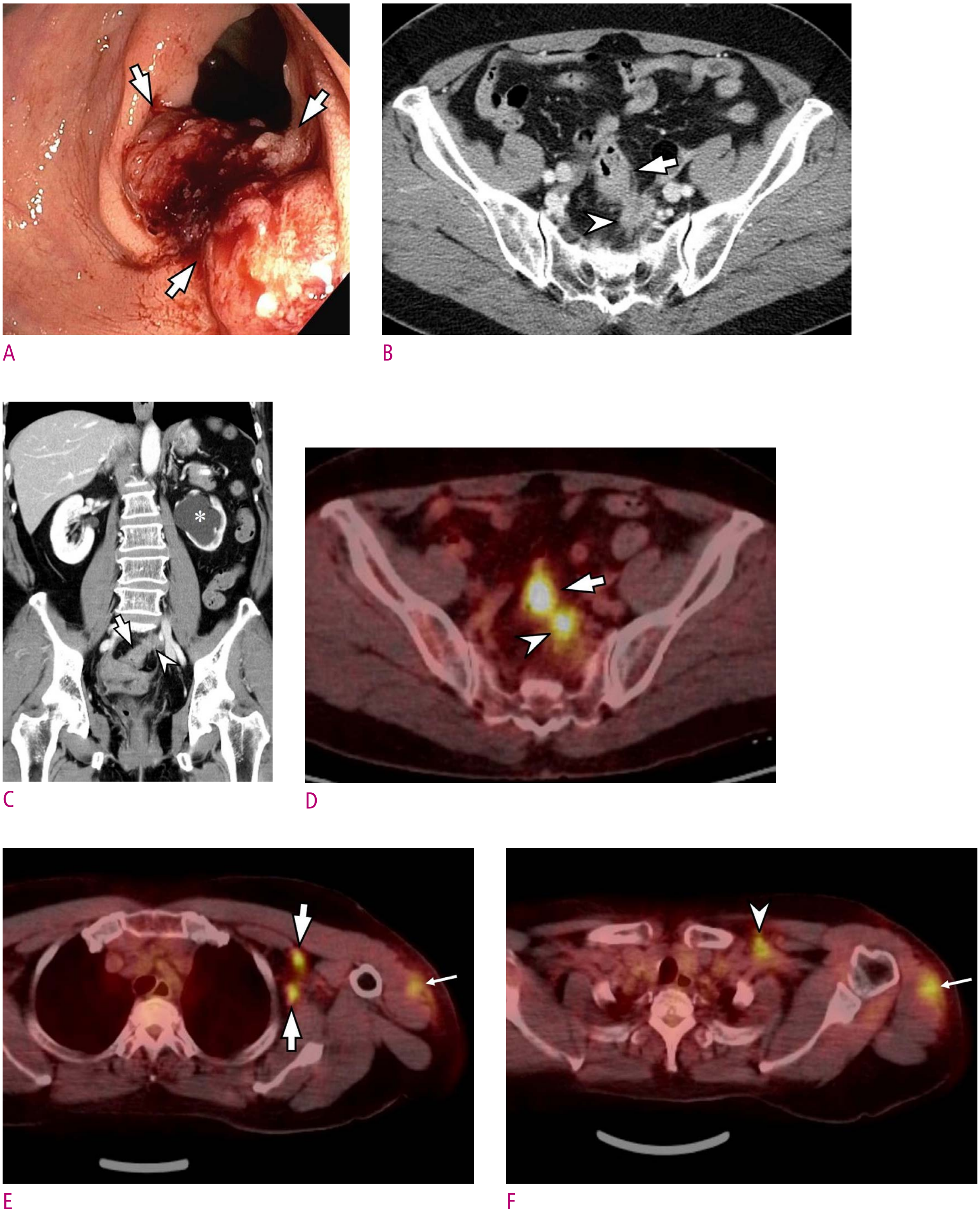

Fig. 1. A 73-year-old female with rectosigmoid junction cancer.

A. On a colonoscopic image, there is a 5 cm ulceroinfiltrative mass (arrows) in the rectosigmoid junction. Colonoscopic biopsy confirmed well-differentiated adenocarcinoma (not shown). B, C. Axial (B) and coronal (C) contrast-enhanced CT images showed well-enhancing wall thickening in the rectosigmoid junction colon (arrow) and adjacent pericolic lymph node (LN) enlargement (arrowhead). Left distal ureter was encased by the enlarged LN, leading to left hydronephrosis (*). D. On a [^{18}F]F-fluorodeoxyglucose (FDG) positron emission tomography/computed tomography (PET/CT) image, colon wall thickening (arrow) and adjacent enlarged LN (arrowhead) showed strong FDG uptake suggesting rectosigmoid junction cancer with pericolic metastatic LN. E, F. On FDG PET/CT images at thoracic level, there were several FDG-avid LNs (arrows) at left axilla area (arrows) and left supraclavicular area (arrowhead). Nuclear medicine doctor interpreted these LNs as metastatic LNs. Therefore, palliative chemotherapy was planned.

G

Fig. 1. G. However, after a thorough image review including coronal PET/CT image for multidisciplinary team discussion by a dedicated gastrointestinal radiologist, the radiologist circumspectly noticed that there was a flat FDG avid lesion at left deltoid area (thin arrows) and suggested the possibility of reactive FDG uptake after COVID-19 vaccination. Note strong hot uptakes at primary colon mass (arrow) and left axillary LN (arrowhead). The patient received COVID-19 vaccination using AstraZeneca vaccine 18 days before FDG PET imaging.

any doubt clinically, serial imaging, discussion in a MDT setting or tissue sampling through biopsy can be helpful in our case. Delaying scans for two to four weeks post-vaccination has been suggested; however, we feel that this may be practically difficult in oncology patients and may cause unnecessary delays.

In conclusion, we hope that this case report will alert radiologists as well as nuclear medicine physicians towards the potential pitfall of reporting LN uptake on [^{18}F] FDG PET/CT in this current vaccination drive and provides a clear illustration of the main patterns of post-vaccine uptake which the reporting physicians or radiologists should be aware of.

ORCID: Jin Sol Choi: https://orcid.org/0000-0002-7034-8243; Se Hyung Kim: https://orcid.org/0000-0001-8664-0356

References

1. Lu R, Zhao X, Li J, Niu P, Yang B, Wu H, et al. Genomic characterisation and epidemiology of 2019 novel coronavirus: implications for virus origins and receptor binding. Lancet 2020;395:565-574.
2. Coronavirus disease (COVID-19) - World Health Organization. [cited 2021 Jun 22]. Available from: https://www.who.int/emergencies/diseases/novel-coronavirus-2019
3. Korea Disease Control and Prevention Agency. Reports for trends in occurrence of adverse reactions related to COVID-19 vaccination in Korea. [cited 2021 Jun 22]. Available from: https://ncv.kdca.go.kr/board.es?mid=a11707010000&bid=0032#content
4. Katal S, Pouraryan A, Gholamrezanezhad A. COVID-19 vaccine is here: practical considerations for clinical imaging applications. Clin Imaging 2021;76:38-41.
5. Schroeder DG, Jang S, Johnson DR, Takahashi H, Navin PJ, Broski SM, et al. Frequency and Characteristics of Nodal and Deltoid FDG and 11C-Choline Uptake on PET Imaging Performed After COVID-19 Vaccination. AJR Am J Roentgenol 2021 May 19. doi: 10.2214/AJR.21.25928. Online ahead of print.
6. Eifer M, Eshet Y. Imaging of COVID-19 Vaccination at FDG PET/CT. Radiology 2021;299:E248.
7. Steinberg J, Thomas A, Iravani A. ^{18}F-fluorodeoxyglucose PET/CT findings in a systemic inflammatory response syndrome after COVID-19 vaccine. Lancet 2021;397:e9.
8. González-Gómez S, Lizarazo DA, Romero J. FDG PET/CT Scan after Vaccination in Times of Pandemic. Radiology 2021;299:E286.
9. Gomez Portilla A, Onaindia E, Larrañaga M, López de Heredia E, Echenagusía V. Periprosthetic seroma with false-positive FDG PET-CT reactive nodes mistaken for metastases in a patient previously treated of metastasic melanoma. Potential source of diagnostic errors. Int J Surg Case Rep 2017;38:66-68.
10. Burger IA, Husmann L, Hany TF, Schmid DT, Schaefer NG. Incidence and intensity of F-18 FDG uptake after vaccination with H1N1 vaccine. Clin Nucl Med 2011;36:848-853.

대장암 환자에서 원격 림프절 전이로 오인된 코로나바이러스감염증 2019 백신 접종 후 FDG PET/CT에서 어깨삼각근 및 동측 액와부와 쇄골위 림프절 FDG 섭취 증가

최진솔[1,2], **김세형**[1,2,3]

[1]서울대학교병원 영상의학과
[2]서울대학교 의과대학 영상의학과교실
[3]서울대학교병원 의학연구센타 방사선의학연구소

초 록

코로나바이러스감염증 2019 (COVID-19)는 코로나바이러스-2 감염에 의해 유발되는 중증 급성 호흡증으로 세계적 대유행 중이다. 감염의 정도와 환자의 동반질환에 따라 다양한 합병증이 나타날 수 있고, 백신은 COVID-19에 대응하는 매우 중요한 조치이다. 본 증례보고는 대장암으로 진단된 환자에서 병기결정을 위해 시행한 FDG 양전자방출단층촬영/컴퓨터단층촬영 (PET/CT)에서 왼쪽 액와부와 쇄골위 림프절에서 FDG 섭취가 증가되어 원격 림프절 전이로 오인하였으나, 동측 어깨삼각근에 비슷한 정도의 FDG 섭취가 관찰되어 백신에 의한 이차적인 림프절 비대 및 FDG 섭취로 최종 진단하였던 73세 여자의 영상소견을 보고하고자 한다. 본 환자는 PET/CT 촬영 18일 전에 AstraZeneca 백신을 1회 접종 받은 기왕력이 확인되었다.

www.e-kjar.org
https://doi.org/10.52668/kjar.2021.00038

pISSN 2586-1719 / eISSN 2799-3299

Korean J Abdom Radiol 2021;5:77-80

Case Report

장중첩증을 유발한 회장의 악성 단발성섬유성종양

이은선
중앙대학교병원 영상의학과

Malignant Solitary Fibrous Tumor of Ileum with Intussusception

Eun Sun Lee
Department of Radiology, Chung-Ang University Hospital, Chung-Ang University College of Medicine, Seoul, Korea

Solitary fibrous tumor (SFT) is rare mesenchymal neoplasm of fibroblastic or myofibroblastic origin. Especially, extrapleural SFT is known to be extremely rare. Here, we report a case of malignant SFT of ileum, resulting in small bowel intussusception in a 74-year-old female patient.

Keywords: Solitary fibrous tumor; Ileum; Intussusception

서 론

단발성섬유성종양 (solitary fibrous tumor, SFT)은 비교적 드문 섬유모세포나 근섬유모세포 기원의 중간엽 신생물이다 (1). 병리적으로는 풍부한 콜라겐 기질을 포함하는 방추 세포로 구성되며 특징적인 면역화학염색결과 (i.e. CD34 양성, Bcl-2 양성, vimentin 양성, S-100 음성, actin 음성, keratin 음성)로 진단을 내리게 되는데 전체 단발성섬유성종양의 약 15에서 20%는 악성으로 알려져 있다 (2). 악성의 경우 병리학적으로는 CD34 반응이 감소하고 S100과 p53에 대한 과발현을 하는 경향이 있는 것으로 알려져 있다 (1). 또한 흉강이 아닌 신체 다른 부위에서 발생하는 단발성섬유성종양은 더욱 드문데, 그 중 위장관에서 생긴 경우는 극히 드물어 현재까지 문헌상 세 개의 증례만이 보고 되어 있다. 이에 74세 여자에서 장중첩증을 유발한 회장의 악성 단발성섬유성종양 1예에 대한 임상적, 영상의학적, 조직학적 고찰을 기존의 문헌조사와 함께 보고하고자 한다.

증례보고

74세 여자가 1주일전부터 시작된 하복부 통증을 주소로 내원하였다. 내원하여 시행한 피검사에서 혈액내 C-reative protein (CRP) 수치가 76.3 mg/L로 상승되어 있었으나, 그 외 특이 소견은 없었다. 복부X선촬영검사에서는 소장 폐색이 의심되는 두 군데 이상의 air-fluid level이 확인되었고, 전반적인 소장의 확장이 있었으며 (Fig. 1A, B), 초음파 검사에서는 하복부 소장에 약 5 cm의 종괴가 선행요인으로 작용한 것으로 생각되는 회장-회장 장중첩증이 확인되었다 (Fig. 2A, B). 추가로 시행한 전산화단층영상검사에서 장중첩증의 선행요인으로 작용한 약 5 cm 종괴는 비교적 균일하게 조영 증강이 잘 되었으나, 일부 조영 증강이 떨어지는 부위가 중심부에서 확인되었고, 경계는 매우 좋았다 (Fig. 3A, B). 주변으로의 침범은 없었

Received: May 20, 2021 **Revised:** June 21, 2021 **Accepted:** June 23, 2021
Correspondence: Eun Sun Lee, MD, PhD
Department of Radiology, Chung-Ang University Hospital, Chung-Ang University College of Medicine, 102, Heukseok-ro, Dongjak-gu, Seoul 06973, Korea
Tel: +82-2-6299-3209 Fax: +82-2-6299-2017 E-mail: seraph377@gmail.com

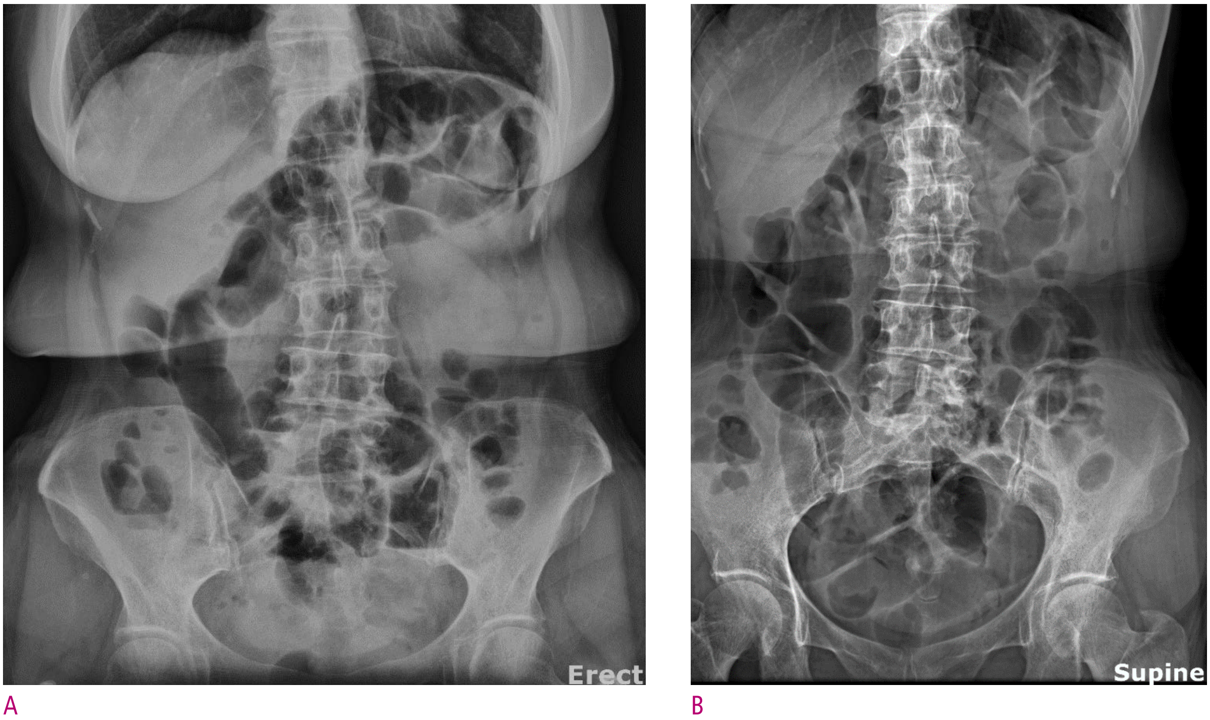

Fig. 1. Abdominal plain radiography on erect (A) and supine (B) position shows bowel obstruction with air-fluid level.

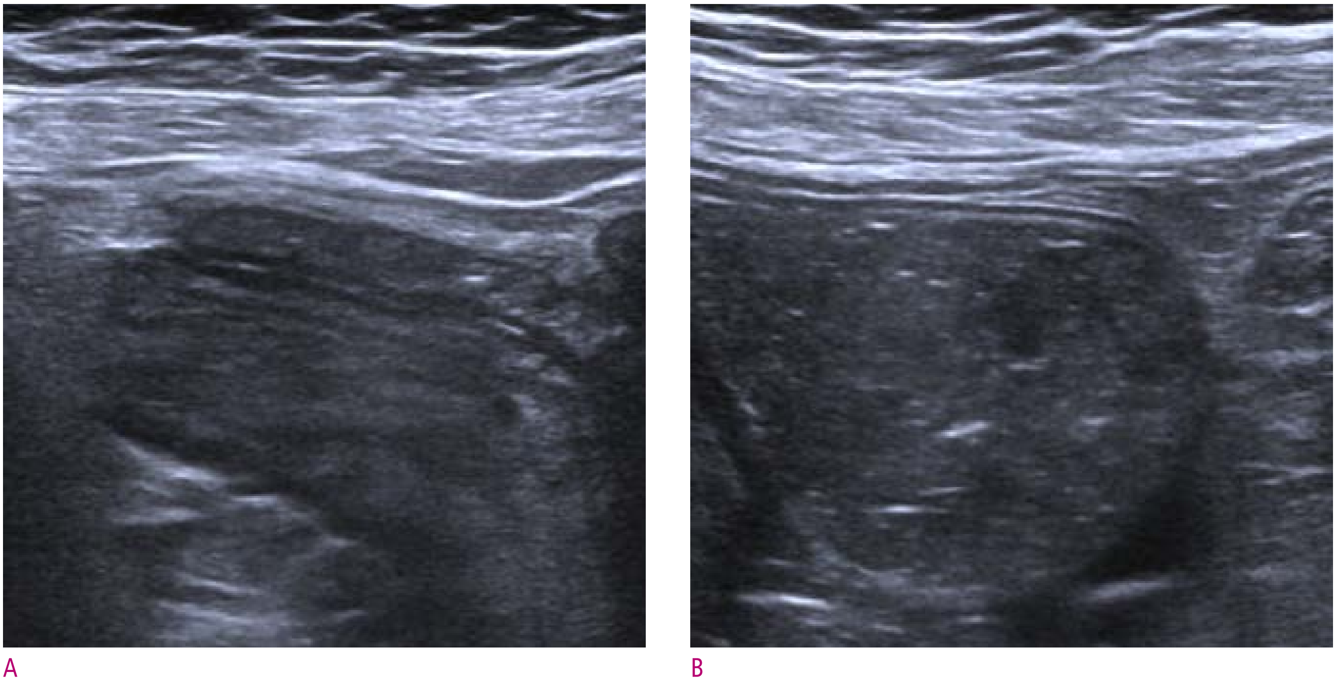

Fig. 2. Abdominal ultrasound shows small bowel intussusception in the pelvic cavity (A). There is 5-cm round and solid mass with internal heterogeneity as a leading point of intussusception (B).

으며, 동반된 복수나 림프절 비대 또한 없었다. 환자는 장폐색이 호전되지 않아 소장 부분절제술을 시행하였으며, 절제조직은 육안상 경계가 매우 좋았고, 고정 후 절제면은 균일한 연노란색을 보였다 (Fig. 4A, B). 현미경 소견으로는 방추세포의 증식, 풍부하고 밀도 높은 콜라겐층, 사슴뿔 모양의 혈관들 및 그 주변과 기질에서 보이는 유리질화 소견이 확인되었다. 세포이형성 또한 관찰되었으며, 10 high power field 당 10개의 유사분열이 확인되었고, 조직 괴사는 전체의 약 5%에서 관찰되었다 (Fig. 5A). 면역화학염색 소견에서는 다음과 같은 결과를 볼 수 있었다: CD34 (+)(Fig. 5B), Vimentin (+), CD99 (+), SMA (+), BCL-2 (focal +), EMA (-), Ki-67 (<5%), CD117 (-), DOG-1 (-), Desmin (-), S-100 (-). 최종적으로 본 증례는 Fédération Nationale des Centres de Lutte Contre Le Cancer (FNCLCC) grade 2에 해당하는 악성 단발성섬유성종양으로 진단되었다.

고 찰

단발성섬유성종양은 비교적 드문 섬유모세포나 근섬유모세포 기원의 중간엽 신생물로 거의 대부분 흉막이나 심막을 포함하는 흉강내 종양이다 (2). 그러나 이론적으로 우

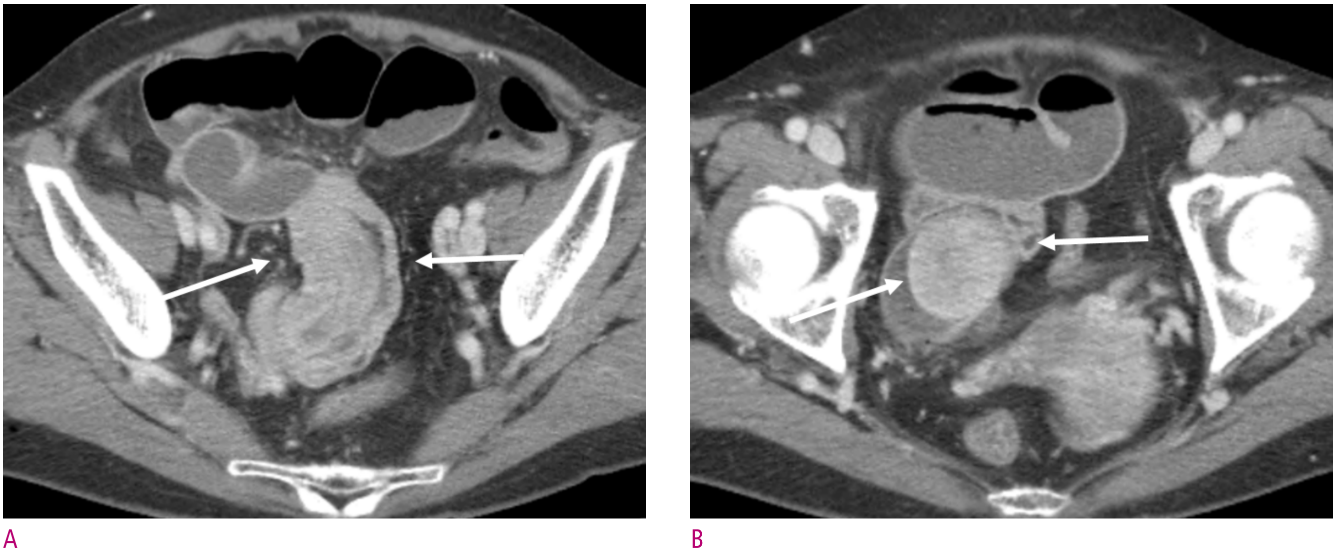

Fig. 3. On computed tomography, there is ileal-ieal intussusception (arrow) with proximal small dilatation (A). At the end intussuception, approximately 5-cm well-enhancing mass (arrow) with subtle central low attenuation is depicted (B).

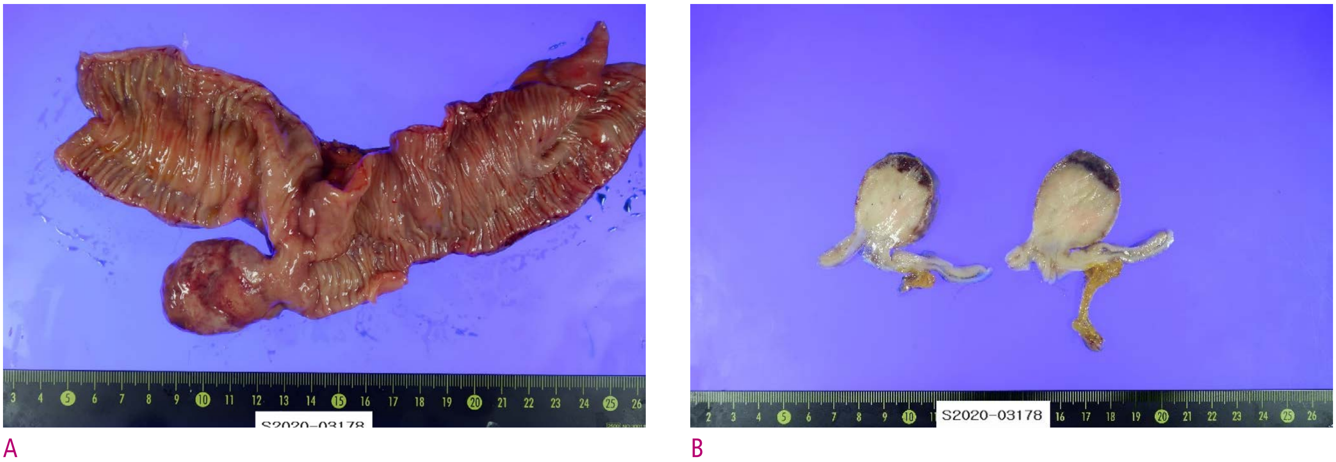

Fig. 4. Surgical specimen shows a 5-cm well-demarcated mass of the ileum (A). After tissue fixation, pale-yellow colored solid mass with focal necrosis at top is identified (B).

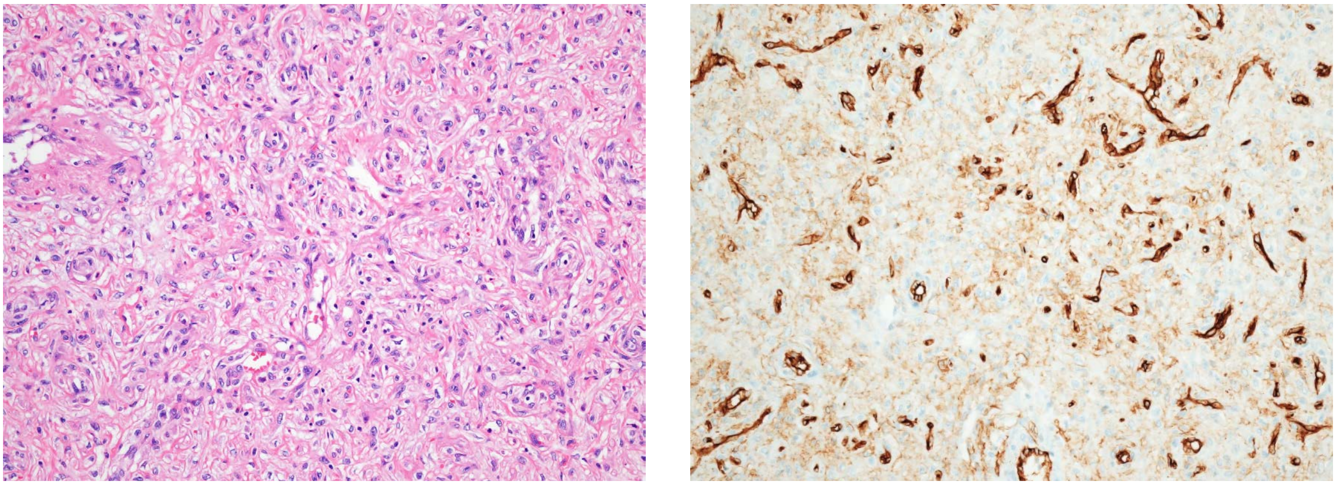

Fig. 5. On microscopy, spindle cell proliferation, collagen stroma and perivascular hyalinazation are found with H&E staining (A). Positivity on CD-34 immunohistochemistry is also noted (B).

리 몸의 어느 곳에서든 발생 가능한 종양으로 극히 드물게 간, 췌장, 위장관에서 발생한 복강 내 증례들이 보고된 바 있다. 위장관은 그 중에서도 더욱 드문 발생 장소로 지금까지 보고된 세 개의 증례에 따르면 비교적 크고 비균질적인 조영증강을 보이는 점막하 종양으로 보이는 경우가 많고, 따라서 비슷한 영상 소견을 보이는 위장관기질종양이나 평활근육종, 슈반세포종, 염증성 근섬유아세포종 등과 감별히 필요할 것으로 생각된다 (1). 본 증례 또한 비교적 균일한 가운데 초음파 및 전산화단층촬영에서 내부 무에코 혹은 저음영이 국소적으로 보였는데 최종 병리소견에서 확인된 약 5%의 조직괴사 부위일 가능성이 매우 높다. 또한 저자가 찾아본 바로는 지금까지의 문헌 보고 상 이러한 위장관 다발성섬유성종양이 장중첩증을 만든 예는 없어, 아마도 본 증례 보고가 그러한 예의 첫번째 보고 일 것으로 여겨진다.

ORCID: Eun Sun Lee: https://orcid.org/0000-0003-0780-7985

References

1. Shanbhogue AK, Prasad SR, Takahashi N, Vikram R, Zaheer A, Sandrasegaran K. Somatic and visceral solitary fibrous tumors in the abdomen and pelvis: cross-sectional imaging spectrum. Radiographics 2011;31:393-408.
2. Ginat DT, Bokhari A, Bhatt S, Dogra V. Imaging features of solitary fibrous tumors. AJR Am J Roentgenol 2011;196:487-495.

장중첩증을 유발한 회장의 악성 단발성섬유성종양

이은선
중앙대학교병원 영상의학과

초 록

단발성섬유성종양(solitary fibrous tumor, SFT)은 비교적 드문 섬유모세포나 근섬유모세포 기원의 중간엽 신생물이다. 특히 흉강이 아닌 신체 다른 부위에서 발생하는 경우는 매우 드문 것으로 알려져 있는데 74세 여자에서 장중첩증을 유발한 회장의 악성 단발성섬유성종양 증례가 있어 보고한다.

www.e-kjar.org
https://doi.org/10.52668/kjar.2021.00052

pISSN 2586-1719 / eISSN 2799-3299

Korean J Abdom Radiol 2021;5:81-83

Case Report

소장폐색을 유발한 회장의 낭성 림프관종

안지현
원주세브란스기독병원 영상의학과

Cystic Lymphangioma of the Ileum Causing Small Bowel Obstruction: A Case Report

Jhii-Hyun Ahn
Department of Radiology, Wonju Severance Christian Hospital, Wonju, Korea

---

Cystic lymphangioma is a rare benign tumor containing chylous or serous fluid. The occurrence of cystic lymphangioma in the small bowel is known to be extremely rare. We would like to report a case of cystic lymphangioma that occurred in the small bowel and caused small bowel obstruction.

Keywords: Cystic lymphangioma; Ileum; Small bowel obstruction

---

서론

낭성 림프관종 (cystic lymphangioma)은 유미성 또는 장액성의 액체를 포함하고 내피세포로 둘러싸인 림프관으로 구성되어 있는 드문 양성 종양이다 (1, 2). 대부분의 낭성 림프관종은 두경부, 액와부에 존재하지만, 그 외에도 위장관, 췌장, 장간막, 후복막 등에서도 나타날 수 있다 (1). 그 중에서 소장에서의 발생은 극히 드문 것으로 알려져 있다 (3-5).

증례보고

68세 여자가 2일 전부터의 복부 통증을 주소로 내원하였다. 환자는 오래전 자궁내막낭으로 오른쪽 난소 절제술을 받은 과거력이 있었다.

복부 전산화단층촬영 (이하 CT)에서 소장폐색이 있었고, 우측 골반강에 위치한 회장에 이행부가 있었다. 이행부에 해당하는 회장벽과 회장 주변에는 조영증강이 되지 않는 낭성 병변들이 있었다 (Fig. 1). 이 낭성 병변들은 구분되어 보이는 벽은 없었고, 경계는 뚜렷하였으며, 주변에 염증소견도 보이지 않았다. 림프절 비대나 복수 소견은 없었고, 다른 복부 장기에도 이상 소견은 없었다. 과거력 및 병변의 위치를 고려하여 회장의 자궁내막증식증의 점액성 퇴화의 가능성을 생각하였고, 그 밖에 회장의 낭성 종양 가능성도 생각하였다.

환자는 회장의 낭성 병변 및 그와 동반된 소장폐색으로 회장 부분 절제를 시행받았다. 육안소견에서 다수의 낭성 병변이 회장 주위에 붙어있었고 장간막에도 병변이 존재하였다 (Fig. 2). 이 낭성 병변들 내부에는 노란색의 장액성 액체가 차있었으며, 회장의 점막부터 장막하층까지 존재하

Received: June 6, 2021 **Revised:** June 22, 2021 **Accepted:** June 24, 2021

Correspondence: Jhii-Hyun Ahn, MD
Department of Radiology, Yonsei University Wonju College of Medicine, Wonju Severance Christian Hospital, 20 Ilsan-ro, Wonju, Gangwon-do 26426, Korea
Tel: +82-33-741-1474 Fax: +82-33-732-8281 E-mail: radajh@yonsei.ac.kr

고 있었다. 병리학적으로 낭성 림프관종으로 진단되었다.

고 찰

위장관에 발생하는 낭성 림프관종은 대부분 증상이 없어 우연히 발견되지만, 위치나 크기에 따라 복통, 장폐색, 또는 장중첩증과 같은 증상을 유발하기도 한다 (1, 3, 6). 이 환자는 회장의 낭성 림프관종이 장폐색을 유발하여 낭성 림프관종이 발견 및 진단되었다.

CT에서 위장관 낭성 림프관종은 점막하층에 위치하는 경계가 좋고 얇은 벽을 가지는 단방 또는 다방성의 낭성 종괴로 보인다. 격막이나 석회화를 보이는 경우도 있다 (1). 그러나 이러한 소견은 비특이적인 소견으로, 수술 전 진단이 어려운 경우가 많다. 소장의 낭성 림프관종은 중복낭종, 기형종, 위장관 기질종양, 혈관종 등과의 감별이 필요하다 (4).

소장의 낭성 림프관종은 수술적 치료를 시행하게 된다. 완전한 수술적 절제를 시행해야 하며, 완전한 절제가 이루어지면 재발하는 경우가 드물지만, 완전한 절제가 이루어지지 못한 경우는 재발의 가능성이 있고 염증이나 출혈을 유발할 수도 있다 (6, 7).

결론적으로, 회장의 낭성 림프관종은 드물고 대부분 증상이 없지만, 이 환자와 같이 소장폐색과 같은 증상을 유발할 수 있다. CT 소견은 비특이적이지만 소장폐색의 이행부에 이와 같은 낭성 종괴가 있을 경우 낭성 림프관종을 감별진단으로 고려해야 하겠다.

ORCID: Jhii-Hyun Ahn: https://orcid.org/0000-0003-3784-9350

References

1. Zhu H, Wu ZY, Lin XZ, Shi B, Upadhyaya M, Chen K. Gastrointestinal tract lymphangiomas: findings at CT andendoscopic imaging with histopathologic correlation.

Fig. 2. Multiple cystic lesions filled with yellow serous fluid were attached around the ileum and lesions were also present in the mesentery.

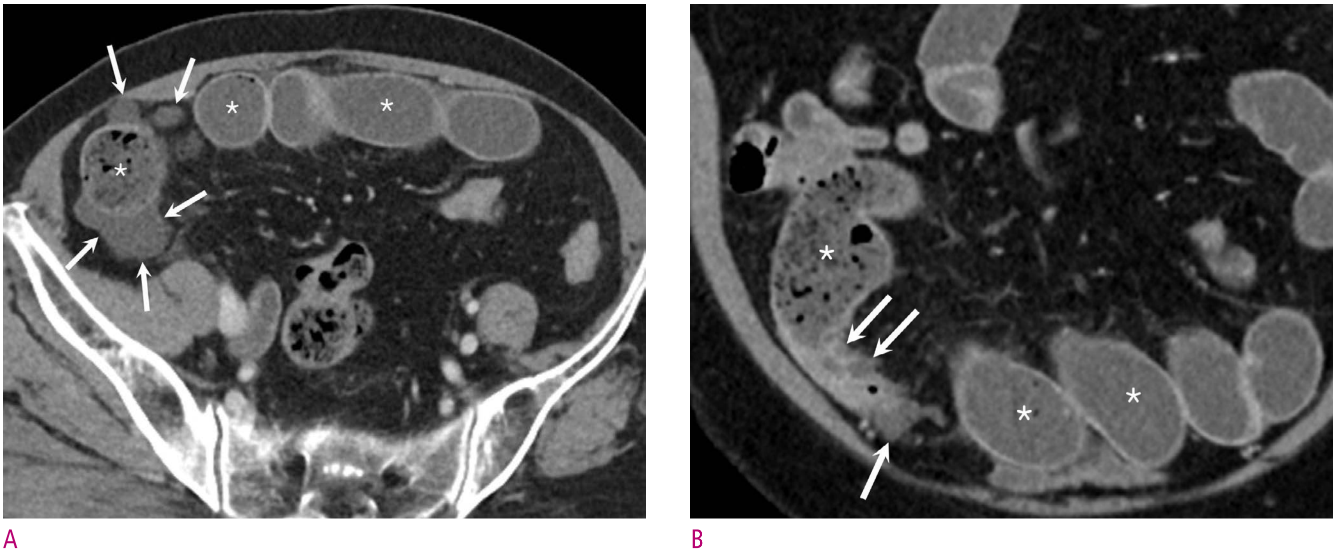

Fig. 1. Contrast-enhanced CT axial (A) and coronal (B) images show small bowel obstruction (*) and transitional zone at the ileum. There area several non-enhancing cystic lesions at the transitional zone of the ileum, adjacent ileum, and mesentery (arrows).

Abdom Imaging 2008;33:662-668.
2. Seki H, Ueda T, Kasuya T, Kotanagi H, Tamura T. Lymphangioma of the jejunum and mesentery presenting with acute abdomen in an adult. J Gastroenterol 1998;33:107-111.
3. Uncu H, Erdem E, Kuterdem E. Lymphangiomas of the ileum: a report of two cases and a review of the literature. Surg Today 1997;27:542-545.
4. Boeck G, Roitzsch E. Submucous cavernous lymphangioma in the ileum ileus of the small intestine. Zentralbl Chir 1982;107:724-726.
5. Calderón-Garcidueñas AL, Padrón-Treviño M, Holguín-Aragón J, Valdéz-Borroel R. Cystic lymphangioma of the ileum. A case report. Bol Med Hosp Infant Mex 1991;48:267-270.
6. Tsukada H, Takaori K, Ishiguro S, Tsuda T, Ota S, Yamamoto T. Giant cystic lymphangioma of the small bowel mesentery: report of a case. Surg Today 2002;32:734-737.
7. Allen JG, Riall TS, Cameron JL, Askin FB, Hruban RH, Campbell KA. Abdominal lymphangiomas in adults. J Gastrointest Surg 2006;10:746-751.

소장폐색을 유발한 회장의 낭성 림프관종

안지현

원주세브란스기독병원 영상의학과

초 록

낭성 림프관종은 유미성 또는 장액성의 액체를 포함하는 드문 양성 종양이다. 낭성 림프관종이 소장에서 발생하는 경우는 극히 드문 것으로 알려져 있는데, 소장에서 발생하여 소장폐색을 유발한 낭성 림프관종 사례가 있어 이를 보고하고자 한다.

KJAR
Korean Journal of Abdominal Radiology
대한복부영상의학회지

투고규정

2017년 1월 6일 제정
2018년 1월 9일 개정
2021년 4월 29일 개정

1. 일반사항

대한복부영상의학회지는 대한복부영상의학회의 공식 학술지로서 연 1회 발간하며, 영문 명칭은 Korean Journal of Abdominal Radiology (KJAR)로 한다. 학술지는 매년 연 1회, 인쇄본의 형태와 온라인(http://e-kjar.org)으로 발간된다.

원고는 국문 혹은 영문으로 작성할 수 있으며, 원고의 종류는 원저, 종설, 임상화보, 증례보고, 특별기고(정책 백서, 원저소개, 편집인에게 보내는 글, 기타) 등으로 구분될 수 있다. 모든 원고는 전자 논문투고 시스템(http://submit.e-kjar.org)을 이용하여 제출한다.

2. 게재윤리사항

2.1. 윤리적 규정

이 학회지에 투고하는 모든 원고는 연구의 대상이 사람인 경우(인체실험의 경우), 헬싱키 선언(Declaration of Helsinki)에 입각하여, 피험자 또는 보호자에게 연구의 목적과 연구 참여 중 일어날 수 있는 정신적, 신체적 위해를 충분히 설명하고, 피험자 또는 보호자로부터 서면 동의서를 받았음을 원고에 명시하여야 한다. 단, 기관 생명윤리 심의위원회 (Institutional Review Boards; IRB)에서 환자 동의서 면제를 승인한 경우는 제외될 수 있다).

연구의 대상이 동물인 경우(동물실험의 경우), 실험 과정이 NIH Guide for the Care and Use of Laboratory Animals에 저촉되지 않고, 소속기관의 동물실험윤리위원회(Institutional Animal Care and Use Committee; IACUC)의 승인을 받았음을 명시하여야 한다.

또한 모든 임상 연구는 공인된 IRB의 승인을 받아야 하고, IRB가 면제를 승인하지 않는 한 연구에 참여하는 모든 피험자(또는 법적 권한이 있는 대리인)로부터 연구 참여에 대한 사전 동의서를 받아야 한다. 또한 필요 시 서면 동의서 및 윤리위원회 승인서의 제출을 요구 할 수 있다. 표절, 중복출간, 연구부정행위 등 연구윤리와 관련된 부분에 대한 처리는 대한의학학술지편집인위원회에서 제정한 '의학논문 출판윤리가이드라인'을 따른다.

2.2. 저자의 정의와 요건

대한복부영상의학회지는 2019년 ICMJE의 저자됨의 권장(http://www.icmje.org/recommendations/)을 따른다. 저자란 출판된 논문에 지적으로 상당한 기여를 한 사람을 말한다. 저자가 되기 위해서는 1) 학술적 개념과 계획 혹은 자료의 수집이나 분석 혹은 해석을 하는 데 있어서 상당한 공헌을 하고, 2) 논문을 작성하거나 중요한 내용을 수정하며, 3) 출간될 원고를 최종적으로 승인하고, 4) 논문의 정확성 또는 완벽성과 관련된 질문에 대해 적절히 설명하고 대답할 수 있는 연구의 모든 측면에 대해 책임을 지는, 이 네 가지의 조건을 모두 만족시켜야 한다. 책임저자는 저자 가운데 1명으로 학술지의 편집인이 보내는 논문 심사의 논평, 수정사항 등을 받아 연락한다. 또한 독자들이 별책(reprints)을 요구하거나 연구팀과의 연락이 필요한 때에 연락이 가능한 연락처가 기재되어 있어야 한다. 논문심사 과정 중 '현재상태로 게재' 결정이 난 후에는 저자의 추가나 책임저자의 변경이 불가능하다. 저자 명단에서 빠지기 위해서는 본인의 의사를 표시하고 서명한 편지를 제출하여야 한다.

2.3 중복게재에 대한 규정

제출된 원고와 동일한 또는 유사한 원고를 다른 학술지(ISSN 등재 학술지)에 게재할 수 없으며, 원고 전체나 원고의 중요한 부분, 표, 그림 등이 다른 학술지에 이미 게재되었거나, 게재 예정인 논문은 게재할 수 없다. 단 사용언어가 다르거나 양측 편집인의 승인이 있을 경우에 허용할 수 있으며, 이때 이차 출간한 논문 표지의 하단(각주, foot note)에 이 논문 전부 혹은 일부가 이미 출간되었음을 알 수 있도록 명시하고 원전을 기술하여야 한다. "This article is based on a study first reported in the [title of journal, with full reference]." 단, 학회 강의록 등과 같이 ISSN 등재 학술지가 아닌 경우에는 해당되지 않는다. 중복게재에 해당하는 것(예; 타 ISSN 등재 저널에 1차로

실린 논문 중 KJAR에 변형, 수록한 경우 등)을 제외하고는 KJAR에 실린 원고도 업적으로 이용할 수 있다. (예; 연수강좌 강의록을 종설로 수정한 경우 등).

2.4. 원고와 관련된 이권과 저작권 양도에 관한 문제

원고와 관련된 연구비를 비롯한 재정적 지원사항과 이권에 대한 문제(conflict of interest, 이해충돌)를 일으킬 수 있는 사항을 빠짐없이 원고의 표지에 명시하여야 한다.

게재 결정된 원고의 저작권은 본 학회에 속하며, 대한복부영상의학회는 원고를 학회지나 다른 매체에 출판, 배포, 인쇄할 수 있는 권리를 가진다.

3. 원고의 종류

A. 원저(Original Article): 원저는 기초 및 임상연구결과의 보고서로서 새로운 정보를 제공할 수 있어야 하고 논문에 포함된 통계기법은 정확해야 한다. 원고의 길이에 제한은 없지만 편집위원회에서 과다한 그림이나 큰 표 등을 제한할 수 있다.

B. 종설(Review): 종설은 특정 주제에 초점을 맞춘 고찰로서 원칙적으로 편집위원회에서 특정 저자에게 위촉한다. 요청받지 않은 논문도 투고 시 편집위원회에서 고려할 수 있다.

C. 임상화보(Pictorial Essay): 임상화보는 질 좋은 사진을 통한 교육이 주목적이며 이미 기정화 된 내용이지만 사진이나 그림들로서 교육적 가치가 크고 훌륭한 경우에 게재한다.

D. 증례보고(Case Report): 복부영상의학분야에 중요한 영향을 줄 수 있는 교육적인 소견을 보고하는 것으로, 영상의학적 진단에 직접적인 관련이 있는 임상소견들을 제시해야 한다.

E. 특별 기고문(Special Report): 본 회지는 위에 기술한 정형화된 원고 이외에 다양한 형식, 다양한 내용의 원고를 게재할 수 있다. 이미 학회지에 출판된 특정 논문에 대한 건설적인 비평 또는 의견, 복부 영상의학 분야의 제반 정책 관련 백서, 혹은 영상의학과 의사의 일반적 관심사항이나 학술분야 특정주제에 관한 기고문을 게재할 수 있다. 별도의 심사과정 없이 편집위원회에서 게재여부를 결정한다. 단 필요에 따라 외부 심사를 의뢰할 수 있다.

4. 원고의 작성

4.1. 일반사항

모든 원고는 한글 또는 영문으로 작성하며 Microsoft Word 최신 버전 사용을 원칙으로 한다. 의학용어의 번역은 가장 최근에 대한의사협회에서 발간한 의학용어집을 사용한다. 글씨 크기는 12 point, 2열 간격(200%)으로, A4용지, letter size용지의 상하좌우에 3 cm의 여백을 둔다. 표지로부터 시작하여 모든 원고에는 페이지 번호를 매겨야 한다. 원고작성에 사용되는 단위는 metric unit이다.

4.2. 표지(Title page)

표지에는 논문 제목과 모든 저자의 이름과 소속기관을 한글과 영문으로 표기하며, 외국인의 경우 영문으로 통일한다. 논문의 제목은 논문 내용을 전달할 수 있는 최소한의 단어로 작성하며 약자는 사용하지 않도록 한다. 다기관 연구에서 소속이 다른 저자들이 포함된 경우 연구가 주로 이루어진 기관을 1번으로 기록하고 그 이외의 기관은 해당 저자 이름에 2번부터 어깨번호를 하고 소속기관을 번호순으로 표기한다. 학위를 포함한 모든 저자명, 모든 저자들의 ORCID ID, 이해 상충, 연구비에 대한 기술이 반드시 포함되어야 한다. 교신저자의 이름, 주소(우편번호), 전화, 팩스번호 및 E-mail 주소, 간추린 제목(running title), 재정지원 등의 순으로 국문과 영문으로 기재한다. 간추린 제목은 국문은 30자, 영문은 12단어가 넘을 경우 표기한다.

4.3. 본문(Main Body)

내표지는 본문 첫째 페이지로서 국문과 영문으로 논문 제목을 기재한다. 내표지와 본문의 모든 페이지에서 저자(소속, 성명)에 관한 사항은 기술하지 않는다. 영문 약어는 최소화하며 이를 사용할 시에는 최초에 풀어 쓴 후 괄호 안에 약어를 기입한다. 색인용어는 영문 초록의 하단에 MEDLINE/PubMed에서 등재된 MeSH 단어를 5개 선정하여 기입한다.

A. 원저

원저의 원고는 표지, 내표지, 영문과 국문초록(목적, 대상과 방법, 결과, 결론을 구분하여 기술한다)과 색인용어, 서론, 대상과 방법, 결과, 고찰, 요약, 참고문헌, 표, 그림 설명의 순서로 구성한다.

원고 종류	초록 최대 글자 수	최대 그림 수	최대 참고문헌수
종설	영문200단어 또는 한글 400자	30	100
임상화보	영문200단어 또는 한글 400자	40	70
원저	영문300단어 또는 한글 600자	20	50
증례보고	영문200단어 또는 한글 400자	10	20

B. 종설

영문과 국문초록을 특별한 구분 없이 기술하며, 서론, 본론, 결론으로 기술하고, 참고문헌, 표, 그림 설명을 작성한다.

C. 임상화보

영문과 국문초록, 서론, 고찰, 참고문헌, 그림 설명의 순으로 한다.

D. 증례보고

영문과 국문초록을 특별한 구분 없이 기술하며, 서론, 증례 보고, 고찰, 참고문헌, 표, 그림설명의 순서로 구성한다.

4.4. 참고문헌

본문에서 참고문헌을 인용할 때에는 인용 순서대로 번호를 부여하여 아라비아 숫자로 각괄호 안에 표기한다. 문헌 인용 시 가능하면 인용논문의 저자 이름을 사용하지 않을 것을 권고하며, 꼭 필요하여 저자명을 언급하는 경우 국내와 외국저자 모두 영문으로 기재하되 1인일 경우 'Kim (1), Bailey (3)', 2인 이상일 경우 'Park 등(2), Brougham 등(4)'과 같이 기술한다. 국내 저자가 서지사항을 영문으로 기재한 경우에는 외국 저자의 예를 따른다. 참고한 문헌은 따로 REFERENCES 난에 본문에 인용한 순서대로 정리하여 나열한다. 논문의 저자는 최대 6명까지 표시할 수 있으며 7명 이상인 경우에는 앞에서 여섯 번째까지의 저자를 나열하고 나머지 저자는 'et al'로 표시한다. 참고문헌이 온라인으로 발간되어 권, 호가 아직 결정되지 않은 경우는 digital objective identifier (DOI)를 표시해야 한다. 학술지명의 표기는 'Index Medicus'의 학술지 약어를 사용하고 그 외 명시되지 않은 기술 양식은 'The NLM Style Guide for Authors, Editors, and Publishers (http://www.nlm.nih.gov/citingmedicine)'에 따라 기술한다.

Journal articles

1. Yoo BM, Lehman GA. Update on endoscopic treatment of chronic pancreatitis. Korean J Intern Med 2009;24:169-179.
2. Caselli RJ, Dueck AC, Osborne D, Gilman AG, Rall TW, Nies AS, et al. Longitudinal modeling of age-related memory decline and the APOE epsilon4 effect. N Engl J Med 2009;361:255-263.

Books

3. Gilman AG, Rall TW, Nies AS, Taylor P. Goodman and Gilman's the Pharmacological Basis of Therapeutics. 9th ed. New York: Pergamon Press, 1996.

Chapters in books

4. Costa M, Furness JB, Llewellyn-Smith IF. Histochemistry of the enteric nervous system. In: Johnson LR, ed. Physiology of the Gastrointestinal Tract. 2nd ed. Vol. 1. New York: Raven, 1987:1-40.

Conference paper

5. Rice AS, Brooks JW. Canabinoids and pain. In: Dostorovsky JO, Carr DB, eds. Proceedings of the 10th World Congress on Pain; 2002 Aug 17-22; San Diego, CA. Seattle (WA): IASP Press, 2003:437-468.

Online publication

6. Suzuki S, Kajiyama K, Shibata K, et al. Is there any association between retroperitoneal lymphadenectomy and survival benefit in ovarian clear cell carcinoma patients? Ann Oncol 2008 Mar 19 [Epub]. http://dx.doi.org/10.1093/annonc/mdn059.

Web content

7. American Cancer Society.Cancer reference information [Internet]. Atlanta (GA): American Cancer Society, c2009 [cited 2009 Nov 20]. Available from: http://www.cancer.org/docroot/CRI/CRI_0.asp.
8. National Cancer Information Center.Cancer incidence [Internet].Goyang (KR): National Cancer Information Center, c2009 [cited 2009 Oct 20]. Available from: http://www.cancer.go.kr/cms/statics.

4.5. 표

표는 그림에서 알 수 있는 내용을 중복하지 않으며 본문의 내용을 읽지 않고도 설명이 가능하도록 간결 명료하게 작성해야 한다. 표는 별도의 페이지에 작성하며 본문에 인용한 순서대로 아라비아 숫자로 'Table 1.'과 같이 표기하고 이어서 제목을 기술한다. 표준 약어 이외의 약어는 하단 주석에서 기술한다(예: EVR, early virologic response; SVR, sustained virologic response.). 표 하단에는 전체적인 내용 설명, 약어 설명, 기호 설명의 순으로 각각 행을 바꾸어 기재한다. 기호 사용 시 *, †, ‡, §, ‖, ¶, **, ††, ‡‡의 순으로 하며 이를 설명 하단에 표기한다.

4.6. 그림

각각의 그림은 본문에 포함하지 않고 개별 파일로 해상도가 300dpi 이상인 TIFF 형식으로 제출해야 한다. 화살표 등이 포함된 그림은 화살표의 위치를 확인할 수 있는 파일(TIFF, PPT, DOCX 등)을 원본과 별도로 제출해야 한다. 그림은 본문에 인용된 순서대로 번호 지어지며, 동일번호에서 2개 이상의 그림인 경우, 아라비아숫자 이후에 알파벳 글자를 기입하여 표시한다 (예: Fig. 1A, Fig. 1B). 원칙적으로 같은 그림 번호 안에 서로 다른 환자의 그림을 포함시키지 않는다. 모든 그림은 설명을 포함해야 하며 구나 절이 아닌 하나의 문장형태로 기술한다. 모든 그림은 출판에 적합하도록 편집자가 조정할 수 있다.

4.7. 기타

상기 기술된 사항 이외는 대한복부영상의학회지의 편집위원회에서 결정한다.

5. 논문의 투고 및 투고 전 확인 사항

5.1. 논문의 제출

- 모든 원고는 온라인으로 투고하여야 한다. 주요문서와 그림파일을 제출해야 하며 주요문서는 표지, 내표지, 초록, 색인용어, 원고 전문, 참고문헌, 표, 그림 설명을 포함한다.

5.2. 제출 전 확인사항

- 원고의 파일 형태가 적절하다. (.doc, .docx, tiff)
- 논문제목, 저자, 저자들의 소속기관을 한글과 영문으로 표기한 표지를 독립된 파일로 작성한다
- 문서는 원고의 종류에 따른 규정을 준수하였다. 그림은 각각의 파일로 이루어져 있다.
- 이전에 출판되었던 내용은 재출판에 대한 편집인의 동의서가 준비되었다.
- 모든 저자의 동의서가 준비되었다.

6. 논문의 심사 및 게재

제출된 원고는 편집위원회에서 해당분야 전문가에게 심사를 요청하고 그 결과에 근거하여 게재여부를 결정하며 원고의 수정 및 보완 사항을 저자에게 권고한다.

논문 심사 후 저자는 심사결과에 따라 심사의견서 내의 지적사항을 토대로 논문을 수정 작성해야 한다.

Scanlux® 300/370

there's more to see...

Dasol Life Science

SANOCHEMIA
Diagnostics International


ulrich
ulrichINJECT
CT motion™

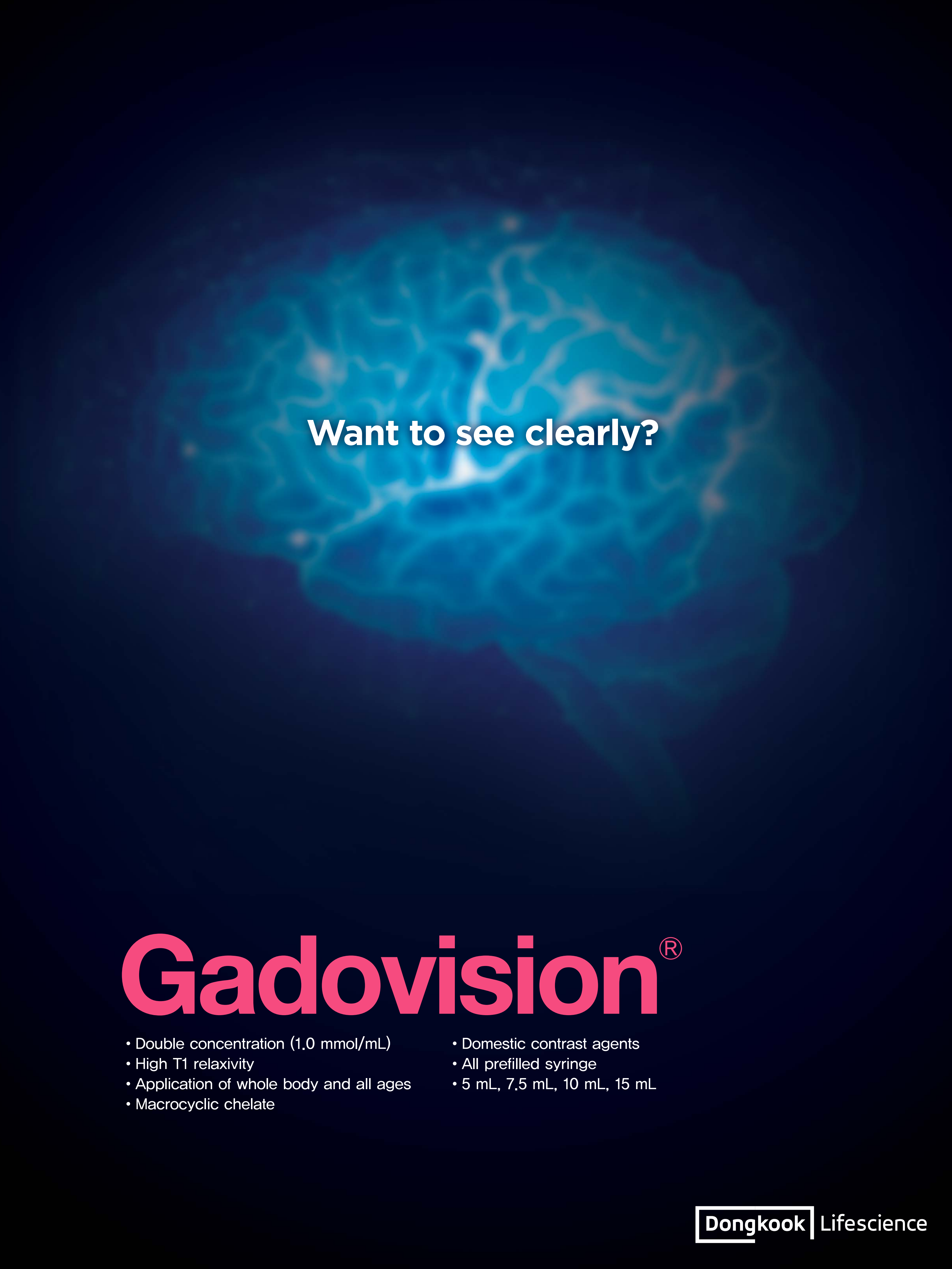
Want to see clearly?

GE Healthcare

There is a Constant On the radiology landscape[1]

OMNIPAQUE · 1982-2018 · 36 YEARS ·

Over 500 million patients

More than 100 countries

Over 36 years' experience

Over 6,500 published clinical articles

PLUSPAK™
(polymer bottle)

Efficient storage and disposal
No sharp alloy ring pull
Efficient labeling

imagination at work

OMNIPAQUE™
IOHEXOL

Reference. 1. Data on file, GE Healthcare Ltd.

효능·효과: 척수조영, 혈관조영, 정맥요로조영 (IVP), CT 조영증강, 체강조영 (관절조영, ERP/ERCP, 헤르니아조영, 자궁난관조영, 침샘조영, 소화관조영) **용법·용량:** 일반적으로 다른 요오드계 X 선 조영제와 같은 요오드 농도, 용량을 사용하며, 투여 전후에 충분한 수분공급을 합니다. 추천 투여용량은 제품설명서를 참고하시기 바랍니다. **금기:** 1) 이 약 및 이 약의 구성성분, 요오드계 약물에 과민반응 및 그 병력이 있는 환자 2) 중증 갑상샘 질환환자 3) 중증 국소감염 또는 균혈증과 같은 전신감염이 있는 환자에 대한 척수조영 **신중투여:** 1) ① 극도의 전신 쇠약 환자 ② 기관지천식 환자 ③ 중증 심장애 환자 ④ 중증 간장애 환자 ⑤ 중증 신장애 환자 ⑥ 급성 췌장염 환자 ⑦ 마크로글로불린혈증 환자 ⑧ 다발성골수종 등의 형질세포질환 환자 ⑨ 강직증 환자 ⑩ 갈색세포종 환자 및 질환 의심자 2) 본인 또는 가족이 기관지 천식, 발진, 두드러기 등의 알레르기를 일으키기 쉬운 체질인 환자 3) 약물 과민반응의 병력이 있는 환자 4) 탈수 증상이 있는 환자 5) 고혈압 환자
※본 제품에 대한 자세한 내용은 제품 설명서를 참고하십시오

서울특별시 강남구 학동로 343번지 POBA 강남타워 7층
Tel: 02-6201-3700 Fax: 02-6201-3801

JB1494KO


YOU
Portfolio
Services
Science


400